الجمهورية الجزائرية الديمقراطية الشعبية

République Algérienne Démocratique et Populaire

Ministère de L'Enseignement Supérieur et de la Recherche Scientifique

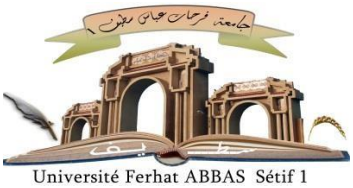

UNIVERSITÉ FERHAT ABBAS - SETIF1

THESE

Présentée à l'Institut d'Optique et Mécanique de Précision

Pour l'obtention du diplôme de

DOCTORAT EN SCIENCES

Option: Optique et mécanique de précision

Par

KARAR Naoual

THÈME

Estimation de la Fiabilité d'un Système Mécanique Multi-Composants « Réducteur de Vitesses » par les Méthodes d'Optimisation

Soutenue, le: 11/12/2025 Devant le jury composé de:

SMATA Lakhdar	**Professeur**	**Univ. Ferhat Abbas Sétif 1**	**Président**
FELKAOUI Ahmed	**Professeur**	**Univ. Ferhat Abbas Sétif 1**	**Directeur de thèse**
DJEDDOU Ferhat	**Professeur**	**Univ. Ferhat Abbas Sétif 1**	**Co-Directeur**
ZIANI Ridha	**M.C.A.**	**Univ. Ferhat Abbas Sétif 1**	**Examinateur**
BOUKHOBZA Abdelyamine	**M.C.A.**	**Centre Univ. Nour Bachir, El Bayadh**	**Examinateur**
FEDAOUI Kamel	**M.C.A.**	**L'École Nationale Supérieure, Batna**	**Examinateur**

الجمهورية الجزائرية الديمقراطية الشعبية

People's Democratic Republic of Algeria

Ministry of Higher Education and Scientific Research

Université Ferhat ABBAS Sétif 1

FERHAT ABBAS UNIVERSITY – SETIF 1

THESIS

Submitted at the Institute of Optics and Precision Mechanics For the attainment of the degree of

DOCTORATE IN SCIENCES

Option: Optics and Precision Mechanics

By

KARAR Naoual

SUBJECT

Reliability Estimation of a Multi-Component Mechanical System "Speed Reducer" Using Optimization Methods

Submitted: 11/12/2025

Members of the assessment committee:

SMATA Lakhdar	**Professor**	**Univ. Ferhat Abbas Sétif 1**	**President**
FELKAOUI Ahmed	**Professor**	**Univ. Ferhat Abbas Sétif 1**	**Supervisor**
DJEDDOU Ferhat	**Professor**	**Univ. Ferhat Abbas Sétif 1**	**Co-supervisor**
ZIANI Ridha	**Associate Professor**	**Univ. Ferhat Abbas Sétif 1**	**Examiner**
BOUKHOBZA Abdelyamine	**Associate Professor**	**Univ Centre. Nour Bachir, El Bayadh**	**Examiner**
FEDAOUI Kamel	**Associate Professor**	**The National Higher School, Batna**	**Examiner**

ACKNOWLEDGEMENTS

First and foremost, I humbly express my deepest gratitude to ALLAH (SWT) for His infinite guidance and blessings throughout my life. Without His grace and mercy, none of this would have been possible. Completing this thesis has been a long and demanding journey, and I am immensely grateful to all those who have supported me along the way.

I extend my heartfelt appreciation to my supervisor, **Prof. FELKAOUI Ahmed**, whose invaluable guidance, insightful advice, and wealth of knowledge made this work possible. His unwavering encouragement and belief in my abilities inspired me to take on this project with dedication and perseverance.

Alongside Prof. FELKAOUI, I would also like to express my sincere gratitude to my co-author, **Prof. DJEDDOU Ferhat**, for his significant contributions and the many enriching discussions we had throughout this journey. His support and camaraderie made the path toward this doctorate a rewarding experience.

I would like to express my sincere gratitude to **Prof. Lakhdar SMATA**, who graciously accepted to serve as President of the Jury.

My heartfelt thanks also go to the distinguished jury members, **Dr. Ridha ZIANI**, **Dr. Abdelyamine BOUKHOBZA**, and **Dr. Kamel FEDAOUI**, for their time, effort, and insightful evaluation of my dissertation. I greatly appreciate their valuable feedback and expertise

Last but certainly not least, I am profoundly grateful to my **family and friends** for their unwavering support, patience, and encouragement over the years. Their understanding and belief in me have been a constant source of strength.

To all who have played a part in this journey; thank you from the bottom of my heart.

KARAR Naoual

ABSTRACT

The reliability assessment of multi-component mechanical systems, such as speed reducers, poses considerable challenges due to the numerous random variables involved and the presence of correlated failure modes. The use of Dimensionality Reduction Methods (DRMs) in structural reliability analysis provides a valuable approach to simplify these complex systems. However, their application raises important concerns related to maintaining accuracy, ensuring interpretability, and achieving computational efficiency.

This thesis evaluates the limitations and applicability of Dimensionality Reduction Methods (DRMs) in solving real-world structural reliability problems. The primary objective is to develop strategies that mitigate inherent drawbacks of DRMs, such as significant information loss, challenges in interpreting principal components and their physical significance relative to the original variables, and high computational complexity.

The research is structured in three stages. First, a Structural System Reliability-Based Dimension Reduction Method (SSR-DRM) is proposed, which leverages the First-Order Reliability Method (FORM) to create reduced-dimensional models based on sensitivity factors and the correlation between failure modes. Reliability is then assessed for the original, reduced-dimensional, and deterministic models to identify which simplified models most accurately represent the original system. Failure probabilities are estimated using FORM and Monte Carlo Simulation (MCS) as benchmark methods. The results consistently show that the reduced-dimensional model provides the most precise approximation of the original system across all subsystems of the speed reducer, effectively capturing essential reliability characteristics while significantly reducing computational effort.

In the second stage, the reduced-dimension models from the previous phase are employed to estimate the overall reliability of the speed reducer, modeled as a series system of its components. First, the first-order failure probability bounds (i.e., the widest upper and lower bounds) are computed for the reduced models. Subsequently, the failure probability is evaluated using Ditlevsen's second-order upper bound method (narrow bounds), incorporating sensitivity factors and the correlation matrix. The results show strong agreement with Monte Carlo Simulation (MCS) outcomes, demonstrating the efficacy of the proposed approach.

The third stage focuses on improving the reliability of the gear pair subsystem under harsh operating conditions. Two distinct approaches are employed: (1) modifying the statistical parameters of the most influential variables, and (2) implementing the proposed Reliability-Based Robust Design Optimization (RBRDO) framework, which utilizes the Sequential Optimization and Reliability Assessment (SORA) method to optimize critical design parameters. The results obtained align closely with findings reported in the literature, validating the effectiveness of the proposed methodology.

This research contributes to the field of mechanical reliability engineering by introducing a systematic framework for (1) system reliability computation and (2) speed reducer design optimization under uncertainty. The proposed approach significantly improves computational efficiency while maintaining rigorous precision in results.

All numerical methods and analytical techniques presented in this thesis were implemented using MATLAB.

Keywords: Dimension Reduction Method (DRM), First-Order Reliability Method (FORM), sensitivity factors, first-order failure probability bounds, Narrow Bounds, Reliability-Based Robust Design Optimization (RBRDO), speed reducer reliability.

RÉSUMÉ

L'évaluation de la fiabilité des systèmes mécaniques multi-composants, tels que les réducteurs de vitesse, pose des défis considérables en raison des nombreuses variables aléatoires impliquées et de la présence de modes de défaillance corrélés. L'utilisation des Méthodes de Réduction de Dimensionnalité (MRD) dans l'analyse de fiabilité structurelle offre une approche précieuse pour simplifier ces systèmes complexes. Cependant, leur application soulève d'importantes préoccupations liées au maintien de la précision, à l'assurance de l'interprétation et à l'atteinte de l'efficacité computationnelle.

Cette thèse évalue les limitations et l'applicabilité des Méthodes de Réduction de Dimensionnalité (MRD) dans la résolution de problèmes de fiabilité structurelle du monde réel. L'objectif principal est de développer des stratégies qui atténuent les inconvénients inhérents des méthodes de réduction de dimensionnalité (MRD), tels que la perte d'informations significative, les difficultés d'interprétation des composantes principales et leur signification physique par rapport aux variables d'origine, ainsi que la complexité computationnelle élevée.

La recherche est structurée en trois étapes. Tout d'abord, une méthode de réduction de dimension basée sur la fiabilité des systèmes structurels (SSR-DRM) est proposée, qui utilise la méthode de fiabilité du premier ordre (FORM) pour créer des modèles de dimension réduite basés sur les facteurs de sensibilité et la corrélation entre les modes de défaillance. La fiabilité est ensuite évaluée pour les modèles originaux, réduits en dimensions et déterministes afin d'identifier quels modèles simplifiés représentent le plus fidèlement le système original. Les probabilités de défaillance sont estimées en utilisant FORM et la simulation de Monte Carlo (MCS) comme méthodes de référence. Les résultats montrent de manière cohérente que le modèle à dimension réduite fournit l'approximation la plus précise du système original dans tous les sous-systèmes du réducteur de vitesse, capturant efficacement les caractéristiques essentielles de fiabilité tout en réduisant considérablement l'effort de calcul.

Dans la deuxième étape, les modèles à dimension réduite de la phase précédente sont utilisés pour estimer la fiabilité globale du réducteur de vitesse, modélisé comme un système en série de ses composants. Tout d'abord, les bornes de probabilité de défaillance du premier ordre (c'est-à-dire les bornes supérieures et inférieures les plus larges) sont calculées pour les modèles réduits. Par la suite, la probabilité de défaillance est évaluée en utilisant la méthode de la borne supérieure du second ordre de Ditlevsen (bornes étroites), en incorporant les facteurs de sensibilité et la matrice de corrélation. Les résultats montrent une forte concordance avec les résultats de la Simulation de Monte Carlo (MCS), démontrant l'efficacité de l'approche proposée.

La troisième étape se concentre sur l'amélioration de la fiabilité du sous-système de la paire d'engrenages dans des conditions de fonctionnement difficiles. Deux approches distinctes sont employées : (1) modifier les paramètres statistiques des variables les plus influentes, et (2) mettre en œuvre le cadre proposé d'Optimisation de Conception Robuste Basée sur la Fiabilité (RBRDO), qui utilise la méthode d'Évaluation de Fiabilité et d'Optimisation Séquentielle (SORA) pour optimiser les paramètres de conception critiques. Les résultats obtenus s'alignent étroitement avec les conclusions rapportées dans la littérature, validant ainsi l'efficacité de la méthodologie proposée.

Cette recherche fait progresser l'ingénierie de la fiabilité mécanique en fournissant un cadre systématique pour optimiser les conceptions de réducteurs de vitesse en cas d'incertitude, en améliorant l'efficacité computationnelle sans sacrifier la précision.

Tous les méthodes numériques et techniques analytiques présentées dans cette thèse ont été mises en œuvre en utilisant MATLAB.

Mots-clés : Méthode de Réduction de Dimension (MRD), Méthode de Fiabilité du Premier Ordre (MFPO), facteurs de sensibilité, bornes de probabilité de défaillance du premier ordre, Bornes Étroites, Optimisation de la conception robuste basée sur la fiabilité (RBRDO), fiabilité du réducteur de vitesse.

ملخص

إن تقييم موثوقية الأنظمة الميكانيكية متعددة المكوّنات، مثل علب تخفيض السرعة، يطرح تحديات كبيرة نظرًا لكثرة المتغيرات العشوائية وتواجد أنماط فشل مترابطة. إن استخدام طرق تقليل الأبعاد (DRMs) في تحليل الموثوقية الإنشائية يوفر مقاربة فعّالة لتبسيط هذه الأنظمة المعقدة. غير أن تطبيق هذه الطرق يثير إشكاليات مهمة تتعلق بالحفاظ على الدقة، وضمان قابلية التفسير، وتحقيق الكفاءة الحسابية.

تهدف هذه الأطروحة إلى تقييم حدود وإمكانية تطبيق طرق تقليل الأبعاد (DRMs) في معالجة مسائل الموثوقية الإنشائية الواقعية. ويتمثل الهدف الرئيسي في تطوير استراتيجيات للتقليل من العيوب الجوهرية لهذه الطرق، مثل فقدان المعلومات بشكل ملحوظ، وصعوبة تفسير المركبات الرئيسية ودلالتها الفيزيائية مقارنة بالمتغيرات الأصلية، إضافة إلى التعقيد الحسابي المرتفع.تم تنظيم هذا البحث في ثلاث مراحل رئيسية:

في المرحلة الأولى، تم اقتراح منهج لتقليل الأبعاد قائم على موثوقية النظام الإنشائي(SSR-DRM) ، يعتمد على طريقة الموثوقية من الدرجة الأولى (FORM) لإنشاء نماذج مخفّضة الأبعاد استنادًا إلى معاملات الحساسية والعلاقات الارتباطية بين أنماط الفشل. بعد ذلك، تم تقييم الموثوقية للنموذج الأصلي، والنموذج المخفّض، والنموذج الحتمي، بهدف تحديد النموذج المبسّط الأكثر تمثيلًا للنظام الأصلي. وقد تم تقدير احتمالات الفشل باستخدام كل من طريقة FORM ومحاكاة مونت كارلو (MCS) كمرجع معياري. وأظهرت النتائج باستمرار أن النموذج مخفّض الأبعاد يقدّم أفضل تقريب للنظام الأصلي عبر جميع الأنظمة الفرعية لعلبة تخفيض السرعة، حيث ينجح في تمثيل الخصائص الأساسية للموثوقية مع تقليل ملحوظ في الجهد الحسابي.

في المرحلة الثانية، استُخدمت النماذج مخفّضة الأبعاد لتقدير الموثوقية الكلية لعلبة تخفيض السرعة، والتي تم نمذجتها كنظام تسلسلي لمكوّناته. في البداية، تم حساب حدود احتمالية الفشل من الدرجة الأولى (أي أوسع حدين علوي وسفلي) للنماذج المخفّضة. ثم تم تقييم احتمالية الفشل باستخدام طريقة ديتلفسن للحد العلوي من الدرجة الثانية (الحدود الضيقة)، مع الأخذ بعين الاعتبار معاملات الحساسية ومصفوفة الارتباط. وأظهرت النتائج توافقًا قويًا مع نتائج محاكاة مونت كارلو، مما يؤكد فعالية المنهجية المقترحة.

أما المرحلة الثالثة فتركّزت على تحسين موثوقية نظام زوج التروس في ظروف تشغيل قاسية. وتم اعتماد مقاربتين مختلفتين:
(1) تعديل المعلمات الإحصائية للمتغيرات الأكثر تأثيرًا،
(2) تطبيق إطار التصميم الأمثل المتين القائم على الموثوقية(RBRDO) ، باستخدام منهجية التحسين المتسلسل وتقييم الموثوقية (SORA)لتحسين المعلمات التصميمية الحرجة.

وقد أظهرت النتائج توافقًا كبيرًا مع ما ورد في الأدبيات العلمية، مما يدعم صحة وفعالية المنهجية المقترحة.

يساهم هذا البحث في مجال هندسة الموثوقية الميكانيكية من خلال تقديم إطار منهجي متكامل من أجل:
(1) حساب موثوقية الأنظمة،
(2)تحسين تصميم علبة تخفيض السرعة تحت تأثير عدم اليقين.

وتُظهر المنهجية المقترحة تحسنًا ملحوظًا في الكفاءة الحسابية مع الحفاظ على دقة عالية في النتائج.

تم تنفيذ جميع الطرق العددية والتقنيات التحليلية الواردة في هذه الأطروحة باستخدام برنامج.MATLAB

الكلمات المفتاحية: طريقة تقليل الأبعاد(DRM) ، طريقة الموثوقية من الدرجة الأولى(FORM) ، معاملات الحساسية، حدود احتمالية الفشل من الدرجة الأولى، الحدود الضيقة، التصميم الأمثل المتين القائم على الموثوقية(RBRDO) ، موثوقية علبة تخفيض السرعة.

CONTENT TABLE

CHAPTER 4: REDUCTION DIMENSION MODEL FOR SPEED REDUCER SUBSYSTEM RELIABILITY

CHAPTER 5: SYSTEM PROBABILITY OF FAILURE BOUNDS BASED ON DIMENSION REDUCTION MODEL OF A SPEED REDUCER

CHAPTER 6 RELIABILITY BASED ROBUST DESIGN OPTIMIZATION OF A GEAR PAIR

FIGURES LIST

TABLES LIST

SYMBOLS LIST

Roman Symbols

b	Width of the contact face
C	Dynamic load capacity for bearing
C_{lim1}	Dynamic load capacity limit selected from SKF
d_p	Pinion pitch diameter
d_i	Shaft diameter
E_{pi}	Elasticity factors of P_f associated with a parameter *pi*
$E_{\mu i}$	Elasticity factors with respect of means
$E_{\sigma i}$	Elasticity factors with respect of means
E_i	Failure events
F_t	Tangential tooth force at transverse pitch, *N*
F_r	Radial force
F_a	Axial force
F_S	Safety factor
f_s	Safety factor for transmission shaft
$G(X)$	Limit state function
$H(u_i)$	Limit state function in the standard space
I_D	Indicator function of the failure domain
K_A	Work condition factor
$K_{F\alpha}$	Longitudinal load distribution factor
$K_{F\beta}$	Transverse load distribution factor
$K_{H\alpha}$	Longitudinal load distribution factor
$K_{H\beta}$	Transverse load distribution factor
K_V	Dynamic load factor
L_{10}	Bearing Life
L_{10h}	Bearing life for general gears
L_{sh}	Shaft length(space between bearings)
m_n	Normal module
M_b	Shaft bending moment

N Total number of samples

N_i Rotational speed

N_F the number of samples leading to failure

P Power

P_{br} The equivalent dynamic load

pi Parameters of random variables

P_f Probability of failure

P_{f-sys} System Probability of failure

$P_{f\_FORM\_red}$ Reduced model Probability of failure using FORM

$P_{f\_MCS\_or}$ Original model Probability of failure using MCS

$P(E_i)$ failure probability of event E_i

$P(A)$ the probability of the intersection of half-spaces limited by the orthogonal hyper-planes Z_i and Z_j

R Reliability

R_d Resistance at the design point

R_C Capacity

R_T The target reliability

S Stress

S_d Stress at the design point

S_{pi} Sensitivity factors of P_f associated with a parameter *pi*

$S_{\mu i}$ Sensitivity factors with respect of means

$S_{\sigma i}$ Sensitivity factors with respect of standard deviations

S_{yt} Yield strength of shafts material

T_i Transmitted torque

u Transmission rapport

$\boldsymbol{x_{red\_i}}$ The reduced variables

Y_β Helix angle factor

Y_F Tooth form factor

Y_{NT} Life factor

Y_{RrelT} Relative surface condition factor

$Y_{\delta relT}$ Relative sensitive factor

Y_S Dedendum stress concentration factor

Y_{ST}	Experimental gear dedendum stress concentration factor
Y_X	Size factor
Y_ε	Contact ratio factor
Z_β	Helix angle factor
Z_E	Elastic factor
Z_H	Nodal field factor
Z_L	Lubricant factor
Z_{NT}	Life factor
Z_R	Tooth fineness factor
Z_V	Velocity factor
Z_W	Work harden factor
Z_X	Size factor
Z_ε	Contact ratio factor
z_i	Tooth gear numbers

Greek symbols

σ_F	Tooth root stress
σ_{Flim}	Experimental gear bending fatigue strength
σ_{FP}	Permissible bending stress
σ_H	Calculated contact stress
σ_{Hlim}	Experimental flank contact fatigue strength
σ_{HP}	Permissible contact stress
σ_i	Standard deviation of random variables
$\boldsymbol{\sigma_{eq\_i}}$	Standard deviation of equivalent random variables
$\boldsymbol{\sigma_{red\_i}}$	Standard deviation of the reduced random variables
μ_i	Mean value of random variables
$\boldsymbol{\mu_{eq\_i}}$	Mean value of the equivalent random variables
$\boldsymbol{\mu_{red\_i}}$	Mean value of the reduced random variables
α_i	The direction cosines
β	Reliability index
β^T	Target reliability index
$\Phi(-\beta)$	The standard normal distribution function

ρ_{ij}	Correlation vector between events E_i and E_j
θ_{ij}	Angle formed by the vectors normal to the two hyper-planes E_i and E_j
τ_{max}	Maximum shear stress

ABREVIATION

COV	**C**oefficient **O**f **V**ariation
FORM	**F**irst-**O**rder **R**eliability **M**ethod
MCS	**M**onte **C**arlo **S**imulation
MPP(P^*)	**M**ost **P**robable **P**oint
PMA	**P**erformance **M**easure **A**pproach
RBDO	**R**eliability-**B**ased **D**esign **O**ptimization
RBRDO	**R**eliability-**B**ased **R**obust **D**esign **O**ptimization
RIA	**R**eliability **I**ndex **A**pproach
SORA	**S**equential **O**ptimization **A**nd **R**eliability **A**ssessment
SORM	**S**econd-**O**rder **R**eliability **M**ethod
SSR-DRM	**S**tructural **S**ystem **R**eliability-**B**ased **D**imension **R**eduction **M**odel

GENERAL INTRODUCTION

Traditional approaches to mechanical system reliability have predominantly relied on deterministic concepts, particularly the safety factor method. However, as modern mechanical systems grow increasingly efficient and complex, this conventional criterion often proves inadequate to address the multitude of uncertainty sources inherent in real-world applications. These uncertainties include variations in operational loads, material properties, dimensional tolerances, environmental conditions, modeling assumptions, and human factors - all of which can significantly impact system reliability.

To overcome these limitations, modern reliability engineering has adopted probabilistic methods that systematically account for uncertainties in system analysis. These advanced techniques enable more precise performance predictions and informed decision-making throughout the product lifecycle - from initial design to operational deployment and maintenance protocols. Crucially, neglecting proper uncertainty quantification can introduce substantial errors in kinematic and dynamic analyses, highlighting the imperative for comprehensive uncertainty integration in failure mode modeling.

In this context, this study conducts reliability analysis for multi-component mechanical systems, with particular emphasis on speed reducers as a representative case study. The system-level reliability fundamentally depends on the probabilistic behavior of its constituent components, necessitating advanced uncertainty quantification methods. Such probabilistic approaches enable rigorous component-level reliability assessment, which forms the essential basis for accurate system-wide reliability evaluation.

Problematic

The reliability of any mechanical system is intrinsically linked to the performance of its constituent components, making accurate component-level reliability assessment indispensable. This dependency underscores the critical role of probabilistic methods in achieving precise reliability evaluations. However, system reliability analysis presents unique challenges when accounting for component interactions, primarily due to the computational complexity of multidimensional integration.

The reliability analysis becomes increasingly demanding in multi-component systems characterized by numerous random variables. While Dimension Reduction Methods (DRMs)

offer a potential solution by reducing either the number of failure modes or random variables through simplifying assumptions, these approaches present notable limitations. The inherent approximations can lead to compromised accuracy, particularly when dealing with highly nonlinear analytical models or correlated events. Such correlations substantially increase system complexity by influencing variable interactions and complicating analytical solutions.

Furthermore, DRMs often entail significant information loss during dimensionality reduction, potentially jeopardizing structural reliability assessments. The transformation to reduced dimensions also obscures the physical interpretation of equivalent variables, hindering engineers' ability to derive practical insights. These challenges emphasize the need for developing robust methodologies that optimally balance computational efficiency with prediction accuracy in failure probability estimation.

The objectives

The main objective of this thesis is to develop an efficient approach for estimating the reliability of a multi-component system—specifically, a speed reducer—by employing a Dimensionality Reduction Method (DRM). This approach aims to address the complexity of high-dimensional reliability problems involving correlated events, while preserving the variability of the reduced variables. At the same time, it seeks to ensure clear and practical interpretability of the results. By striking this balance, the thesis aspires to contribute a robust and scalable framework for reliability analysis in complex engineering systems. Then, improving the reliability and optimizing the design of the gear reducer, taking into account uncertainties in all model input variables, this goal is carried out in three stages:

Objective 1:

Conventional Dimension Reduction Methods (DRMs) often suffer from accuracy limitations due to their inherent simplifying assumptions, which can compromise reliability estimations. To overcome this challenge, we propose a novel methodology for assessing failure probability in mechanical systems characterized by correlated failure modes and high-dimensional random variables. Our approach, termed the Structural System Reliability-Based Dimension Reduction Method (SSR-DRM), builds upon the First Order Reliability Method (FORM) to develop reduced subsystem models that preserve essential variability while maintaining computational efficiency.

The methodology begins with a reliability-based design framework incorporating three complementary models for each failure mode: (1) a physical model describing stress distributions, (2) a probabilistic model characterizing variable statistics, and (3) a performance model defined through limit state functions. Following the Stress-Strength approach, we employ structural reliability method —specifically FORM—to compute failure probabilities and sensitivity factors, with Monte Carlo Simulation (MCS) serving as the reference benchmark.

A comprehensive comparative analysis is conducted across three model representations for each component failure mode: the original model, the reduced-dimensional model, and the deterministic model, in order to determine which of the latter two can properly reflect the original model.

Objective 2:

This stage evaluates the reliability of the speed reducer system by analyzing reduced-dimensional component models arranged in series configuration. The assessment proceeds through two sequential analytical phases: initial estimation of subsystem and system failure probabilities using first-order bounds (providing the widest possible upper and lower probability limits), followed by refined probability estimation through Ditlevsen's second-order upper bound method (narrow bounds) to achieve greater precision in the reliability assessment.

Within this framework, the First-Order Reliability Method (FORM) computes the sensitivity factors (direction cosines), which subsequently enable construction of the failure mode correlation matrix for the speed reducer. This matrix is then integrated with reliability indices and failure probabilities to calculate second-order failure probability bounds for each subsystem. The system-level reliability bounds are ultimately determined using Ditlevsen's second-order upper bound method, with rigorous validation against Monte Carlo Simulation (MCS) results to verify the accuracy of the proposed approach.

Objective 3

The reliability of the gear pair subsystem is critically analyzed under severe operating conditions that simulate real-world challenges and degrade its performance.

This part of the thesis focuses on enhancing the reliability and optimizing the design of this subsystem. The objective is to achieve a robust design that can withstand uncertainties effectively. A robust design refers to one that exhibits minimal sensitivity to changes in the statistics of input random variables.

Normalized sensitivity, called elasticity factors, are used to compare variables in terms of importance in the model. Based on elasticity factors analysis, the desired reliability and robust design of a cylindrical gear pair are obtained in the following ways:

- ✓ By modifying the mean of the most significant random variables and by reducing the standard deviation or truncating their distribution law.
- ✓ By combining Robust Design Procedures (RDP) and the Reliability-Based Design Optimization method (RBDO), this method is called **R**eliability-**B**ased-**R**obust **D**esign **O**ptimization (RBRDO)**.** The RBRDO employs the decoupled method of Sequential Optimization and Reliability Assessment SORA to calculate the optimum values of critical parameters to achieve the desired reliability and robust design.

Thesis organization

The thesis is composed of six chapters, including an introduction and a conclusion.

The first chapter provides an overview of the fundamental principles of system reliability methods. It synthesizes existing studies that have applied these methods specifically to speed reducer or gearbox systems.

The second chapter focuses on presenting the speed reducer's components along with their corresponding failure modes. The components considered include gears, bearings, and shafts.

The third chapter offers a comprehensive literature review on reliability methods. It covers approximation methods like **FORM** (**F**irst-**O**rder **R**eliability **M**ethod) and SORM (**S**econd- **O**rder **R**eliability Method), as well as simulation methods such as Monte Carlo simulation, along with their mathematical formalisms. Additionally, the chapter presents various approaches for reliability-based design optimization (RBDO), including Sequential Optimization and Reliability Assessment (SORA), Reliability Index Approach (RIA), and Performance Measure Approach (PMA). Finally, this chapter discusses the integration of structural reliability methods in the calculation of the first and second-order system failure

probability bounds.

In the fourth chapter, a Structural System Reliability-Based Dimension Reduction Method (SSR-DRM) is built based on the First Order Reliability Method (FORM) to develop a reduced subsystem model using sensitivity factors and correlation between several failure modes. Both FORM and MCS methods were employed to conduct a comprehensive reliability analysis of speed reducer system components.

In the fifth chapter, the reduction dimension model obtained in the previous chapter is examined to calculate the first and second-order failure probability bounds for each subsystem. Then, the overall system bounds are established utilizing Ditlevsen's second-order upper bound method and compared with the results from Monte Carlo Simulation (MCS) of both the original and reduced dimension models.

In the sixth chapter, critical parameters of variables that exhibit higher elasticity factors have been modified. These modifications aim to enhance reliability and optimize the design of gear pairs. The changes can be implemented by adjusting the statistical parameters of critical parameters or by employing the proposed RBRDO process.

The conclusion of the thesis examines the achieved results and explores potential future directions for this research.

The MATLAB code has been implemented for all the techniques utilized in this thesis.

CHAPTER 1: RELIABILITY ANALYSIS OF GEAR SPEED REDUCERS: A COMPREHENSIVE REVIEW

1.1 Introduction

"Reliability," as defined by ISO 8402, refers to the ability of an element to complete the intended task within the specified operating and environmental conditions for a predetermined period. The word "element" includes components, subsystems, or the entire system. The required function may include mutually dependent operations to get a single work or a specified service.

The system can be analyzed using two main approaches: the functional approach and the structural approach. The functional approach identifies the system based on its functions and breaks it into its essential operating components. However, the structural approach treats the system as a collection of interconnected structural elements or subsystems. A system with multiple failure modes or is made of various structural elements, its reliability is judged on consideration of the reliabilities of the individual components and their potential failure modes.

A speed reducer is a complex multi-component system comprising various elementary components such as bearings, shafts, and gearings. It plays an important role in changing the speed and torque with a defined ratio and can also change the direction of rotation.

To effectively analyze the reliability of a speed reducer, it is essential to model its configuration by examining the arrangement of its components and the standard failure modes. Different reliability approaches are used to develop precise models that evaluate the overall system reliability.

This chapter thoroughly explores the different approaches used to evaluate system reliability and highlights their application to gear reducers. It aims to synthesize these methods while highlighting the advancements they have enabled so far.

1.2 Multi components system reliability techniques

Continuous daily advancements have made Significant progress in system reliability assessment and design techniques. Over time, various methods have emerged, demonstrating their effectiveness in evaluating the reliability of multi-component systems while integrating multiple constraints. This chapter explores two fundamental system reliability concepts, highlighting their importance and applications.

- System reliability methods
- Structural reliability methods

1.2.1 System reliability methods

Various system modeling methodologies have been proposed for reliability analysis.

Rausand and Høyland (2003) provided extensive coverage of the terminology and major models adopted in reliability studies, including analytical methods that form the basis of reliability engineering and reliability data analysis. Likewise, Billinton and Allan (1992) conducted a comprehensive system reliability assessment through probability methods. The authors touched on the concepts and fundamentals of probability theory, statistics, and reliability evaluation, aiming to present a range of theoretical methods and practical applications for quantitative reliability analysis. A classic source for mechanical engineering and gearbox standards reliability, including probability calculation, is Bertsche (2008); the author focused extensively on techniques for assessing reliability in automobiles and mechanical engineering sectors concerning components and systems.

The literature has explored and proposed numerous system-reliability assessment methods, such as fault tree analysis (FTA), reliability block diagrams, Markov chains, and Bayesian networks (BN). Numerous studies have confirmed that these methodologies have significantly impacted gearbox system reliability.

1.2.1.1 Reliability Block Diagram

The reliability block diagram RBD functions as a structural representation that illustrates the logical interconnections among faults within a system. This diagram frequently examines extensive and complex systems that represent network interactions, including series, parallel, or combined configurations (Rausand & Høyland, 2003).

The RBD method is extensively utilized in assessing gearbox system reliability, as evidenced by several relevant studies, a few of which are referenced below.

Abdi et al. (2021) developed a comprehensive reliability model using block diagrams for gearbox systems for two wind turbine drivetrain types. The model evaluates failure and repair rate indices for both configurations.

Zheng (2023) proposed a failure correlation-based technique for estimating the reliability of wind power system gearboxes. The gearbox RBD was created. The results

indicated that failure correlation produced by external dynamic stresses between components can drastically affect gearbox system reliability.

The RBD approach has several advantages. Bryan (2023) states that RBD can be used to examine parallel and series systems. Block diagrams visually represent how system components are connected and how these connections influence overall system reliability. Companies can utilize RBD data to predict manufacturing system performance. They may also locate high-risk production assets within systems. RBD also has other benefits, such as improved communication, a deeper understanding of system reliability, and enhanced decision-making.

Unfortunately, Several deficiencies are associated with RBD analysis. One primary concern is its dependence on precise process data, which affects analytical accuracy. Although RBD accounts for internal human errors and external conditions, a system's performance can still fail for different reasons. Furthermore, RBD requires detailed explanations of component failures and their impact on overall system reliability.

These limitations highlight the need for alternative methods for more accurate system reliability analysis.

1.2.1.2 Fault Tree Analysis (FTA)

According to the SAE ARP4761 Standard, Fault Tree Analysis (FTA) is a deductive failure analysis method used to examine a specific undesired event. It provides a systematic approach to identifying the causes of such an event. FTA follows a 'top-down' assessment approach involving a qualitative analysis of an undesirable occurrence and its evaluation.

Loc (2021) conducted a reliability analysis using the FTA for single- and double-stage reducers. Additionally, the study explored probabilistic design methods and a sensitivity analysis during the design phase. According to Calderon-Salmeron et al. (2023), tribological reliability parameters are key in determining potential cost savings. An improved Fault Tree Analysis (FTA) incorporating tribological failure rate links was used to assess the reliability of a gearbox.

A key advantage of Fault Tree Analysis (FTA) is its ability to model complex system configurations using simple and comprehensible Boolean logic (Liang et al., 2022). FTA provides unique insight into a system's operation and potential failures, allowing for the consideration of undesirable events caused by software failures and human errors during system operation and maintenance. Moreover, FTA accounts for environmental influences on

the system, ensuring a more comprehensive assessment of its reliability.

Several disadvantages of using FTA to represent system inoperability have been highlighted by Tchangani and Pérès (2020). These include neglecting physical interactions between components, assuming independent component operation, and defining components in a binary state (normal or faulty) despite the possibility of intermediate states such as functional degradation. Additionally, FTA struggles to incorporate numerical indicators of overall system health instead of individual component health and often disregards external influences. According to Wu et al. (2011), the limitations of fault trees include the need for prior knowledge of basic event probabilities, challenges in automating quantitative analysis, and difficulties in identifying weak links within the system.

According to Shafiee et al. (2019), FTA is a static approach that cannot effectively analyze multiple failures. It is also unintuitive and fails to account for dynamic interactions between components. Additionally, several other limitations hinder FTA's ability to simulate complex dynamic systems.

1.2.1.3 Failure Modes Effects and Analysis (FMEA)

Failure Modes and Effects Analysis (FMEA) is a systematic approach to identifying potential failure modes for each system component or function, determining their causes and effects, and assigning corresponding severity, occurrence, and detection ratings.

The primary objective of FMEA is to eliminate, reduce, or mitigate the impact of the failure modes deemed most critical.

FMEA can include FMECA (Failure Modes, Effects, and Criticality Analysis). According to the Standard (MIL-STD), FMECA is a reliability evaluation and design technique that identifies potential failure modes within a system and its equipment to assess their impact on the system and equipment performance. Each failure mode is classified based on its effect on mission success and the safety of personnel and equipment. Another extension of FMEA is the HAZOP (Hazard and Operability) study. These approaches have a wide range of applications in reliability engineering, aiming to maximize the reliability and performance of various systems, including gearbox systems.

Tazi et al. (2017) developed a hybrid cost-FMEA to assess criticality by incorporating cost considerations. A subsequent quantitative comparison analysis determines the average failure rate, the significant causes of failure, estimated failure costs, and failure detection methods. The FMEA also illustrates how each component impacts the gearbox and wind

turbine systems. Hoogeveen and Mao (2022) conducted an FMEA to identify the gearbox components requiring the most attention and those most likely to fail. The analysis revealed the need for a detailed examination, digital testing, and verification of the gears and planetary gear system to enhance their strength and durability.

According to Christiansen (2023), the FMEA process reduces the probability of failure in an operational environment by maintaining reliability during manufacturing, ensuring product quality, and enhancing process safety. This improves customer satisfaction and helps lower operational costs by preventing unexpected breakdowns.

FMEA also has certain limitations: it requires a significant investment of time and resources, and the analysis can be influenced by the team's experience and skills, which may introduce biases. Incorrect assumptions, the omission of specific failure modes, or the use of outdated data can compromise the accuracy of the evaluation. Peeters et al. (2018) note that FMEA adopts a bottom-up approach, which is less formalized and more guided by expertise than FTA. Due to time constraints, these two methods are rarely applied comprehensively.

Moreover, traditional FMEA has certain limitations that require solutions. These include managing imprecise failure data, integrating expert opinions, lacking weighting for risk parameters, and neglecting the conditionality of failure events (Yucesan et al., 2021). Additional challenges must be addressed to enhance FMEA for more effective risk assessment and mitigation.

1.2.1.4 Markov model

The quantitative Markov (MC) model analysis is practical for systems with complex maintenance strategies and interdependent components. A Markov process is a mathematical model that describes the evolution of a system over time, where the future state depends only on the current state and not on past states. This property, known as the memory-less property of a stochastic process, simplifies the analysis of system behavior by focusing solely on present conditions. As a result, Markov models are widely used in reliability assessment, maintenance optimization, and performance evaluation of engineering systems.

Li et al. (2017) used two Markov reliability models to assess offshore wind turbine gearbox failure rates, availability, and failure times in multi-state degraded systems. A comparison of the computed results with European wind farm failure data validated their findings. Gu et al. (2020) collected vertical vibration data from normal, worn, and fractured teeth of a gearbox in a vibration experiment to monitor and understand gearbox function. They also proposed an online diagnostic and performance evaluation model integrating a Hidden

Markov Model (HMM) and fuzzy comprehensive evaluation. Their results demonstrated that the proposed performance evaluation method performed satisfactorily.

Jia et al. (2024) present a fault detection diagnosis scheme for harmonic reducers under practical operating conditions. The Hidden Markov Model (HMM) represents the dynamic rules, extracting new features related to state transition probability and observation probability to establish the mapping relationship between external excitations and monitoring signals.

Markov models offer several benefits for system reliability analysis. Markov analysis allows for formula-based estimation of system reliability parameters, providing fast, precise, and efficient outcomes (Amanda, 2016).

However, Markov chains have certain drawbacks. Kabir and Papadopoulos (2019) noted that Markov chains (MC) are limited to exponential distributions, meaning they can only simulate systems with exponentially distributed lifespans, which may be too restrictive for complex systems. Liang et al. (2022) highlighted that a key limitation of the Markov model is the exponential growth of states as more components and factors are added to the system.

Classical Markov chain analysis requires accurate knowledge of all probabilities or rates within the Markov model, which can be a significant challenge. Markov analysis relies heavily on the modeler's expertise and judgment to determine parameters.

1.2.1.5 Bayesian Network

A Bayesian Network (BN) is a directed acyclic graph that uses Bayesian techniques to compute the probability of occurrence of events the node represents. Each node is associated with a probability function that takes a specific set of values from the node's parent variables and provides the probability for the variable represented by the node.

In reliability engineering, Bayesian network techniques are employed in gear transmission system analyses:

Elusakin and Shafiee (2022) developed a dynamic Bayesian Network (DBN) framework for offshore wind turbine gearbox fault detection and reliability analysis. The framework estimates the reliability, availability, and MTBF of each subassembly. The results indicated that gearbox system failures are most often caused by bearing subassembly failures.

Bayesian networks are an excellent methodology for updating probabilities and learning sequentially in risk analysis due to their dependence on the events they represent.

According to Singh et al. (2022), BNs are flexible with various probability

distributions and, therefore, are recommended for modeling uncertainties. Another advantage is the control over the dependencies of events when evidence is incorporated, which further enhances learning in Bayesian networks.

In practice, Bayesian networks have significant limitations in their application to system reliability analysis. Some major drawbacks include the high computational resource demands and the complexity of managing probabilities when developing Bayesian network models for systems with numerous parameters. Another challenge is the necessity for accurate data to estimate probabilities and their interrelationships within Bayesian networks. This requires handling large datasets, which can be a potential constraint. Furthermore, the practical application of Bayesian networks for reliability analysis demands substantial knowledge of probability and statistics. Additionally, implementing Bayesian learning can be expensive and resource-intensive.

1.2.2 Structural Reliability Methods (SRM)

Structural reliability methods (SRM) assess failures in engineering structures. They account for various uncertainties, such as material properties, loads, and environmental conditions. SRM helps estimate failure probabilities using statistical or probabilistic models. It allows engineers to quantify risks and optimize structural safety designs, balancing cost and performance.

The most important contribution of structural reliability methods to system reliability analysis is the reliability-based design and calibration of safety factors within design codes. Overall, methods to measure the reliability of a structure can generally be divided into five categories (Lemaire et al., 2009; Madsen et al., 2006). While the general concept remains consistent, classifications vary among authors. We have adopted the following classification:

1. **Level 0:** Represents deterministic approach.
2. **Level I**: Semi-probabilistic methods.
3. **Level II:** Partial application of probabilistic techniques.
4. **Level III**: Fully probabilistic method.
5. **Level IV:** Uses cost as the optimization criterion

1.2.2.1 Level 0: The deterministic approach of reliability

In the deterministic approach to reliability, it is assumed that there is no uncertainty in the design variables and modeling parameters. This approach was used in traditional design methods, where the system is oversized by a safety factor, which indicates security. While this method ensures system safety, it often results in an overly large and inefficient design.

A. Safety Factor concept

Safety is a critical concept in mechanics and the design process of mechanical engineering. It significantly influences various design aspects, such as geometry, dimensions, and material selection. However, it is often an ill-defined quantity in practice. In the 1860s, A. Wohler, a German railroad engineer, proposed a safety factor of two for tension. The term 'factor of safety' began to be widely used in the early 1880s. Generally, the safety factor is the ratio between the maximum load that does not cause failure and the corresponding applied load (Randall, 1976). Various norms and standards exist, and design criteria are based on applying safety factors.

B. Parameters in the selection of a safety factor

Ideally, excellent engineering judgment, based on information and experience, should guide the balancing of safety factors. The design engineer uses engineering analysis and judgment to set the safety factor. According to Musto (Musto, 2010), this judgment is based on:

- ✓ Knowledge of uncertainties related to materials, manufacturing techniques, and the analysis used to determine part dimensions.
- ✓ Understanding of the product's usage and maintenance during its service life.
- ✓ Potential risks and costs associated with possible product failure during service.
- ✓ Relevant standards and codes for the specific industry.
- ✓ Contractual obligation to customers.

The structure safety factor (overall factor), Fs, is traditionally expressed as the ratio of the breaking strength (capacity) Rc to the applied stress S:

$$F_S = \frac{R_C}{S} \tag{1.1}$$

Several analyses of gearbox systems and deterministic design investigations have been conducted on safety factors and deterministic approaches to reliability.

Kissling and Stangl (2017) converted component safety factors into failure probabilities based on the Weibull distribution. This procedure applies to ISO, DIN, and AGMA standard computations. Reliability can also be determined at the system level, identifying the weakest parts of a gear unit.

Beermann (2018) explores alternative methodologies and the relationship between safety factors and gearbox system reliability calculations. To meet the required criteria, the safety factor must exceed the 'required safety factor''. Two common approaches define this criterion: the minimum necessary safety factor for a given lifespan or the minimum probability of achieving the expected lifetime. The built-in reliability coefficients of ISO 281 (2007) and AGMA 2001-D04 (2001) are compared with Bertsche's (2008) generic method. The application of Bertsche's approach yields reasonable results.

Rupesh et al. (2017) investigated bending and wear safety factors by computing bending and wear stresses using ANSI/AGMA (2001) and finite element techniques. They compared analytical safety factors with those obtained from ANSYS simulations. The results demonstrated that the bending and wear safety factors estimated through analytical and finite element methods were nearly identical.

Santana et al. (2024) examined a two-stage gearbox with a 10:1 gear ratio designed to reduce output speed and enhance motor torque for safe and easy maintenance. Gearbox design parameters were computed using Excel and simulated in Solid Works. The pinion, gear, and material validation safety factors confirmed the accuracy of the gear analysis. (Hristovska, 2024) proposed a method for evaluating safety by incorporating safety factors, operating data, load capacity, and applied loads. Three different methods were employed to analyze a reducer under specific operating conditions. Based on their findings, the results apply to similar reducers operating under comparable conditions, and the proposed method can effectively assess the safety of dynamically loaded gear reducers. Traditionally, a safety factor has been used to account for unknowns. However, historical safety factor trends may not reliably predict future requirements, especially in rapidly evolving technologies and environments. Over-engineering due to an excessively high safety factor can lead to increased costs, added weight, and design inefficiencies. Conversely, an overly low safety factor may compromise system safety and reliability. Therefore, determining an appropriate safety factor is crucial to achieving optimal design functionality, maximizing reliability, and ensuring cost-effectiveness.

1.2.2.2 Level I: called the semi-probabilistic method

In semi-probabilistic methods, a representative value incorporates a certain degree of statistical significance into the applied load or stress within design rules. These rules also include partial safety coefficients, which account for uncertainties in material properties, loading conditions, and structural behavior. This approach is widely used, particularly in code

calibration—a specialized process by an authoritative body (such as a code committee). Code calibration involves employing advanced methods to assign values to the variables within the code format, ensuring a specific design code is formulated. The key variables in a partial safety factor-based code format include characteristic values, partial safety coefficients, and load reduction factors (Cremona et al., 2013).

A. Design Codes Assessment Approaches

Standards, norms, and regulations serve to standardize engineering constructions through design codes. Each design code methodology addresses specific technological challenges and adheres to established standards to ensure structural reliability, safety, and performance (Baravalle, 2017). These rules ensure engineering process regularity, reliability, and safety.

- **Level 4 involves a risk-informed approach.** In this approach, decisions are made based on a full risk analysis, where all potential hazards and uncertainties are evaluated and considered. This approach integrates both the probability of failure and the consequences of failure, aiming for optimal safety without overdesign. According to International standard ISO 2394 (1998), safety and reliability are integral to the design process, where the goal is to manage risks effectively while ensuring the design's structural integrity.

- **Levels 3 and 2 are reliability-based method**s. Probabilistic models are often used in reliability-based design and assessment, which help design structures that can perform reliably under uncertain conditions. Failure consequences and damage potential are critical factors that help simplify or refine the design process. The Joint Committee on Structural Safety JCSS (2001) is a recognized authority that sets standards for structural reliability, focusing on modeling standards that incorporate safety factors and reliability assessments into the design process.

- **Level 1 or semi-probabilistic approach** combines elements of both deterministic and probabilistic methods. It offers a simplified version of the more complex reliability-based designs (Level 2), allowing for more straightforward implementation in situations where uncertainties are less critical or well understood. Eurocode (2002) play a significant role in this approach, providing standardized guidelines for representing uncertainties and categorizing failure modes. These codes allow for the consistent application of semi-probabilistic methods, making it easier to assess structural safety by focusing on categorized failure modes and the consequences of those failures.

B. Partial Safety Factors

In the design process, partial safety factors are used for loads subjected to uncertainty or strengths concerning their uncertainties. The resistances and stresses are analyzed using those partial safety factors, which can be calculated from the mean values μ_R and μ_S:

$$R_d = \frac{\mu_R}{\gamma_R} \tag{1.2}$$

$$S_d = \gamma_S . \mu_S \tag{1.3}$$

γ_R and γ_S are the partial resistance and stress safety factors, respectively.

To verify the security of any structure, the following relation must therefore be satisfied:

$$R_d \geq S_d \tag{1.4}$$

C. Code objective

The common objective of a design code should be to ensure that structures designed under it meet the required safety standards. Many codes aim to establish a clear objective: determining the target reliability index, $\boldsymbol{\beta^T}$. This safety target can be defined for specific structures, components, and/or limit states. The optimal value of $\boldsymbol{\beta^T}$ depends on the expected costs associated with failure and the costs of upgrading, such as increasing the safety margin (Andrzej & Lind, 1995).

D. The calibration techniques

Calibration techniques are generally categorized into global methods and approximate methods. The Global Optimization Method (GOM) aims to determine the most accurate partial safety factors; however, it requires a relatively large number of reliability analyses to achieve optimal results. In contrast, approximate methods can provide reasonable results with fewer reliability analyses. The choice between GOM and approximate methods depends on the complexity of the mechanical model and the computational time required for each reliability analysis (Gayton, 2004). While calibration techniques have been widely applied in engineering, particularly in the design process, there are limited studies that apply partial safety factors, specifically in gearbox reliability analysis.

The Norwegian classification society Det Norske Veritas DNV (2012) has developed standards for the marine and electrical sectors, such as the classification note CN 41.2-DNV-GL. The society uses ISO 6336 Parts 1-5 to estimate gears' fatigue life. ISO/TR 13989 calculates seizure safety factors, while ISO 53 applies to cylindrical gears, and ISO 23509 pertains to bevel gears. These standards help develop guidelines to protect life, property, and the environment through proper gear design and reliability assessment.

Grączewski and Ligaj (2015) presented the ISO 6336 standard and CN 41.2-DNVGL rules for calculating cylindrical toothed gears in ships and oil rigs.

Keller (2017) redefined gearbox designs to enhance load-sharing characteristics, thereby improving fatigue life prediction.

When working within the semi-probabilistic framework for defining safety factors, ambiguity can arise regarding including various sources of uncertainty. It is important to note that partial safety factors do not account for all uncertainties. Large partial safety factors may be applied when significant uncertainty is present. However, excessive rigor in design can lead to overly conservative safety margins, undermining efficiency and cost-effectiveness. Achieving a well-balanced compromise in determining safety factors is crucial for ensuring both the reliability of the design and its competitiveness.

1.2.2.3 Level II: Partial application of the probabilistic method

These approaches employ an approximate probability-based limit state function and incorporate statistical parameters for each uncertain variable, typically the mean and variance. Additionally, they include a measure of the interaction between the parameters, usually represented by the covariance.

A. Uncertainty representation

According to Zhang and Mahadevan (2000), uncertainty in engineering analysis arises from three sources:

1. ***Physical uncertainty,*** or inherent variability, is typically measured by a probability distribution derived from observed data;

2. ***Statistical uncertainty,*** which refers to uncertainty in the statistical distribution parameters of random variables encountered in the first source, often due to a lack of sufficient data;

3. ***Modeling uncertainty***, which includes uncertainties in both probabilistic and mechanical models.

Numerous comprehensive evaluations, such as those by Helton and Davis (2003) and Helton (1994), maintain a distinction between two classifications of uncertainty:

Stochastic uncertainty arises from the system under examination exhibiting several potential behaviors, and ***subjective uncertainty*** arises from insufficient information regarding quantities presumed to possess fixed values in a specific analysis. Consequently, ***stochastic***

uncertainty pertains to the system being examined, whereas ***subjective uncertainty*** relates to the analysis and the analysts involved.

Other alternative terminology includes aleatory, variability, irreducible, and "type A" as substitutes for the word stochastic, and epistemic, state of knowledge, reducible, and "type B" as substitutes for the term subjective.

B. Techniques of partial application of the probabilistic approach

This approach involves the theoretical application of uncertainty to reliability analysis and reliability-based design optimization (RBDO). Uncertain conditions are incorporated to apply various techniques to assess system reliability, including probabilistic modeling, sensitivity analysis, and failure probability estimation. Various techniques employed for reliability analysis include:

1) ***First-order Second Moment (FOSM) Method***: The FOSM method, often referred to as the Mean Value First-Order Second Moment (MVFOSM), assumes that the limit-state function can be approximated by a first-order Taylor series expansion at the mean point.

2) ***First-Order Reliability Methods (FORM):*** In the FORM techniques, the limit state function (failure function) is linearized, and the reliability is evaluated using Level II or Level III methods.

3) ***Second-order Reliability Methods (SORM):*** In SORM methods, a quadratic approximation of the failure function is derived, and the probability of failure for the quadratic failure surface is estimated.

Chapter 3 provides further details on these methods. The techniques discussed above are applied to analyze the reliability of the gear-reducer system.

In Hu et al. (2015), a method is developed for the intelligent reliability analysis of spur gear contact fatigue under electrohydrodynamic lubrication. The approach employs Hertz contact zones, quadratic polynomials, artificial neural networks, genetic algorithms, and advanced first-order second moment (AFOSM) methods to estimate oil film pressure and design parameters.

Loc (2021) proposes a reliability-based approach for mechanical transmission systems using moment-matching methods (MMM), FORM, and Monte Carlo Simulation (MCS), along with Reliability-Based Analysis And Design Of The Mechanical Systems (RADME) computer programs and post-design sensitivity analysis techniques to address the reliability design problem.

Pei, J. et al. (2021) estimate the probability of lubricant failure in gears in real-time using gear stochastic dynamics and an electro hydrodynamic reliability model based on the FOSM technique. Wang. J et al. (2022) compute reliability using the Regional Equivalent Conversion Index (RECI) for each limit state function boundary and sub domain. The proposed method also calculates the parallel linear performance function RECI. Additionally, reliability is precisely calculated using the (AFOSM) method, and RECI-reliability mapping is performed. The impact of relative errors in sample parameters is analyzed to determine the optimal value.

In Fan et al. (2024), an enhanced version of the FORM and SORM is proposed to balance accuracy and efficiency. First, an improved modified symmetric method for FORM iterations eliminates the need for a line search approach to determine step length. At the same time, an adaptive Kriging model with rational update criteria enhances FORM efficiency. Second, since the adaptive Kriging model provides high accuracy at the final design point, a more efficient SORM is introduced, maintaining the same efficiency level as the improved FORM.

Radoń and Zabojszcza (2025) emphasize the importance of structural reliability and sensitivity analysis in design. They compute failure probability and perform global sensitivity analysis, which can be effectively integrated into routine design practice. Two probabilistic design methods are employed: the FORM, SORM, and MCS.

Lobato et al. (2025) analyzed the reliability of a flexible-link manipulator subjected to uncertain parameters using direct FORM, SORM, and RIA. They addressed a reliability-based design challenge through multi-objective optimization, applying the multi-objective optimization differential evolution algorithm to SORM and RIA.

Deep Neural Network-based FORM and SORM recently found many practices in SRA. Malakzadeh and Daei (2020) propose a hybrid FORM-sampling simulation to reduce time expenses in structural analysis, such as reliability index, design point, and important vector computation. The procedure is based on important sampling combined with stepwise standard deviation correction of variables correlated with the sampling density function to analyze structural reliability with a few random samples. Moreover, Artificial Neural Networks ANN have relatively efficiently simulated limit state function, reducing computation time remarkably.

Widely known analytical approximation methods, such as FORM and SORM, are extensively used by engineers because they offer a good compromise between accuracy and efficiency for realistic problems. However, these methods can produce inaccurate results when applied to highly nonlinear systems. Moreover, reliability calculations generally require the evaluation of the gradients of the limit state function, which complicates the computation of the reliability index, especially when the limit state functions are highly complex.

Reliability-Based Design Optimization (RBDO) integrates structural reliability analysis into the design optimization process to ensure performance under uncertainty. Its goal is to minimize cost, weight, or other objectives while ensuring the probability of failure remains below an acceptable threshold. In RBDO, the objective function and probabilistic constraint specifications capture both the deterministic and stochastic aspects of the design and constraint problems. Probabilistic constraints are used to define the required reliability level for the overall system. Several methods have been developed to solve RBDO problems, including the following:

- ***The Performance Measure Approach (PMA)*** facilitates efficient evaluation of constraint violations. In this approach, the performance measure is determined by solving inverse reliability problems (Tu & Choi, 1999).

- ***Reliability Index Approach (RIA)***: This approach incorporates the FORM approximation for reliability analysis. This method highlights the efficiency of the double loop using FORM, where Lee and Kwak (1995) used Neumann expansion to solve the structural problem.

- Du and Chen (2004) developed **sequential optimization and reliability assessment (SORA)**. This method reformulates the RBDO problem as a series of deterministic optimization sub-problems. An inverse reliability analysis is performed after achieving the final optimized design through deterministic optimization. SORA significantly improves computational efficiency by decoupling the RBDO problem into a sequential process involving deterministic optimization and reliability analysis, effectively forming a single-loop approach.

- ***Reliability-Based Robust Design Optimization (RBRDO)*** is an extension of RBDO that explicitly considers uncertainties in the design optimization process. The primary goal of RBRDO is to develop more robust designs that are less sensitive to variations in input parameters. By incorporating the probabilistic nature of uncertainties, RBRDO helps engineers and designers make better-informed decisions, leading to systems or products that

are both more robust and more reliable.

Much research has been conducted on probabilistic design optimization for gearboxes. RBDO methods have found widespread application in the design of robust gearbox components. The following sections present a synthesized overview of the reported studies in this area, highlighting the improvements and insights gained from these research efforts.

Yang et al. (2013) developed evidence-based design optimization (EBDO) for planetary gear reducer designs subjected to two uncertainties. They applied the FORM to evaluate performance function reliability.

Huang et al. (2013) developed an enhanced version of the SORA method, called Enlarged SORA (ESORA), which can handle random design variable variances that remain constant or change over time. Their method achieves superior computational performance while maintaining the usability of the original SORA methodology. ESORA's effectiveness was mathematically validated and confirmed through its application to the design of a speed reducer.

He et al. (2017) used a speed reducer model that accounts for manufacturing process faults to evaluate an uncertainty-based multidisciplinary optimization technique for RBRDO. The results demonstrate the approach's feasibility and efficacy.

Li et al. (2016) also explored Multidisciplinary Robust Design Optimization (MRDO) under multidimensional uncertainties, utilizing uniform and normal random uncertainty distributions. They developed mathematical models for multidimensional uncertainty quantification and applied them to speed reducer and bulk carrier optimization as case studies.

In 2018, Chen et al. (2018) introduced a SORA-based method for developing a Probabilistic Feasible Region (PFR) to enhance efficiency. The iteration of the PFR refines and expands the probabilistic feasible zone without additional computations. The computational performance of the PFR is compared with that of SORA when applying a speed-reducer design. In the same year, Yang et al. (2018) proposed a method for Reliability-Based Optimal Design (RBOD), which implements a simultaneous design and calibration procedure based on a local domain approach. This method treats the unknown design parameters as calibration parameters and optimizes them within local domains while adhering to reliability constraints. The best values are determined using a programmable transmission shaft optimization model.

In 2019, Zaman (2019) proposed a modified probabilistic speed reducer ultimate strength and strain probabilistic design method. They demonstrate a standard decoupled RBDO method.

The same year, Chen et al. (2019) introduced a Markov Decision Process (MDP) framework to enhance design-point-based RBDO procedures. The MDP generates SORA shifting vectors by tracing the design points from previous reliability analysis iterations. When multiple design points exist, the probabilistic constraints are adjusted to better align with the feasible design space. A speed reducer model was used to evaluate the MDP approach, demonstrating its ability to overcome challenges associated with multiple design point issues.

Liu et al. (2021) conducted an RBDO study focused on gear transmissions. They estimated dynamic fatigue reliability sensitivity to identify optimal structural parameters. The gear transmission's dynamic fatigue reliability was evaluated using the stress-strength interference theory, providing a basis for earlier and more efficient design iterations. This approach enables volume reduction while maintaining fatigue reliability.

Several Machine Learning (ML) techniques have been applied to RBDO in recent years, leading to significant systematic advancements. Zhang et al. (2024) discussed using instance-based transfer learning in RBDO to eliminate the need for repeated reliability analyses, where the source domain remains fixed while the target domain is continuously updated throughout the optimization process.

Ebrahimi and Bataleblu (2024) presented a systematic survey of past developments and future trends in RBDO. The study highlights a range of methodologies aimed at enhancing performance, including Cross-Entropy (CE) methods, uncertainty-based design optimization, and their integration with machine learning. Additionally, it identifies emerging trends, such as digitalization and model-based systems engineering, which increasingly influence the evolution of RBDO practices.

RBDO helps to maximize designs by quantifying uncertainty using probabilistic constraints. It makes design optimization more realistic and strict, producing more consistent technical solutions. A primary challenge of RBDO is the recurring dependability analysis problem solution in every iteration. This iterative process might be time-consuming for advanced mathematical models or computationally expensive simulations. RBDO optimization requires more time as reliability analysis is usually the main computational restriction. Still, another RBDO challenge is gradient computation for probabilistic constraints. Improving RBDO approaches depends on reducing these flaws and finding

effective computation techniques.

Goswami et al. (2019) noted that the Reliability Index Approach (RIA) is unstable and sluggish to converge. In addition, very nonlinear probabilistic restrictions might reduce the optimality of RIA outcomes. Probabilistic Optimization with Multiple Approaches (PMA) solves a more complex optimization problem with fewer constraints. Thus, PMA is more stable than RIA. PMA involves solving many inverse reliability analysis problems, which is computationally expensive. Finding the best strategy for a problem requires balancing stability and computing efficiency. SORA trades computational performance for reliability estimate accuracy. It may help when computing resources are limited and reliability evaluation and design optimization must be balanced. The shift vector's dimensionality increases with the number of design variables, so SORA is limited to academic problems. The shift vector is also built using the Hasofer-Lind reliability index, which may be inaccurate in some cases.

1.2.2.4 Level III is called the fully probabilistic method

The most accurate reliability analysis approach, Level III, models design uncertainties using joint distribution functions. Failure probability is computed using the probability integral. Many textbooks describe these reliability analysis methodologies. The reliability analysis calculates system reliability using all conceivable failure mechanisms. Level-III approaches include:

- **Analytical Integration (AI)** Analytical integration is only suitable if the failure surface is simple and a few design factors are involved.

For example, if the failure function,

$$G(x)=R-S \tag{1.5}$$

With stress S and the resistance R

The failure probability will be calculated as the probability distribution function.

$$P_f = Prob[G(X) \leq 0] = \int \dots \int_{G(X)\leq 0} f_x(d,x)dx \tag{1.6}$$

Nevertheless, analytical integration is not feasible in practice due to complex distributions, complicated limit state functions, several fundamental variables, and a very complicated failure surface.

- **Numerical Integration (NI):** Analytical integration cannot always be performed; hence, numerical integration is used to evaluate the probability of failure P_f in such cases. For this purpose, all the basic random variables in the original space were

transformed into the independent standard normal distributed variables. Then, the integration was numerically accomplished according to Eq. (1.6). Thus, numerical integration can only be performed at moderate numbers of random variables, e.g., up to a maximum of n=10. Beyond this, computing time increases astronomically and becomes hardly manageable for high-dimensional problems. In most applications, this method is used as complementary validation for other methods with few variables.

Zhang et al. (2018) calculated dynamic reliability using the Gauss-Legendre quadrature. A Gauss-Legendre numerical integration tool accurately transforms the integral into the sum of polynomials. The case study concerns the reliability of three-stage spur gear reducer contact fatigue under varied situations. We compare the accuracy of the suggested method against MCS. Results show that the suggested strategy is feasible.

- **Monte Carlo Simulation (MCS):** Analytical and numerical integrations are inefficient owing to challenging failure circumstances and time-consuming calculations. This limitation may be avoided using MCS, which is always viable. MCS is a straightforward approach for predicting P_f by simulating many variable X realizations x. Failure probability is the ratio of failures to samples. This approach is briefly discussed in Chapter 3.

Gao et al. (2018) modeled planetary gear system random longevity and dynamic dependability. Failure dependency and dynamic random load redistributions are models. MCS verifies models. System functioning reveals load distribution unpredictability. External load dispersion affects planetary gear systems' reliability, longevity, and redundancy. At the system level, Zheng (2023) calculated time-varying reliability linked to failure correlation for major gearbox components (gear and bearing) using a complete probability differential technique and stress strength interference theory. MCS confirmed the findings. The failure correlation caused by external dynamic loads between components may severely impact gearbox system reliability.

The fully probabilistic approach has a distinct disadvantage: it is pretty obscure and requires thorough knowledge of probability, rendering it impractical for many engineers. Also, a fully probabilistic approach usually requires a lot of computation power and resources since it is mainly based on countless repeated analyses, especially for large structures with a very low probability of failure.

Monte Carlo Simulation (MCS) is a standard sampling system employed in reliability analysis. Its downfall is the time and resources exhausted in performing a large number of

iterations. This may become a challenge for engineers in terms of costs and computational efficiency. Thus, it is pivotal that the reliability analysis method selected for a certain engineering problem balances accuracy and computational feasibility.

1.2.2.5 Level IV Methods use cost as the optimization criterion: An acceptable design maximizes the utility function (benefits minus costs). The aforementioned methods apply to economically important structures, apply the principles of engineering economic analysis under uncertainty, and consider costs and benefits, including construction, maintenance, repair, consequences of failure, interest on capital, etc. Level IV designs are suitable for extremely sensitive projects like nuclear power projects, transmission towers, and highway bridges.

Only a limited number of studies address time-dependent reliability calculations, and these work only with simplifying assumptions.

Singh et al. (2009) introduced a linear and nonlinear Cumulative Probability of Failure method. The roller clutch design study found that lowering failure probability over time lowers lifetime cost. Higher longevity cost due to initial quality does not guarantee reliability. Li et al. (2012) maximize preventive maintenance time by improving system reliability to reduce lifetime costs. The lifecycle cost includes production, inspection, and projected variables. All pricing depends on quality/reliability. Whenever increased reliability falls below an acceptable level, preventative maintenance is done. The approach determines the most critical components or failure modes that, if fixed, would improve system reliability.

Reliability-based design with longevity cost has received little attention because of the complexity and computing effort necessary to determine time-dependent reliability. Few studies use lifetime cost in reliability, maintenance, and warranty design.

Clark et al. (2022) developed reliability-based, computationally efficient layout optimization techniques. Wind conditions may be used to calculate globe gearbox bearing life, and failure cost and power production models can be used to set reliability objectives. Results indicate that a reliability-power production multi-objective function minimizes failure costs without reducing power output.

1.2.3 Dimension Reduction Methods (DRM) and its applicability in structural system reliability

Dimension Reduction Methods (DRM) play a crucial role in enhancing the analysis of structural system reliability by simplifying complex datasets while retaining essential

information. In structural system reliability, DRM further simplifies complex probabilistic models by reducing the number of random variables while retaining essential uncertainty attributes.

Rahman and Xu (2004) proposed that univariate DRM assists in calculating statistical moments of mechanical system responses in the presence of uncertainties in geometry, material properties, and loads. It makes calculations more efficient while maintaining accuracy by dividing complex problems into one-dimensional functions and simplifying them. However, this method may not be sufficient in systems with considerable random variation and/or non-linearity owing to residual error integrations of two or more dimensions. Xu and Rahman (2004) present a new, generalized DRM for predicting the second-moment characteristics of mechanical systems' response.

1.2.3.1 Main Techniques used in Dimension Reduction Methods

The main Techniques used in DRM are:

1. ***Principal Component Analysis (PCA):*** Especially in structural reliability contexts, PCA is considered one of the most popular DRM. It aims to transform correlated variables into a smaller set of uncorrelated variables called principal components. This is done by finding the directions (or components) in which the data varies the most. The first principal component will capture the most significant variance; the second will capture the second greatest, and so on. In the case of structural reliability, such simplification of input variables like material properties, load, or environment of interest could all be included in the model to keep the engineer focused on the most important aspects affecting reliability. More details about this method are found in Jolliffe (2002).

2. ***Independent Component Analysis (ICA):*** ICA is less commonly used in structural reliability and more typical in signal processing, fault detection, or health monitoring of structures (e.g., vibration signal analysis). Unlike PCA, the ICA identifies statistically independent components, which seeks to maximize variance. This technique proves helpful when the data contains mixed components that require separation for analysis. Therefore, the basics of ICA are provided in Tharwat (2021) to show how this method works and serve as a comprehensive source for researchers interested in this field.

3. ***Singular Value Decomposition (SVD):*** This technique is more concerned with model order reduction or solving linear systems than directly utilizing structural reliability frameworks. SVD is the cornerstone of matrix decomposition and numerical linear algebra. The technique can be used for dimension reduction by expressing a

matrix in terms of its components. It is usually employed together with PCA for efficiently extracting the principal components. Wall et al. (2003) discuss gene expression analysis using Singular Value Decomposition (SVD) with stress on the data's preliminary characterization.

Lee and Choi (2010) employ the most probable point (MPP)--based DRM to estimate the risk of failure in a series system. The study includes design sensitivity analysis for system RBDO. MCS and finite difference approaches agree well with the results.

Park (2023) proposed an efficiency and accuracy method based on SORM, DRM, and sampling-based RBDO. First, an improved convolution integration method is proposed to make accurate improvements in the general form of SORM to enhance efficiency in novel SORM. Second, for improving accuracy in existing univariate DRM, a method called 'Selectively Extending to Bivariate Dimension' by the statistical model selection method is also proposed.

Zhang. Y et al. (2025) proposed an advanced adaptive Kriging-based candidate sample reduction strategy (AK-CSR) approach to improve rare event reliability analysis of complex structures. The updated Kriging model and increased first-order reliability approach may identify the probable failure area.

1.2.3.2 Dimension Reduction Methods (DRM) challenges

In structural reliability analysis, the Reduction Dimension Method (RDM) is designed to tackle complex issues, but it also has its own set of challenges.

a) Balancing Information Loss and Dimensionality Reduction reducing a data set's dimensionality to two or three dimensions may result in significant information loss [Jolliffe (2002); Bibal & Frénay (2019); Kim et al. (2005)], techniques like PCA focus on preserving variance but may miss task-specific details. According to Soleimani et al. (2021), dimensionality reduction may result in considerable information loss, thus compromising the correctness of structural reliability evaluations. In structural health monitoring, dimensionality reduction on approaches can diminish detection accuracy by as much as 60%. The primary objectives of the research by Jia et al. (Jia et al., 2022) are to apply "low loss" in feature DRM, preserve the characteristics of the original data, identify the most effective mapping, and get the ideal low-dimensional representation.

b) Interpretability Challenges: Reduced dimensions can lead to difficulty interpreting the principal components and understanding their physical significance in

the context of the original variables. This can make drawing practical conclusions from the results challenging for engineers. Bibal and Frénay (2019) asserted that linear methods like PCA are often seen as easier to understand among the various DRM because their parameters combine. However, nonlinear dimensionality reduction (NLDR) embeddings are hard to understand, which makes them less useful for tasks that require clear explanations (Mylonas et al., 2024).

c) Assumption of Linearity: Many DRM techniques, including PCA, assume linear relationships among variables, which may not always hold in real-world applications (Van Der Maaten et al., 2009). In particular, nonlinear dimensionality reduction techniques offer an advantage because real-world data will likely be highly nonlinear. The performance of the nonlinear techniques is investigated in artificial and natural tasks. According to Van Der Maaten et al. (2009), the results of the experiments reveal that nonlinear techniques perform well on selected artificial tasks but do not outperform the traditional PCA on real-world tasks.

d) Computational Complexity: Depending on the dataset's implementation and size, some DRM techniques can be computationally intensive, especially for high-dimensional data. This can negate some of the time-saving benefits of dimension reduction.

These drawbacks highlight the importance of careful consideration when applying DRM techniques in practice, especially in the context of structural system reliability. Proper understanding and analysis are essential to mitigate these limitations. The DRM facilitates the numerical computation of reliability; however, its application in engineering is minimal. So, this method needs to be examined when applied to real reliability problems.

1.2.4 Applicability of structural reliability methods in system multi-components

Structural reliability methods are crucial for assessing the performances of a multi-component system. These methods allow the calculation of upper and lower bounds of failure probability by considering system dependencies and chain-of-failure effects.

In 1968, Kounias (1968) created mathematical formulas to calculate the bounds of the failure probabilities of a system in series configuration. In order to find a linear upper-bound estimate formula for a series system event, Hunter (1976) expanded the formulation. Vanmarcke (1973) published the upper probability bound in 1973. Ditlevsen (1979) and many others have demonstrated the bounds' extensive use for structural reliability assessments in various examples.

Hohenbichler and Rackwitz (1982) proposed a First-order concept to assess the reliability of structural systems by calculating probability estimates for components and establishing derived probability bounds on the union of failure events. This method is thoroughly examined and shown to be adequate for practical applications, accompanied by a straightforward example highlighting its effectiveness. Murotsu (1983) proposed a method for estimating upper bounds on the reliability of redundant frame structures.

Kiureghian and Der Kiureghian (2003) developed the linear programming (LP) bounds method, which applies to various configurations, facilitates efficient computations, and yields robust results. Byun and Song (2020) introduced an alternative formulation of the linear programming (LP) bounds method for evaluating the reliability of intricate systems. It employs binary integer programming (BIP) grounded in inclusion relationships among events, mitigating memory demands while decreasing computational expenses for more minor problems.

Song et al. (2021) examined the theories and applications of structural system reliability methods, emphasizing Boolean system events, sequential failures, and SSR-based design and topology optimization. They presented a literature review of these methods, categorizing them according to their characteristics and approaches.

Structural reliability techniques are indispensable because they help to balance the consequences of failure against material consumption and the probability of failure by directly handling the uncertain or random nature of loads and capacities (Jiang et al., 2017).

These techniques are applied in many domains, such as the design of new structures, calibrating safety factors for simplified procedures, reassessing existing structures, taking into consideration degradation factors such as corrosion and wear, and for inspection planning, taking into account the uncertainties posed by non-destructive testing methods. They are also helpful in decision-making under uncertainties and probabilistically assessing various failure scenarios.

1.3 Conclusion

This chapter provided a comprehensive overview of system reliability modeling and structural reliability methods, explicitly focusing on their application to speed reducer systems. Additionally, we explored various widely used reliability assessment techniques for gearbox systems, synthesizing key findings from scientific research. By examining the advantages and limitations of each approach, we evaluated factors such as computational

efficiency, time constraints, and data requirements.

The selection of an appropriate reliability method depends on multiple considerations, including product characteristics, manufacturing processes, regulatory standards, and available resources regarding time, computation, and finances. Since different techniques vary in complexity and precision, they offer distinct levels of insight into system behavior and response variability. Hybrid and combinatorial models have emerged to overcome the inherent limitations of individual methods, providing more robust reliability assessments.

In the next chapter, we provide an overview of the key components of a speed reducer and examine their predominant failure modes across various stages, including design, manufacturing, and operational phases. This analysis aims to identify critical failure mechanisms and their underlying causes, contributing to a deeper understanding of reliability challenges in speed reducer systems.

CHAPTER 2:MAIN SPEED REDUCER SYSTEM FAILURE

2.1 Introduction

A speed reducer, also known as a gearbox, is a mechanical device consisting of a set of gears used to reduce the rotational speed from an input source, typically a motor, while increasing torque and potentially changing the direction or axis of rotation. It consists of multiple gear sets housed within a structure that supports bearings and shafts.

Speed reducers are continuously operated under challenging conditions, which inevitably lead to fatigue and high service loads. These conditions can give rise to defects in the speed reducer, potentially resulting in failure and significant system downtime. However, the speed reducer must have a long lifespan that meets the customer's needs.

To address this issue, it is important to focus on the key factors and modes responsible for component failures in the speed reducer. Furthermore, failure modes must be addressed during both the design and operation stages to ensure the safety, reliability, and prevention of catastrophic failures in the gear reducer.

This chapter analyzes speed reducers' common failure modes and investigates their underlying causes in the design, manufacturing, and operating stages.

2.2 Failure analysis

Failure analysis is the systematic procedure for gathering and considering data to determine the cause of failure and avoid future occurrences (Scutti & McBrine, 2002). According to Noor (2007), failure analysis has three primary duties.

A. Identifying failure modes, which may also take place on-site or in laboratory settings. Common techniques used in identifying failure modes include fractography, metallographic analysis, and mechanical testing.

B. Determining the root causes for the failures include a consideration of the unit’s design, loading conditions, and environmental context. Laboratory investigations may require comparative samples or failure reproduction in order to substantiate the diagnosis.

C. Performing a root cause analysis that combines knowledge of failure modes and their causes with system-specific factors such as design, operation, maintenance history, and environmental influences. Typical examples of root causes include fatigue due to cyclic loading, corrosion-related degradation, stress corrosion cracking, and both ductile and brittle fractures.

An all-rounded understanding of these factors is important for good failure prevention and reliability of the systems.

2.3 Failure statistics of gearbox system

Statistical explorations of failures gathered from systems containing gearboxes or speed reducers indicate that the gearbox is one of the most crucial subsystems in terms of failure frequency and the effects resulting thereof. Because of complicated mechanical interaction and keeping up with rigorous working conditions, it is comparatively prone to degradation mechanisms such as wear, fatigue, and misalignment.

Musial et al. (2007) pointed out that gear systems are among the most expensive components in a wind turbine. In fact, their rates of failure tend to be higher than anticipated, adding to the cost of wind energy.

Ribrant (2006) conducted an analysis of component downtimes in wind power systems between 2000 and 2004, revealing that gearbox related failures accounted for 32.8% of the total downtime in wind power plants. The mean downtime per gearbox failure was approximately 600 hours, which is more than double the average downtime associated with blade or pitch system failures.

In an effort to estimate average failure rates and reliability growth curves for maintained onshore wind turbines in Germany and Denmark, Tavner et al. (2007) used failure data from wind turbine model. Their results indicate that although electrical control systems account for higher proportions of failures in Germany, gear failures have a more serious effect on turbine availability owing to their high mean time to repair (MTTR).

Analyzing the Vestas V44-600kW and V90-2MW wind turbine models, Fischer et al. (2011) found that gearbox downtime amounted to 9% and 13% of total downtime, respectively, coming after generator downtime with 18% and 24%, respectively. These findings point out the degree of emphasis that has to be taken regarding gearbox reliability for wind turbines in their economic and operational efficiencies.

Chengbing and Xinxin (2012) conducted a study on the structural components and failure modes of wind power plants, revealing that gearboxes accounted for 19.4% of total downtime, followed by the control system (18.3%) and electrical system (14.3%). Thus, although the downtime is rather close in value, most of the downtimes are attributed to the gearbox.

Nie and Wang (2013) conducted a comprehensive survey of wind turbine subsystems across wind farms in Europe and America, identifying the gearbox as the most failure-prone component.

Between 2005 and 2010, wind turbines frequently experienced failures within just 3 to 5 years of operation, despite gearboxes being designed for a 20-year service life. This discrepancy led to substantial economic losses due to increased maintenance costs and operational downtime. Wang et al. (2016) emphasized the critical nature of this issue, identifying the gearbox as the most failure-prone component in wind turbines. They advocated for enhanced reliability measures and maintenance strategies to address this vulnerability.

Repeated studies have shown that the gearbox is a very significant cause of unplanned downtime. The resulting downtime has one of the highest impacts on overall operational efficiency. Therefore, it is necessary to make a comprehensive study of such influential factors and establish key failure modes in a gearbox system. Understanding this is required for the application of effective maintenance strategies, less downtime, and higher overall reliability of the system.

2.3.1 Main influential factors on the failure behavior of a speed reducer

The main influential factors on the failure behavior of gearboxes are:

A. **Design:** Gearbox failure may occur due to design errors such as unreasonable material (Akinci et al., 2005; Lanzuttiet al., 2017), an improper heat-treatment process (Pan & Yang, 2022), and improper geometrical parameters (Maláková et al., 2021), or inadequate lubrication (Liu et al., 2020).

Musial et al. (2007) argued that design defects are major contributors to the premature failure of wind turbine gearboxes. Also, Nwosu and Iwuoha (2010) raised design errors to the level of prime causative factors in gear tooth overload and tooth tip interference, thus accentuating the role of bad design in causing reliability problems with gearboxes.

Throughout the design process, engineers and designers must design a product and generally carry out a systematic analysis for potential failure modes. The thorough definition of failure modes should involve a detailed examination of their severity, probability of occurrence, and delectability. With this systematic approach, engineers may assess how each type of failure could affect performance and reliability. Such severity enables one to prioritize the most critical failure modes, which can lead to significant consequences or safety hazards.

B. Material Defects and Processing Defects

Impropriety in manufacturing procedures may cause insufficient surface hardness, which diminishes a gearbox's life span. Accuracy in assembly, on the other hand, plays a vital role in ensuring the gearbox's longevity (Gear Handbook, 2013).

These failures may be due to poor machine operations or very bad heat treatment of components, followed by improper assembly of a given gear set (Pandey & Lim, 2020). It was further informed by Liu (2014) who said that the failure was actually because of the heat treatment that was not adequate, which led to insufficient tooth flank strength and, thus, developed into sudden fatigue failure. Nwosu and Iwuoha (2010) observed that manufacturing errors contribute to misalignment by mismatch of the profiles of the gears and that this misalignment translated into an uneven load distribution of the teeth of the gears. Moreover, this issue was further complicated due to the misalignments of pinions and gears because of surface finishes that were out of tolerances.

C. Service Environment and Maintenance Faults

The gearboxes are manufactured with sturdy shapes to withstand harsh industrial conditions like high temperatures, dust, load, humidity, and contact with chemicals. However, such extreme environmental factors may be the cause of premature failure from the system before it can achieve its expected service life (Goswami & Rai, 2023). The work of Tavner et al. (2013) and Su et al. (2016) further addresses the outdoor environmental influence factors, wind speed, and temperature, on the reliability and discusses how these factors affect the failure rates of offshore wind turbine (WT) components. Their work also indicates the inherent importance of operation and maintenance in determining WT failure rates.

Maintenance faults may lead to incredible financial loss as well as disastrous accidents in certain instances. In the opinion of Öztürk (2006), 60% of gearbox faults are due to some gear-related failures, while 24% happen as a result of the ineffectiveness of maintenance acts. Hence, it became inevitable to monitor the health of gearbox systems while diagnosing various faults. Several papers have been written on fault diagnosis (Wang et al., 2023; Tang et al., 2023) and condition monitoring (Inturi et al., 2023; Alvarado-Hernandez et al., 2022). These papers use new technologies to help find faults more accurately, which lets maintenance professionals make better decisions.

2.4 Failure modes of speed reducer components

Gears, shafts, and bearings are the main components susceptible to failure in a speed reducer, each subjected to various failure mechanisms that impact their performance within the system. According to Sann et al. (2024), shafts, gears, and bearings are also the primary sources of noise and vibration in vehicle gearboxes. Therefore, the different failure modes associated with these components are discussed below.

2.4.1 Gears and their Failure Modes

Gears are a crucial elements found in nearly all mechanical machines, serving several vital purposes. Their principal function is to facilitate gear reduction, which is essential for maintaining sufficient power and torque transfer.

2.4.1.1 Geometry of Gears

Gears are designed in different types to serve different co-functional purposes. Gear types include spur gears, helical gears, straight and spiral bevel gears, and hypoid gears. The kind of gear and some special design features directly relate to the operating features (Bhaumik et al., 2007). Usually, factors dealing with several aspects, such as geometry, materials of manufacture, and conditions of operation, may define the lifetime of a speed reducer system. The tooth profile, contact ratio, and pressure angle are some of the most important design factors that go into choosing the right gearing for a given application (Herring, 2004). The nomenclature of a typical spur gear is shown in **Figure 2.1.**

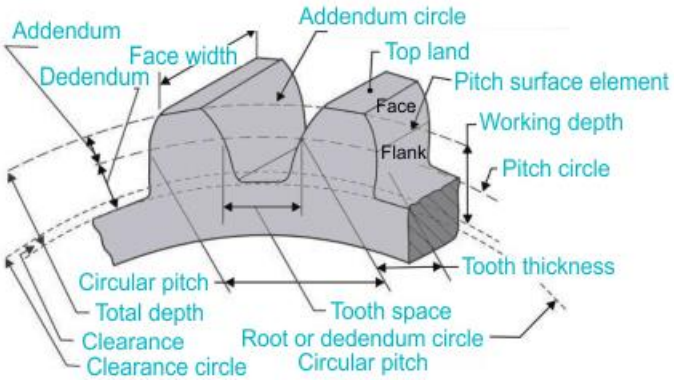

Figure 2. 1: Nomenclature of typical spur gear (testbook, 2026)

2.4.1.2 Failure Modes of Gears

The gear system is subject to numerous degradation processes that can diminish performance or life. These failures can usually be analyzed through multiple techniques, visual inspection, macroscopic and microscopic examination, analysis of fracture appearance, chemical composition testing, hardness testing, mechanical testing, microstructural analysis,

and surface roughness evaluation (Wang et al., 2016). Errichello and Muller (2002) created a comprehensive classification system for the six main classes of gear failures. The outline of these classifications are:

A. Bending Fatigue

Bending fatigue represents a progressive failure mechanism in gears resulting from cyclic loading. This process evolves through three distinct phases: crack initiation at stress concentrators, stable crack propagation, and final catastrophic fracture. In gear systems, the root fillet region proves particularly susceptible to high-cycle fatigue (HCF) failures, where operational stresses remain below the material's yield strength while exceeding 10,000 load cycles.

The fillet's geometric stress concentration, combined with sustained cyclic loading below yield limits, creates ideal conditions for fatigue crack nucleation and growth, ultimately leading to tooth fracture without plastic deformation.

Figure 2. 2: Bending fatigue fracture in gear root fillet (Errichello, 2013)

B. Contact Fatigue

Surface contact fatigue (Hertzian fatigue) represents the predominant failure mode in gear systems (Fernandes & McDuling, 1997). This damage mechanism manifests on contacting surfaces through progressive microstructural deterioration that significantly compromises load-bearing capacity. The failure process initiates with subsurface crack formation at stress concentrators, evolving into either localized micropitting (<1mm) or macroscopic spalling (>1mm). These surface-initiated cracks propagate under cyclic Hertzian contact stresses, ultimately leading to material exfoliation through two synergistic mechanisms: (1) mechanical fatigue from repeated stress cycles and (2) tribochemical reactions at crack tips that accelerate

corrosion fatigue. The resultant metal fragment detachment creates surface discontinuities that further amplify stress concentrations, establishing an autocatalytic failure progression **(Fig. 2.3).**

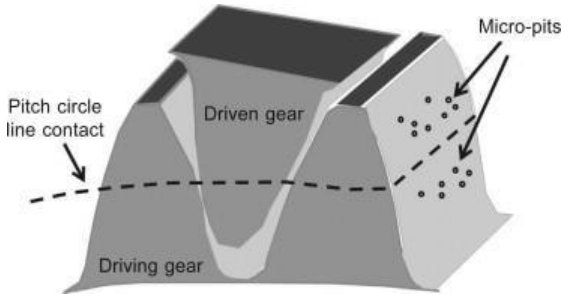

Figure 2. 3: Spatial positions of micro-pits in relation to pitch circle contact (free rolling) on gear flank surfaces (Oila, 2003)

Surface fatigue failures predominantly manifest as either macro-pitting or micro-pitting. Oila and Bull (2005) identified seven key factors governing micro-pitting initiation and progression: (1) gear steel material properties, (2) lubricant characteristics, (3) surface finish quality, (4) applied load magnitude, (5) thermal conditions, (6) operational speed, and (7) slide-roll ratio. The pit formation process creates localized stress concentrations that accelerate fatigue crack development, ultimately leading to tooth fracture (Li & Kahraman, 2014). As pitting damage accumulates, adjacent micro-pits coalesce into macro-scale spalling, which severely degrades the gear's load-carrying capacity through progressive surface deterioration (Fernandes & McDuling, 1997). This evolutionary damage process transitions from initial surface distress to catastrophic failure through three distinct phases: microstructural surface alterations, pit nucleation, and final spall formation.

C. Wear on gear

Wear on gear tooth surfaces results from the loss or displacement of material by mechanical or chemical actions. Two kinds of wear may be distinguished: adhesion and abrasion.

1) Adhesion: This phenomenon arises when the material is transferred from one tooth surface to another through welding and tearing, as shown in **Fig. 2.4.a**. It is generally restricted to the oxide layer on the tooth surface.

2) Abrasion: Affected by the presence of contaminating agents lying within the lubricant, like sand, scale, rust, machining chips, grinding dust, welder splatter, and wear debris. These appear as relatively smooth, parallel scratches or gouges on the surface. Severe abrasion may produce wear steps at both ends of the contact surface within the dedendum.

a) 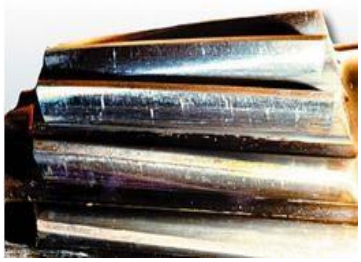 b) 

Figure 2. 4: Type wear of gear teeth: **a)** Adhesion and Polishing; **b)** Abrasion (Errichello & Muller, 2002)

Additional wear mechanisms in gear systems manifest through various mechanisms, including polishing, corrosion wear, erosive wear, scuffing, and overload, each influencing gear performance and longevity (Errichello & Muller, 2002).

3) Polishing: A fine-scale abrasive wear that results in bright, mirror-like surfaces on gear teeth, typically caused by chemically active lubricants contaminated with fine abrasive particles. **(Fig. 2.4.a).**

4) Corrosion Wear: Caused by chemical reactions involving acids, additives, or moisture in the lubricating oil, this type of wear leads to uniform, fine pitting on gear contact surfaces.

5) Erosive Wear: Material loss resulting from relative motion between a surface and a fluid containing solid particles. The severity of erosion is influenced by factors such as particle impact angle, velocity, and the hardness of the surface material.

6) Scuffing: Unlike fatigue failure, scuffing can occur early in the gear's service life, as noted in ASTM D5182–9. It is caused by severe adhesive contact, leading to metal transfer between mating gear teeth (see Fig. 2.5). Scuffing typically appears in the addendum or dedendum regions along the direction of sliding.

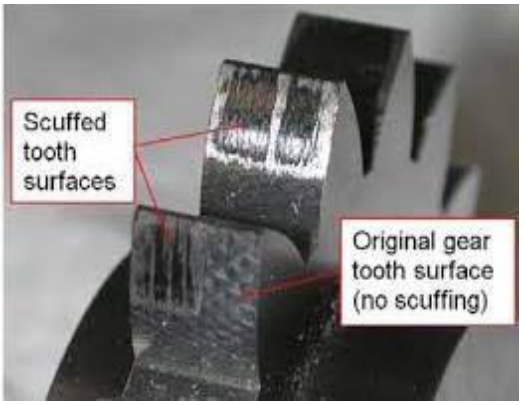

Figure 2. 5: Scuffing of gear tooth surfaces (Wink, 2012)

7) Overload: Tooth fracture occurs when gears are subjected to multidirectional forces that exceed the material's tensile strength. These may be due to seizure of the bearings, failure of the driven equipment, foreign objects in the gear mesh, or sudden misalignment (Armaan et al., 2020).

Wear considerably impacts gear performance, varying the dynamic transmission error, vibration impact condition, and amplitude (Sheng et al., 2022). The wear coefficient relies on lubrication conditions, surface roughness, temperature, load, and sliding velocity (Huangfu et al., 2020).

2.4.2 Rolling bearings and their failure modes

According to statistics from the gearbox failures database published in several sources, such as Chengbing and Xinxin (2012; Sheng, 2016; Zhang et al., 2020; Jiang et al., 2022; Mankhi et al., 2022; Karpat et al.2022) and others, the majority of failures are caused by rolling bearing elements.

2.4.2.1 Rolling bearings geometry

Rolling bearings are essential mechanical components used in a wide range of applications. They support and guide rotating or oscillating elements—such as shafts, axles, or wheels—while enabling effective load transmission between machine parts. These bearings offer high precision and low friction, allowing for increased rotational speeds and reduced noise levels.

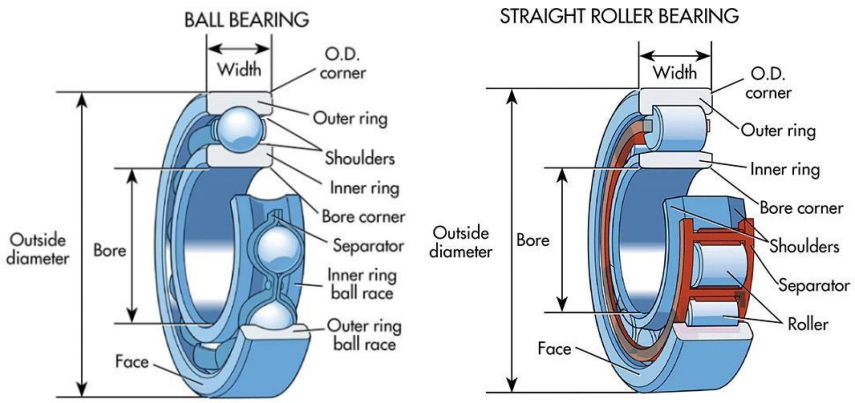

Figure 2. 6: Ball bearings are straight or cylindrical roller bearings (Carlos, 2015)

2.4.2.2 Classification of Bearing Failure Modes

Failure or damage to rolling bearings can result in partial or complete machine breakdown, often leading to significant economic losses. According to research (World Pumps,

2015), approximately 35% of rolling bearing failures are attributed to lubrication issues. More broadly, tribological factors—including friction, wear, and lubrication—account for nearly 80% of all bearing failures, as illustrated in **Fig. 2.7**.

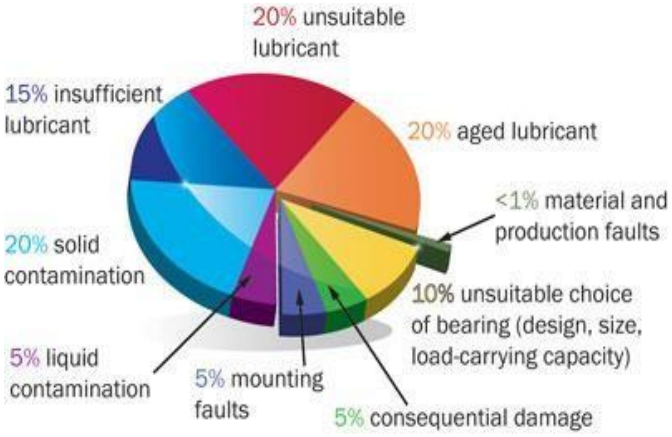

Figure 2. 7: Bearing Failure Modes classification

Failure statistics show that a significant portion of premature rolling bearing failures are directly or indirectly linked to the lubricant used. Selecting the appropriate lubricant is therefore essential for ensuring proper functionality and prolonging bearing life. While various publications may use different terminology to classify bearing failures, it is widely recognized that there are six principal failure modes, each with its own sub-modes. Further understanding of bearing damage mechanisms has been established through ISO 15243(2004).

a. Rolling Contact Fatigue

In terms coined by ISO 15243 (2017), rolling contact fatigue is caused by repeated stresses occurring at the contact points between rolling elements and raceways. This type of fatigue typically leads to both microstructural and macrostructural changes in the material, and in most cases, results in material spalling.

➢ **Subsurface Initiated Fatigue**: The conditions responsible for cyclic loading, as described by Hertzian contact theory, also cause the development of subsurface stresses and material alterations that lead to the initiation of microcracks deep within the material. The depth at which these cracks form depends on several factors, including the applied load, operating temperature, material properties, and the material's cleanliness and microstructure. As these cracks propagate toward the surface, they eventually cause spalling **(Fig. 2.8).**

Figure 2. 8: Advanced subsurface spalling in a tapered roller bearing, Stationary inner ring (ISO 15243, 2017)

➢ **Surface-initiated fatigue:** caused by plastic deformation of surface asperities, surface- initiated fatigue is characterized by the very nature of its cause. This surface damage is the result of insufficient lubrication and an inadequate lubricant film thickness. Surface micro-deformation, such as micro-cracking of asperity **(Fig. 2.9(a)),** micro-spalling of asperity **(Fig. 2.9(b))**, and microscale areas of pitting as grey stains **(Fig. 2.9(c)),** may occur due to contact between the asperities of the rolling elements and the bearing raceway.

a) 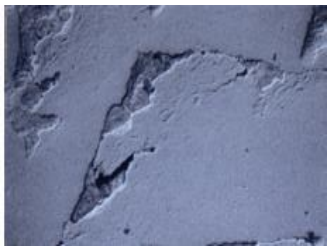 b) 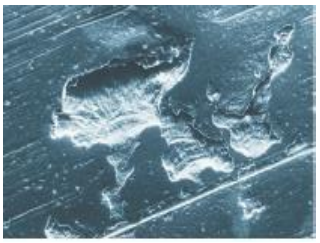 c) 

Figure 2. 9: Surface-initiated fatigue: **a)** asperity micro-cracks, **b)** asperity micros-palls, **c)** micros-palled areas (ISO 15243,2017)

b. Wear

According to ISO 15243 (2017), wear refers to the gradual removal of material as a result of the engagement of asperities from two contact surfaces, which can either be sliding or rolling/sliding. Wear occurs in two ways: through abrasive wear and adhesive wear.

1) Abrasive wear

Abrasive wear occurs when hard debris particles become entrained in the contact area, leading to scoring or abrasion of the surface (Fig. 2.10). Two main mechanisms are typically involved: first, the action of loose hard particles that scratch the surfaces; and second, the penetration of harder asperities into softer material surfaces, forming grooves (Liu et al., 2001).

The extent of damage depends on factors such as the size and shape of the debris particles, as well as the hardness and properties of the contacting materials (Dwyer-Joyce et al., 1990). Key parameters influencing abrasive wear include lubricant viscosity, sliding speed, applied load, and the thickness of the lubricant film.

To mitigate abrasive wear, Loewenthal et al. (1982) recommended increasing the lubricant's viscosity and regularly monitoring its cleanliness to prevent contamination.

2) Adhesive wear

Adhesive wear is a form of lubricant-related damage that occurs between two surfaces sliding relative to each other. It is typically characterized by the transfer of material from one surface to another, often observed as smearing. According to Liu and Zhou (2001), the wear mechanism in rolling contact evolves with increasing tangential friction force. When this force is minimal, a moderate and consistent level of wear occurs, predominantly due to abrasive mechanisms. However, as the tangential friction force increases, adhesive wear becomes the dominant mechanism. This transition highlights the critical influence of contact conditions on wear behavior.

Figure 2. 10: Bearing surfaces damaged by adhesive wear (Vencl et al., 2017)

Smearing can be mitigated through several strategies, including increasing the applied load, using smaller or hybrid bearings (with lighter rolling elements), applying protective surface coatings, modifying the cage design, and optimizing the selection of lubricants such as oil or grease.

3) Corrosion

Corrosion denotes the removal of reaction products generated on contact surfaces as a result of interactions with the surrounding environment. Oxygen in the atmosphere is a prominent reactive agent that facilitates the rusting of rails, resulting in this form of degradation (Kimura et al., 2002).

➢ **Moisture Corrosion**

Surface oxidation or corrosion (rust) is caused by moisture and contact of the bearing parts with aggressive media such as water or acids **(Fig. 2.11a).** Consequently, corrosion pits will form and can develop into spalling **(Fig. 2.11b).**

a)  b) 

Figure 2. 11: Bearing surfaces damaged by moisture corrosion (ISO 15243, 2017)

Effective prevention of corrosion primarily requires proper sealing of the application to ensure that the lubricant remains uncontaminated by water or aggressive liquids. Additionally, the use of lubricants with strong rust-inhibiting properties significantly contributes to minimizing corrosion risk (Vencl et al., 2017).

➢ **Frictional Corrosion**

According to the ISO 15243 (2017), frictional corrosion is classified into two types: fretting corrosion and false brinelling.

• **Fretting Corrosion**

Fretting corrosion arises from small-amplitude relative motion between the bearing ring and its seat on a shaft or in a housing (see **Fig. 2.12**). It is most often associated with excessively loose fits or form inaccuracies. Effective countermeasures include specifying tighter fit tolerances and applying anti-corrosion pastes or protective surface coatings.

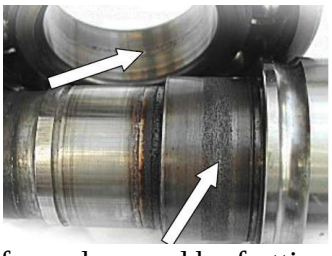

Figure 2. 12: Bearing surfaces damaged by fretting wear (Vencl et al. 2017)

• **False brinelling**

False brinelling can be physically mitigated by ensuring that rolling elements do not remain stationary in the same position for extended periods (see **Fig. 2.13**). Regular

movement helps prevent localized wear and surface damage associated with this phenomenon.

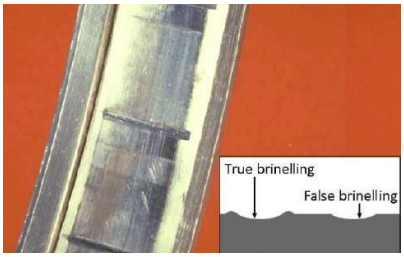

Figure 2. 13: Bearing surfaces damaged by false brinelling (Venclet al. 2017)

The primary strategy to prevent both fretting corrosion and false brinelling is to eliminate vibration, thereby stopping the sliding or rocking motions that cause damage. This can be accomplished by using vibration isolators and tightening connections to increase friction through higher applied loads.

4) Electrical erosion

Electrical erosion in rolling bearings occurs when electric current passes through the thin lubricant film between the rolling elements and the raceway. This phenomenon is especially common in electric motor bearings and can lead to localized damage and accelerated wear.

5) Plastic deformation

Plastic deformation occurs when excessive force is applied to a bearing, resulting in permanent changes to its shape. It can arise from several conditions, including:

✓ ***Overload Deformation:*** Caused by excessive static loads, sudden shocks, or mishandling during operation or installation.

✓ ***Indentations from debris***: Solid particles may enter the bearing through seals, contaminated lubricant, or wear of adjacent components such as gears. As rolling elements pass over these particles, the debris becomes embedded and causes indentations on the raceway surface.

6) Fracture and cracking

Forced fracture occurs when the applied stress exceeds the material's strength, usually due to high loads or overstressing. Fatigue fracture results from repeated bending cycles, starting as small cracks that gradually grow until the bearing ring or cage fails. Thermal cracking arises when excessive heat generated at sliding surfaces causes cracks to form, typically perpendicular to the direction of sliding

In conclusion, addressing the failure mechanisms of rolling element bearings is crucial for maintaining a gearbox system's safe and reliable functioning. Actively addressing these failure types has numerous substantial advantages, such as improved reliability, extended service life, cost efficiency, optimum performance, and the capacity for proactive maintenance via condition monitoring.

2.4.3 Shafts and their failure modes

The failure of shafts can significantly affect the overall system, potentially leading to severe consequences. Therefore, it is essential to proactively identify and understand the primary failure mechanisms associated with shafts.

2.4.3.1 Shaft Geometry

A shaft is a rotating machine element with a circular cross-section that supports components such as rollers and gears while transmitting power. Typically, shafts are designed with a stepped configuration, featuring the largest diameter in the middle and tapering to smaller diameters at the ends. This design helps balance strength and weight.

Shafts must possess sufficient rigidity to prevent excessive deflection, which can cause uneven gear tooth loading and premature wear. By nature, shafts are subjected to varying cyclic bending and torsional loads, often compounded by stress concentration factors. To ensure durability, shafts need to withstand shock loads without yielding and resist fatigue caused by reverse bending combined with torsional stresses (Hariom et al., 2016). **Fig 2.14** shows the common shaft configurations used in vehicle transmissions.

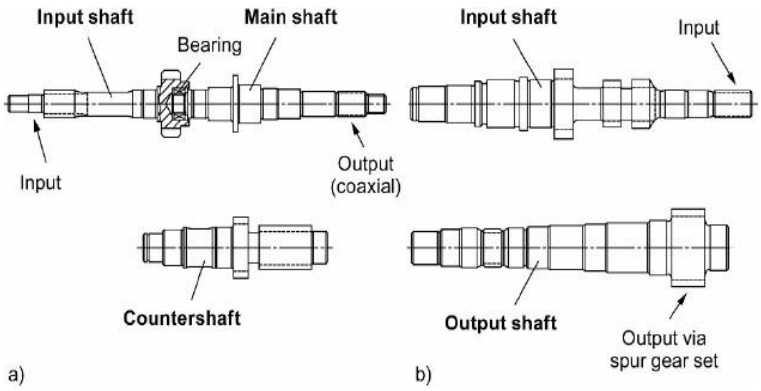

Figure 2. 14: Characteristic shaft configurations in vehicle transmissions. **A)** Two-stage coaxial countershaft transmission; **b)** single-stage countershaft transmission for front-transverse mounting (Naunheimer et al., 2011)

2.4.3.2 Shafts failure modes

The shaft may fail due to a variety of causes, including metallurgical defects, cyclic fatigue, excessive torque, and additional stresses arising from misalignment or impact. The primary mechanisms of shaft failure are corrosion, wear, overload, and fatigue. Among these, wear—particularly abrasive wear—is a common issue, as it reduces the shaft's dimensions and alters its geometry, potentially compromising its performance. According to the Handbook of Reliability Prediction Procedures for Mechanical Equipment (Center, N. S. W, 1998), the major modes of shaft failure include:

a. Shaft fatigue /fracture

Fatigue fracture is one of the most common causes of shaft failure. Broken shafts frequently occur in gearboxes and rotating machinery (Eftekharnejad et al., 2012). Shafts subjected to high torsional loads combined with repeated bending moments are especially prone to developing fatigue cracks (see Fig. 2.15). Fatigue failure is often initiated by stress raisers such as fillets, stress concentrations at keyways (Fig. 2.16a), abrupt changes in shaft diameter, bending fatigue, and the effects of high rotational speeds. Additionally, variations in temperature and environmental conditions during operation can accelerate fatigue crack initiation and propagation.

According to Pantazopoulos et al. (2010), fatigue fracture occurs in three stages. The first stage involves crack initiation, where microscopic flaws develop under cyclic loading. The second stage is characterized by the progressive growth of these cracks with each load cycle. Finally, in the third stage, the shaft experiences immediate rupture due to overload of the reduced cross-sectional area caused by the advancing crack.

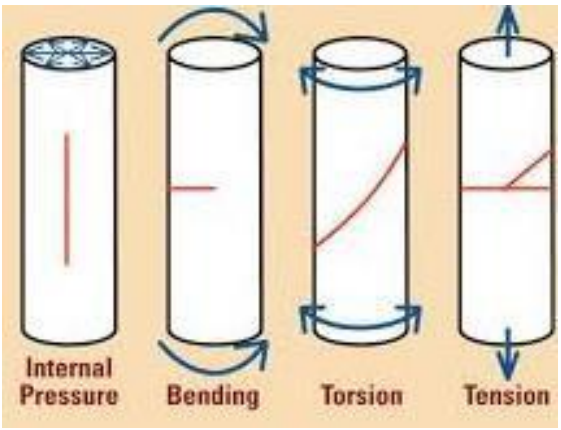

Figure 2. 15: The fracture planes caused by four common fatigue forces (Bhaumik et al., 2002)

a)  b) 

Figure 2. 16: a) The battered end of a motor shaft, **b)** torsional fatigue failure of a fan shaft (Efficient plant, 2012)

b. Fretting corrosion

Corrosion failures in shafts are primarily caused by the combined effect of environmental factors and mechanical stresses acting on the shaft material. The underlying issue is an electrochemical reaction that gradually deteriorates the shaft surface (Raut, S and Raut, L 2014). . Such failures are commonly observed at critical stress concentration areas like the shoulder fillets and the bottom edges of keyways (Loganathan et al., 2010). Studies indicate that pitting corrosion is a major contributor to premature shaft failure. Additionally, damage in the fracture zone, including fretting and abrasion, has been identified as a significant factor in shaft degradation Sara (2020) **(Fig 2.17).**

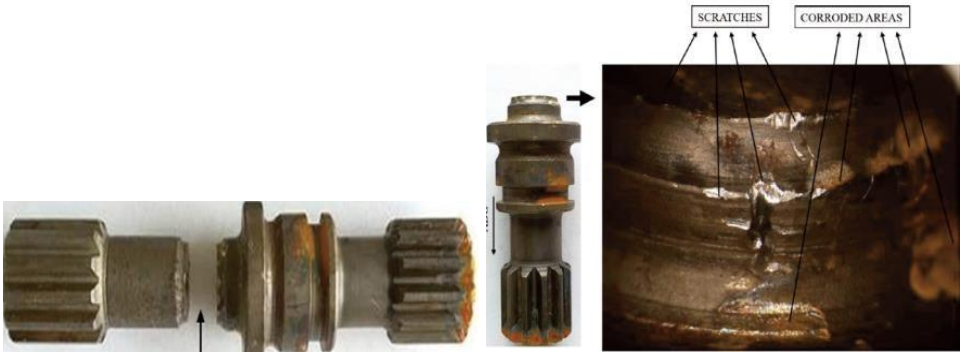

Figure 2. 17: The fretting and scratching in the fracture zone of the corroded side of the shaft (Sara, 2020)

Preventive measures against fretting corrosion can be classified based on their effectiveness in mitigating the underlying causes. These include reducing relative movement by increasing friction force—such as through applying higher normal loads—or by lowering friction via lubrication or using low-friction inserts. Another approach is to exclude the corrosive atmosphere by employing rubber gaskets or flooding the area with lubricant. Increasing the abrasion resistance of contacting surfaces and physically separating them are also common strategies.

It is important to note that a measure effective in one situation may worsen the problem in another, emphasizing the need for careful diagnosis before implementation.

c. Shaft misalignment

Misalignment is a common cause of premature spalling in shafts. It occurs when the centerlines of two shafts connected by a coupling are not properly aligned (Forsthoffer, 2011). **Figure 2.18** illustrates various forms of misalignment and the resulting variations in shaft end positioning that can occur during operation.

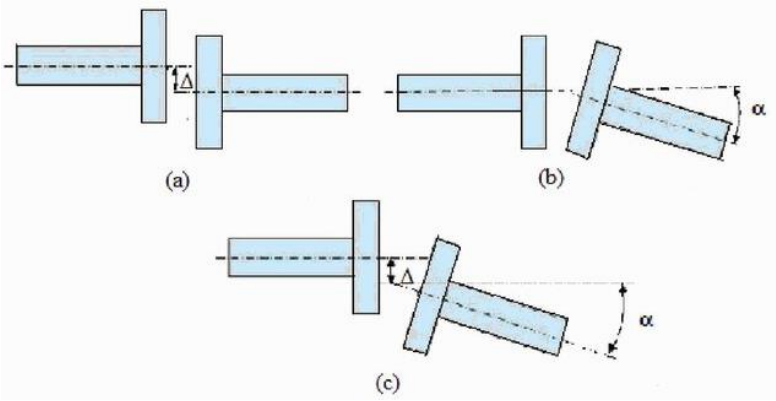

Figure 2. 18: Shaft misalignment conditions (a) Parallel, (b) Angular, (c) Combined (Forsthoffer, 2011)

Noor (2007) states that misalignment can occur either during the initial assembly of equipment or throughout subsequent repairs. Additionally, deflection or deformation of supporting components during operation may cause misalignment. Significant misalignment between the driver and driven machines can result in excessive vibration, increased bearing stress, shaft fracture, and coupling failure. Therefore, accurate alignment of turbomachinery requires a thorough understanding of thermal expansion effects in the radial direction of both machine casings (Bloch, 1998).

d. Bent shaft

Shaft bending can result from various factors such as creep, thermal distortion, large unbalanced forces (Mogal & Lalwani, 2017), excessive heat, or cold bowing—where gravity causes a long, slender shaft to bend while at rest. Other causes include the shaft's length, physical deformation, excessive loads, high torque, impact forces, and bearing failures. A bent shaft generates significant vibrations depending on the extent and location of the bend, which can impose substantial loads on adjacent components during operation, potentially leading to further damage.

e. Excessive shaft deflection

Shaft deflection refers to the bending or displacement of a shaft when subjected to forces such as axial stress. All rotating shafts experience some degree of deflection during operation, regardless of external loading. However, excessive shaft deflection can result from factors including dynamic loading, reversing loads, operating above critical shaft speed, and unbalanced loads. In vehicle gearboxes, shafts tend to be long with significant distances between support bearings and are often subjected to asymmetrical loads, which further contribute to substantial deflections (Gunjegaonkar et al., 2009).

Saleem et al. (2012) demonstrated that vibrations caused by imbalance can damage critical machine components such as bearings, seals, gears, and couplings. Toothed gearing systems are particularly sensitive to changes in shaft geometry; for instance, even slight shaft tilting can lead to gearwheel misalignment (see **Fig. 2.19)** or increased edge pressure on the bearings, accelerating wear and potential failure.

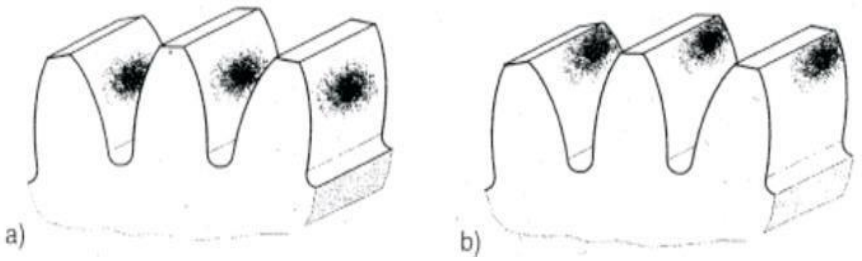

Figure 2. 19: Contact pattern **a)** Uniform Contact Pattern. **b)** One Sided Contact Pattern (Lechner and Naunheimer 1999)

To prevent excessive deflection. Gunjegaonkar et al. (2009) asserted that shaft deflection and strength predictions should be carefully verified, ideally including the deformation of the housing and bearings.

f. Damaged surface finish

The surface finish of a shaft plays a critical role in its performance and longevity. If the surface is too smooth, it may lack the necessary asperities or “pockets” to retain an adequate lubricant film, potentially leading to lip damage and premature seal leakage. Conversely, a surface that is too rough can cause metal peaks to protrude through the lubricant film, resulting in severe wear and reduced seal life. Such failures can stem from corrosion, contaminants, manufacturing defects, and thermal expansion at elevated temperatures (Glenn,2002).

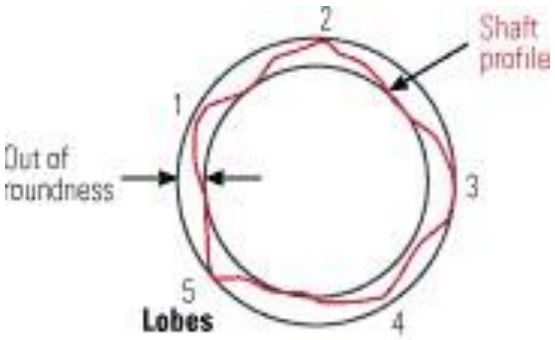

Figure 2. 20: Rounding and lobing also have an impact on sealability (Glenn, 2002)

Several finishing processes are employed to optimize the shaft surface in the seal contact region, including plunge grinding, paper polishing, roller or diamond burnishing, and high-speed ceramic turning. Investing in high-quality, precision-manufactured shafts for gearbox systems is highly recommended, as such shafts contribute directly to extended service life by reducing wear and tear, increasing load-bearing capacity, improving alignment, minimizing vibration and noise, enhancing lubrication efficiency, and providing greater resistance to corrosion and fatigue.

2.5 Conclusion

Failure modes analysis plays a crucial role in improving machine reliability by enabling corrective actions to be taken. Throughout this chapter, our focus has been on comprehending the impact of various components within a speed reducer system and understanding their primary failure modes. This process entails studying the system's behavior under different conditions and identifying all potential failure modes or ways in which both the system and its components can fail.

It is important to highlight that calculating a speed reducer system's reliability can be conducted by considering its elements. When multiple failure modes are present, the concept of system reliability comes into play. This involves estimating the overall system's reliability based on the reliabilities of the individual elements while establishing specific performance criteria.

The next chapter introduces mathematical approaches to structural reliability methods, which establish a basis for evaluating the probability of failure in mechanical engineering.

CHAPTER 3: MATHEMATICAL APPROACHES OF STRUCTURAL RELIABILITY METHOD

3.1 Introduction

Structural reliability is a discipline of structural engineering that deals with the assessment and quantification of the failure probability of structures such as buildings, bridges, dams, and offshore platforms under different load conditions. Moreover, structural reliability methods are not limited to structural systems alone. In recent decades, they have been widely used in various fields, and they play a crucial role in assessing the reliability of different systems, particularly mechanical components.

Structural Reliability Methods (SRM) offer a systematic approach to evaluating structural reliability while considering diverse uncertainties. These methods use probabilistic analysis and sensitivity analysis, employing techniques such as the first-order reliability method (FORM), the second-order reliability method (SORM), and simulation methods to quantify and analyze uncertainties related to structural performance.

Reliability-based design optimization (RBDO) is a significant tool in structural reliability methodologies. RBDO combines reliability analysis with optimization methodologies to determine an optimal design. This chapter aims to introduce the key mathematical concepts used in structural reliability methods.

3.2 Fundamental principles of structural reliability methodology

Below, we present several fundamental principles in the SRM.

3.2.1 Stress - Resistance Approach

Reliability is evaluated by determining the probability that a functional parameter associated with the performance of a product exceeds its admissibility limits, leading to failure. This evaluation is based on the statistical distributions of two fundamental parameters: **Resistance** and **Stress**. In this context, *resistance* represents the inherent capacity of a system or component to withstand external solicitations, while *stress* denotes the external demand or load applied to the system during operation. For a system to be considered reliable, its resistance must exceed the applied stress. The technical definitions of these terms are detailed below:

- **Stress Load effect (internal strength)**

Stress defines the effect of external loading that induces internal forces within a structure (Lemaire et al., 2013). It is quantitatively expressed as the **internal force per unit area** and is denoted by SSS. Stress represents the intensity of these internal forces that develop to resist

deformation when a material or structural component is subjected to external actions such as mechanical loads, thermal variations, or other environmental influences.

- **Resistance (strength or capacity)**

Resistance characterizes the capacity of a material or structural component to withstand external actions without failure. It is commonly referred to as the strength of materials**,** encompassing mechanical properties such as tensile strength, compressive strength, fatigue strength, and more. Resistance reflects the internal ability of a system to oppose deformation or damage under applied loads. (Lemaire et al., 2009).

3.2.2 Limit-state function

A limit state refers to a condition beyond which a system or component can no longer fulfill its intended function in a safe or satisfactory manner. This condition arises when a critical performance threshold is exceeded, resulting in failure or unacceptable performance**.**

The limit state function, commonly denoted by G(x), is a fundamental concept in structural and reliability analysis used to define the boundary between safe and failure domains. It is a mathematical expression that establishes a relationship among key performance parameters of the system, notably resistance (R) and stress (S**)**, which are both subject to uncertainty.

In this context, the variable x represents the vector of basic random variables**,** which may include material properties, geometric dimensions, loads, and environmental conditions—each characterized by statistical variability. The general form of the limit state function is expressed as:

$$G(X) = R - S \tag{3.1}$$

The limit-state function can be classified as either linear or nonlinear according to its characteristics. In addition, the limit-state function can be explicitly defined in terms of the random variables and constants, which directly represent the relationship between the variables and the performance criterion. Conversely, an implicit limit-state function is not defined by an explicit equation; rather, it is defined by an equation that must be numerically solved. The limit state of the majority of systems can be classified into two categories:

- **Ultimate limit states (ULS):** This category deals with extreme or worst-case scenarios where the structure or system is subjected to loads or actions that push it to its maximum capacity, such as fatigue, corrosion, fracture, etc. This limit state possesses a low probability of occurrence, but it may risk the element's life.

- **Serviceability limit-states (SLS):** This category focuses on ensuring that the structure or system performs adequately during normal service conditions throughout its expected lifespan. Serviceability limit states take into account variables, including excessive deflection, excessive vibration, leakage, and localized damage. Due to the reduced risk compared to ultimate limit states, a higher probability of occurrence may be accepted in these limit states (Ditlevsen and Madsen 1996).

A limit state function comprises two types of variables:

A. Design variables d: These variables are deterministic and can include various parameters that affect the behavior, performance, and characteristics of the system.

B. Random variables X represent uncertainties and fluctuations, whose realizations are noted x. Each random variable is characterized by its probability distribution and corresponding statistical characteristics (generally, mean and standard deviation).

3.2.3 Probabilistic Analysis

Probabilistic analysis involves quantifying the uncertainties associated with various input variables, such as material characteristics, geometric dimensions, and loads. The probabilistic treatment of the performance function, which translates to a stress-resistance balance, is performed to analyze the failure probability of mechanical components under uncertainty.

3.2.4 Failure Probability and Reliability Index

The reliability index is another important notion in the SRM. It provides a measure of the safety margin or the level of confidence in the structural performance.

The fundamental objective of SRM is to determine the failure probability P_f under uncertainty. To ensure this purpose, the SRM follows these steps:

1. Defining the failure criteria: mode of failure.
2. Probability distribution modeling: statistical distributions are often used to represent the variability of these uncertain parameters.
3. Formulate a mathematical model: develop a mathematical model (performance or limit stat function) that describes the behavior of the structure.
4. Perform reliability analysis, which involves evaluating the probability of failure.
5. Sensitivity analysis: Evaluate the impact of various uncertain factors on the overall structure's reliability.

6. Design optimization: Utilize the reliability analysis results to optimize the structure's design.

3.3. Overview of Structural Reliability Methods

Structural reliability methods (SRM) refer to assessing the failure probability of components or systems. This criterion is based on the model parameters, and it involves the separation of space into two zones: Reliability and failure zone, $\boldsymbol{G(d, x)}$ with positive values $\boldsymbol{G(d, x)} > 0$ define the safe space, and negative ones $\boldsymbol{G(d, x)} \leq \mathbf{0}$ define the failure space. The probability of failure is presented by:

$$P_f = Prob[G(d,x) \leq 0] \tag{3.2}$$

$$P_f = Prob[G(d,x) \leq 0] = \int \dots \int_{G(d,x)\leq 0} f_x(d,x)dx \tag{3.3}$$

Estimating this integral is not easy because the joint probability distribution of $f_x(d,x)$ is rarely known (Lemaire et al., 2013).

There are many techniques to overcome this drawback. In the next section, we present three techniques, which are among the most commonly used in mechanical systems. The first technique includes methods based on the knowledge of the reliability index β such as the First-Order Reliability Method (FORM) and Second-Order Reliability Method (SORM); the second one is the Monte Carlo Simulation (MCS), and the third technique includes the Reliability-Based Design Optimization Methods (RBDO).

3.3.1 Methods based on the knowledge of reliability index $\boldsymbol{\beta}$ (FORM and SORM)

In this method, the level of reliability is estimated by a reliability index noted $\boldsymbol{\beta}$. It offers an estimation of the probability of failure $\boldsymbol{P_f}$.

3.3.1.1 Reliability Index $\boldsymbol{\beta}$

Finding the Most Probable Point MPP(P^*) on the limit-state surface is a key step in determining the reliability index β. There are several types of reliability index, including:

A. ***Cornell reliability index***

Reliability techniques have been established to address a category of issues related to structural design and statistical data, taking into account the resistance and load of components as random variables.

The mean and standard deviation of the limit state *G(d, x)*, can be determined as:

$$\mu_G = \mu_R - \mu_S \tag{3.4}$$

μ_G is the mean of $G(d,x)$

μ_R and μ_S are the means of R and S, respectively.

The standard deviation

$$\sigma_G = \sqrt{\sigma_R^2 + \sigma_S^2 - 2\rho_{RS}\sigma_R\sigma_S} \quad (3.5)$$

Where ρ_{RS} is the correlation coefficient between R and S, and σ_R and σ_S are the standard deviations of $\boldsymbol{R}$ and $\boldsymbol{S}$, respectively.

The reliability index β_c, is defined as:

$$\beta_c = \frac{\mu_G}{\sigma_G} = \frac{\mu_R - \mu_S}{\sqrt{\sigma_R^2 + \sigma_S^2 - 2\rho_{RS}\sigma_R\sigma_S}} \quad (3.6)$$

If the resistance and the loading are uncorrelated (ρ_{RS} =0), the reliability index becomes:

$$\beta_c = \frac{\mu_G}{\sigma_G} = \frac{\mu_R - \mu_S}{\sqrt{\sigma_R^2 + \sigma_S^2}} \quad (3.7)$$

$$P_f = \Phi(-\beta) \quad (3.8)$$

Where Φ (.) is the standard normal distribution function

B. The Hasofer-Lind reliability index

To calculate the reliability index β for each failure mode, the distance between the origin of the standard space and the limit state in U_{space}, $H(u_i) = 0$, is determined.

The reliability index search constitutes an iterative optimization problem given by equation.

$$\begin{cases} min\ \beta = \|u\| \\ under\ the\ constraint\ \ H(u_i) = 0 \end{cases} \quad (3.9)$$

The algorithm for calculating this index was initially proposed by Lind and Hasofer (Hasofer & Lind, 1974) and improved by Rackwitz Fiessler (Rackwitz & Flessler, 1978).

The reliability index is defined in equation (3.6) as:

$$\beta = \frac{\mu_G}{\sigma_G}$$

In this case, the mean of the limit state function μ_G is defined as:

$$\mu_G = G(U^*) - \sum_{i=1}^{n} \frac{\partial G(U^*)}{\partial x_i} \sigma_{x_i} . U_i^* \quad (3.10)$$

Moreover, the standard deviation σ_G is calculated as:

$$\sigma_G = \sqrt{\sum_{i=1}^{n} \left(\frac{\partial G(U^*)}{\partial x_i} \sigma_{x_i}\right)^2} \quad (3.11)$$

The point $U^* = (u_1^*, u_2^*, u_3^* \dots\dots\dots u_i^*)$ on $G\ (U)\ = 0$ is the design point in U_{space}.

The failure probability is given by equation (3.2):

$$P_f = Prob[G(X) \leq 0]$$

However, the reliability is defined by the equation:

$$R = 1 - P_f \quad (3.12)$$

3.3.1.2 Analytical methods (Approximation methods) steps

The main steps of the approximation method are:

Step1: Iso-probabilistic transformation

The first step is the iso-probabilistic transformation T, which moves the physical variables xi to normalized Gaussian variables ui (Lemaire & Pendola, 2006). The transformed space is termed U_{space}. The resultant variables will be uncorrelated and correspond to a normal distribution with a mean of 0 and a standard deviation of 1.

$$T: \quad u_i = \Phi^{-1}(F(x_i)) \quad (3.13)$$

$(F(x_i))$ the distribution function of the variable x_i.

After the transformation, the mathematical representation of the performance function G(X) will be modified. H(U) is used to represent the modified performance function in U-space. **Fig (3.1).**

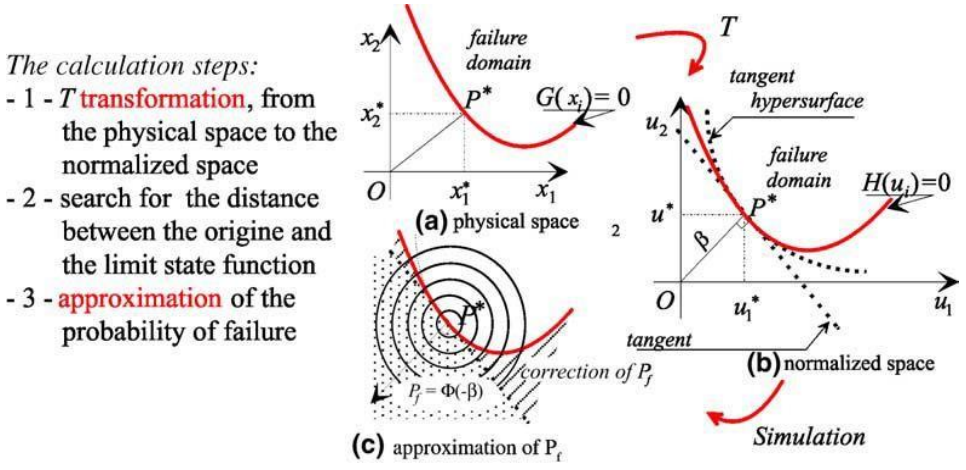

Figure 3. 1: Calculation steps of β and $Pf_$f using approximation techniques (Lemaire & Pendola, 2006)

An overview of the various Isoprobabilistic transformations and their classification from the richest to the poorest information are found in (Lemaire *et al.*, 2009).

The simplest transformation is the Rosenblatt transformation; the resulting variables are written as:

- For a normal distribution of x_i:

$$u_i = \frac{x_i - \mu_i}{\sigma_i} \tag{3.14}$$

- Case of lognormal distribution of x_i:

$$u_i = \frac{\ln(x_i) - \lambda_i}{\xi_i} \tag{3.15}$$

where, $$\lambda_i = \ln \mu_i \,, \tag{3.16}$$

$$\xi_i = \sqrt{\ln(1 + \delta_i^2)} \quad , \quad \delta_i = {}^{\sigma_i}/_{\mu_i} \tag{3.17}$$

Step 2: Optimization algorithm choice

Three criteria should be considered while choosing an optimization algorithm (Lemaire et al., 2009):

- ***Efficiency*** refers to the number of calls to the limit-state function (mechanical model) required to meet a given numerical accuracy level.
- ***Algorithm Robustness*** refers to its ability to locate the optimal design point.
- ***The capacity*** refers to the method's ability to handle huge problems with several random variables or complicated limit states.

Several methods can optimize equation (3.9), including:

1. **Sequential Quadratic Programming (SQP).** SQP improves convergence by using performance gradients and curvatures to learn more about the limit state function. For quadratic functions, the solution is precise (convergence in one iteration). SQP algorithm is effective and resilient. Its sole drawback is that it needs the assessment of second-order derivatives (Hessian), which is costly, especially with many random variables. Finite element studies are needed for (n) random variables. For algorithm specifics, see (Lemaire et al., 2013).

2. **Hasofer-Lind Rackwitz Fiessler algorithm** in the Hasofer-Lind method, the random variables X are assumed to be normally distributed. The Rackwitz-Fiessler algorithm is similar to the Hasofer-Lind iteration method except that necessary to implement the calculation of the mean and standard deviation of the equivalent normal

variables. The Rackwitz-Fiessler method is also called the HL-RF method since Hasofer and Lind originally proposed the iteration algorithm, which Rackwitz and Fiessler later extended to include random variable distribution information (Choi *et al*., 2006). A flow chart of the algorithm is given in **Fig (3.3)**

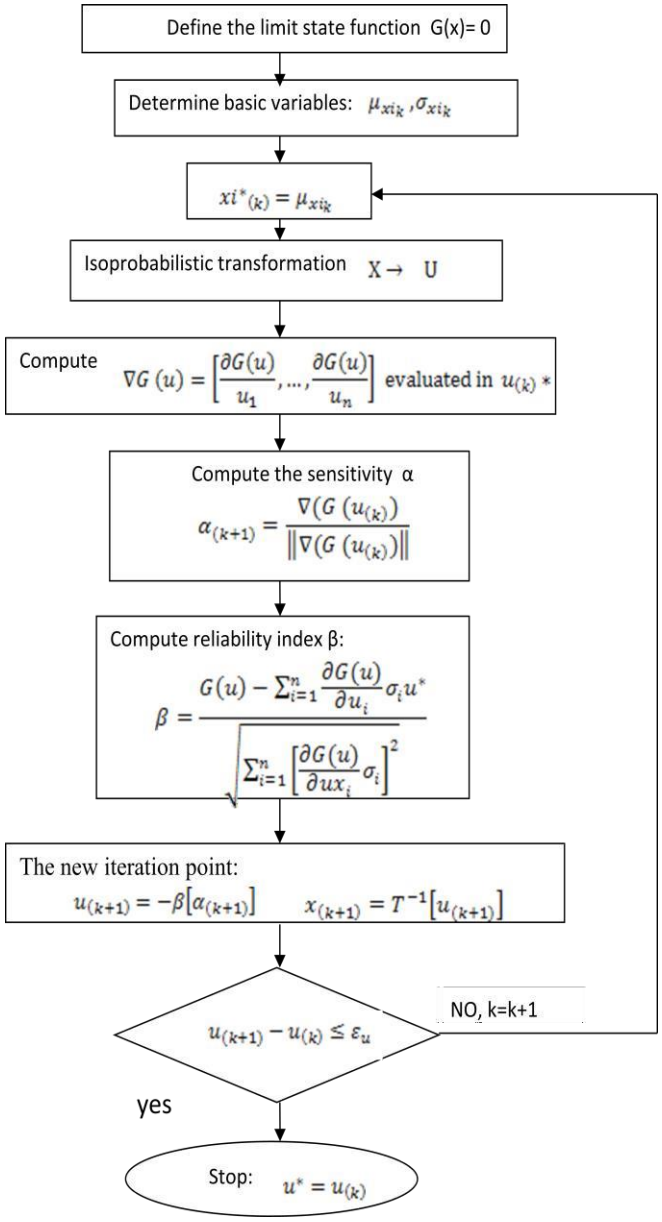

Figure 3. 2:Flowchart of Hasofer-Lind Rackwitz Fiessler algorithm

This algorithm is very effective, but it lacks robustness. Abdo and Rackwitz (1991) and Liu and Der Kiureghian (1991) proposed a more robust version of the HL-RF method.

1) Abdo-Rackwitz algorithm: To avoid the calculation of the Hessian matrix, Abdo and Rackwitz suggested replacing the Hessian with the identity matrix (first order approach -

HLRF). The iterative system obtains the minimization of the Lagrangian. The optimization problem can be written as:

$$\begin{cases} \text{minimize } \|u^2\| \text{ , as objective function} \\ \text{subject H(u)} \leq 0 \end{cases} \tag{3.18}$$

Several strategies, including feasible directions, penalty methods, dual methods, and the Lagrange multiplier approach, are available to address this optimization problem.

The advantage of the Abdo-Rackwitz technique is the time savings achieved by eliminating Hessian computations. This approach is highly efficient for a substantial quantity of random variables exceeding 50. It converges marginally slower than the SQP approaches but significantly faster than the traditional Rackwitz-Fiessler algorithm. The Abdo-Rackwitz algorithm offers the optimal balance between cost and accuracy.

Step3: Line search

The solution of the iterative optimization of equation (3.9) involves determining the direction of descent. To ensure the convergence of the algorithm, a convergence acceleration factor based on the Augmented Lagrangian Technique can be introduced. This factor denotes the length of the increment. The new iteration point becomes:

$$u^{k+1} = u^k + \alpha^k \Delta u^k \tag{3.19}$$

where (α^k) is found by minimizing the descent function (Merit function) proposed by Abdo and Rackwitz (Abdo & Rackwitz, 1991), (Liu & Der Kiureghian, 1991).

Step4: Stopping criteria

Convergence is attained at iteration $(k+1)$. The three convergence criteria applicable for concluding the MPP search process in FORM and SORM are:

$$u_{(k+1)} - u_{(k)} \leq \varepsilon_u \tag{3.20}$$

$$\left|\frac{G(x^*)}{G(x_0)}\right| \leq \varepsilon_G \tag{3.21}$$

$$\left|\frac{\beta^{k+1}-\beta^k}{\beta^k}\right| < \varepsilon_\beta \tag{3.22}$$

Where ε_u, ε_G, and ε_β are convergence values specified by the user. For example, we can take $\varepsilon_G = 10^{-4}$ and $\varepsilon_\beta = 10^{-3}$ (Lemaire & Pendola, 2006).

3.3.1.3 Results of a reliability analysis

Reliability analysis produces different products. In addition to the reliability index β and failure probability P_f, there are important factors and design point coordinates.

1. Approximation of the failure probability

The FORM and the SORM are widely used in reliability estimation. They provide an approximate solution to estimate a system's failure probability based on a limit state function **(Fig 3.4).**

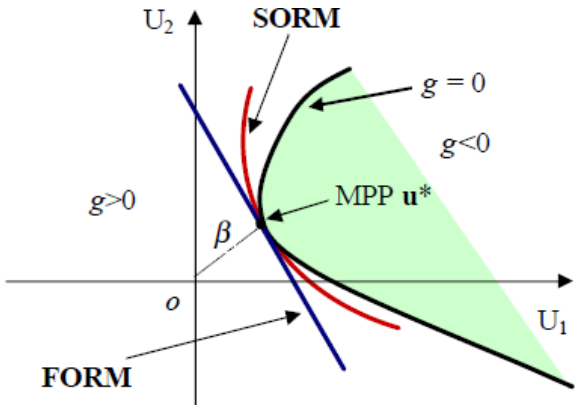

Figure 3. 3: Principle of the FORM and SORM approximation [Phimeca Software]

A. First Order Reliability Method *FORM*

The designation "First Order Reliability Method" (FORM) is derived from the approximation of the performance function G (x, d) using the first order Taylor expansion (linearization), as illustrated in Fig (3.4). The FORM method is utilized to calculate the reliability index β, followed by the approximation of the failure probability. (Choi *et al.* 2006). The failure probability is given by:

$$P_f = \int_{-\infty}^{0} \frac{1}{\sigma_G \sqrt{2\pi}} exp\left(-\frac{1}{2}\beta^2\right) dG \quad (3.23)$$

$$P_f(FORM) = \Phi(-\beta) = 1 - \Phi(\beta) \quad (3.24)$$

This method gives a good estimation in the case of a low-performance surface curvature. However, it does not take into account the curvatures of the limit stat surface at the MPP. This negligence can lead to incorrect and unsatisfactory results.

B. Second Order Reliability Method (SORM)

As its name implies, this method uses the second-order Taylor expansion to approximate the performance function at the MPP ($\boldsymbol{u}*$).

The limit stat is approached by an osculating parabolic at the design point (***Fig 3.4)***.

So, calculating reliability is then more complex. We assume that $H(u)$ is twice differentiable at the design point, then the second-order development of Taylor around the point u^* is defined:

$$H_Q(u) = H(u^*) + \nabla H(u^*)^T(u - u^*) + \frac{1}{2}(u - u^*)^T \nabla^2 H(u^*)(u - u^*) \quad (3.25)$$

$H_Q(u)$ Quadratic approximation of $H(u)$

$\nabla^2 H(u^*)$ Hessian matrix of $H(u)$ at the design point u^*.

The process to generate principal curvatures κ_j is given in (Haldar & Mahadevan, 2000) (Choi *et al.*, 2006).

The computational cost associated with this method exceeds that of the FORM approximation. SORM employs analytical quadratic surfaces to approximate the limit state function. The practical algorithms utilized are:

- Breitung's formula (Breitung, 1984) presents a hyper-parabolic surface that shares the same tangent plane and curvatures as the performance function at the design point. The probability of failure is estimated using the following equation:

$$P_f = \Phi(-\beta)\left(\prod_{i=1}^{n-1}\frac{1}{\sqrt{1+\beta_{k_i}}}\right) \text{ , For } \beta \to \infty \text{ and } \beta\kappa j < 1 \text{ for all } j. \quad (3.26)$$

κ_i (κ_1,..., κ_{n-1}) are the main curvatures of the limit stat function G at the design point.

The hypersphere method consists of estimating the probability based on the average curvature at the design point (Der Kiureghian & Liu, 1986).

- Tvedt's (Tvedt L., 1983) method is more sophisticated, but the result is often very close to Breitung's value.

2. Design point

This result gives the coordinates of all random variables at MPP in the physical and normalized spaces.

$$u^* = \beta.\alpha^* \quad (3.27)$$

$$x^* = \sigma.u^* + \mu \quad (3.28)$$

3. Important Factors

The FORM method products contain important factors. In general, they identify the weight of different variables and distinguish the types of variables that have resistance or loading effects. These factors include direction cosines, sensitivity, and elasticity reliability factors.

A. direction cosines

The Direction Cosines define the sensitivity of the reliability index with respect to normalized variables *U**. Direction Cosines, also known as α_i, represent the relative weights of the various normalized variables. So, a random variable that has a low direction cosines can be considered deterministic; on the other hand, a variable whose high direction cosines indicate that the variable has deviated from its average value to cause failure. Furthermore, each variable has a positive sign (+), represents a loading, or a resistance variable with a negative sign (-). The direction cosines can be calculated by:

$$\alpha_i = -\frac{\partial \beta}{\partial u_i}\Big|_{u_i^*} \tag{3.29}$$

$$u_i{}^* = \beta_{HL}.\alpha_i \tag{3.30}$$

$$\sum_{i=1}^{n} \alpha_i{}^2 = 1 \tag{3.31}$$

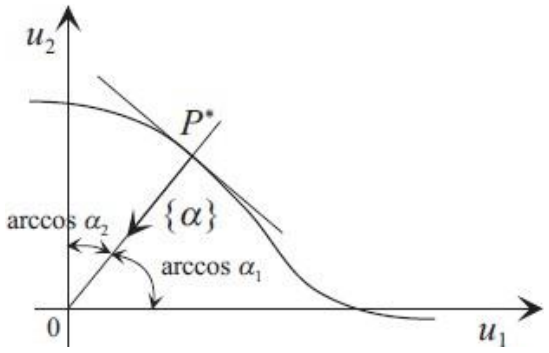

Figure 3. 4: Direction cosines at the MPP [Phimeca Software]

B. Sensitivity and elasticity of the reliability index

The sensitivity factors define the influence of parameter variation on the progression of the reliability index. The calculation of these factors is performed using the derivative of the reliability index with respect to each parameter. It is possible to define the sensitivity factors S_{pi} of β associated with a parameter *pi* (the mean value or the standard deviation of a stochastic variable or a constant in the failure function) by:

$$S_{pi} = \frac{\partial \beta}{\partial pi} = \frac{\partial \beta}{\partial u_i}.\frac{\partial u_i}{\partial pi}\Big|_{u_i^*} \tag{3.32}$$

For independent Gaussian random variables, the sensitivity factors of the reliability index with respect to the average are $S_{\mu i}$ and standard deviations $S_{\sigma i}$ are expressed very simply by:

$$S_{\mu i} = \frac{\alpha_i}{\sigma_i} \tag{3.33}$$

$$S_{\sigma i} = -\frac{\beta \alpha_i{}^2}{\sigma_i} \tag{3.34}$$

The sensitivity is a real measure and does not allow the comparison between different variables. Some time, for reasons of interpretation, it is necessary to use elasticity rather than sensitivity. Elasticity is a normalized sensitivity which is expressed in the following way:

The elasticity factors E_{pi} of β associated with a parameter *pi*:

$$E_{pi} = \frac{\partial \beta}{\partial p_i} \frac{p_i}{\beta} \tag{3.35}$$

The elasticity factors of the reliability index relative to average $E_{\mu i}$ and standard deviations $E_{\sigma i}$ for Gaussian random variables are expressed as:

$$E_{\mu i} = -\frac{\alpha_i u^*}{\beta} \tag{3.36}$$

$$E_{\sigma i} = -\alpha_i^2 \tag{3.37}$$

C. Reliability Sensitivity and elasticity factors

The The sensibility S_i and elasticity E_i of R around u_i^* are defined as:

The reliability sensibility relative to average: $S_{\mu i} = \frac{\partial R}{\partial \mu_i}$ (3.38)

The reliability sensibility relative to standard deviation: $S_{\sigma i} = \frac{\partial R}{\partial \sigma_i}$ (3.39)

The reliability elasticity relative to average: $E_{\mu i} = \frac{\mu_i}{P_f} \frac{\partial R}{\partial \mu_i}$ (3.40)

The reliability elasticity relative to standard deviation: $E_{\sigma i} = \frac{\sigma_i}{P_f} \frac{\partial R}{\partial \sigma_i}$ (3.41)

Based on sensitivity and elasticity results, all parameters can be treated according to their impact on the calculated results.

FORM is highly efficient for problems with many random variables (over 50) and performs well when the limit-state surface has a single minimal distance point and is nearly linear around the design point. However, its accuracy decreases for highly nonlinear failure surfaces. SORM, while requiring more computational effort, provides better second-order estimates. However, it does not inherently verify whether the Most Probable Point (MPP) is a global or local minimum.

3.3.2 Monte Carlo Simulation

Monte Carlo Simulation (MCS) is a probabilistic method that evaluates a system's response by randomly sampling input variables (***Fig 3.6)***. Failure probability is calculated by the estimated value of the analytical integral of equation (3.2). From the computation time viewpoint, simulation methods are the most expensive. However, from the accuracy perspective, they may be the best way to assess failure probability. The simulations facilitate the acquisition of reference results and enable the monitoring of second-order estimates.

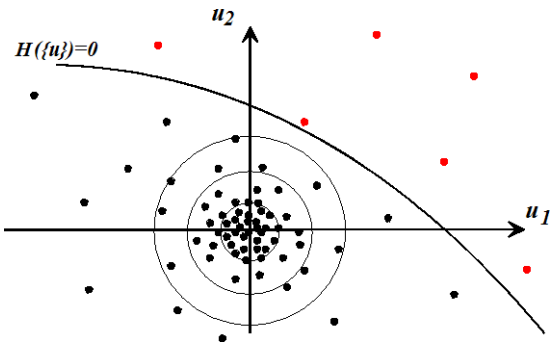

Figure 3. 5: Classical Monte Carlo simulations (Lemaire et al., 2013).

To estimate failure probability using a Monte Carlo method, we generate a large number of random values according to known statistical laws and count the number of cases where $G(x)$ is negative(failure cases).

$$P_f = \frac{N_F}{N} \tag{3.42}$$

N_F: the number of samples leading to failure, and N: the total number of samples.

3.3.2.1 Monte Carlo Simulation steps

According to Haldar and Mahadevan (2000), MCS is implemented in six steps:

1) Define the problem using all random variables.;

2) Model the probabilistic characteristics of all random variables based on the probability density function and its parameters.;

3) Generate N samples of random variables;

4) Evaluate the failure rate using the performance function for each set of values generated by the random variables;

5) Extract probabilistic information from the number of assessments;

6) Determine the accuracy and efficiency of the simulation.

3.3.2.2 Statistical estimates

The indicator function of the failure domain denoted $I_D(X)$ takes the following values

$$\begin{cases} I_D(G(d,x)) = 1 & \text{si } G(d,x) \leq 0 \\ I_D(G(d,x)) = 0 & \text{si } G(d,x) > 0 \end{cases} \quad (3.43)$$

Thus, the probability estimator is written then for N prints $U_1, \ldots\ldots, U_N$ performed

$$P_f = \frac{1}{N}\sum_{i=1}^{n} I_D(X_I) \quad (3.44)$$

The estimate's coefficient of variation is expressed as:

$$cov = \sqrt{\frac{1-P_f}{NP_f}} \quad (3.45)$$

For an objective $cov = 0.1$ and a probability $P_f = 10^{-n}$, we obtain $N = 10^{n+2}$ (Lemaire *et al.*, 2013).

3.3.2.3 Features of Monte Carlo simulation

Monte Carlo Simulation is easy for engineers without knowledge of probability and statistics. It supports any performance function and probability distribution. It is computationally resilient and converges after enough runs. Unlike other approaches, the number of random variables does not affect its accuracy. However, Monte Carlo Simulation may be computationally intensive in reliability analysis.

3.3.3 Reliability-based Design Optimization Methods

Reliability-based design optimization (RBDO) is a methodology that combines principles of structural reliability analysis and mathematical optimization to design engineering systems that meet certain reliability criteria. RBDO methods aim to find the optimal design that maximizes the system performance while satisfying specified reliability constraints.

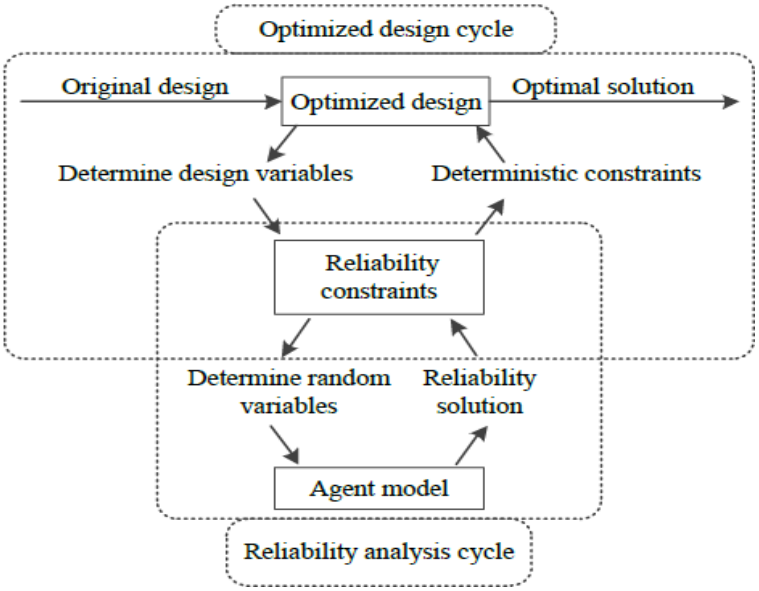

Figure 3. 6: Schematic diagram of the RBDO problem (Dawei et al., 2021)

RBRDO stands for "Reliability-Based Robust Design Optimization." It combines the approach of robust design with reliability analysis to ensure that all unknowns are taken into account during the design process. This procedure aims to achieve a reliable design that fulfils all performance requirements with the least possible sensitivity to changes in input variables. The RBDO involves optimization performed simultaneously, considering performance objectives and reliability constraints. The most commonly used solution techniques are single-loop, double-loop, and decoupled approaches.

3.3.3.1 Single-Loop Method

The single-loop method, or nested approach, integrates optimization and reliability analysis into a single loop, reducing computational cost compared to the double-loop method. It treats uncertain parameters as random variables and updates design variables while considering probabilistic behavior. However, its accuracy may be affected as it relies on the mean values of uncertain parameters during each iteration.

3.3.3.2 Double-loop method

The double loop method is a classical approach for the RBDO challenge. It consists of nesting the reliability analysis within the optimization loop. The design optimization loop is considered external, while the reliability assessment loop is classified as internal, as shown in Fig (3.8). This approach is expressed via two techniques: The Reliability Index Approach (RIA) and The Performance Measure Approach (PMA).

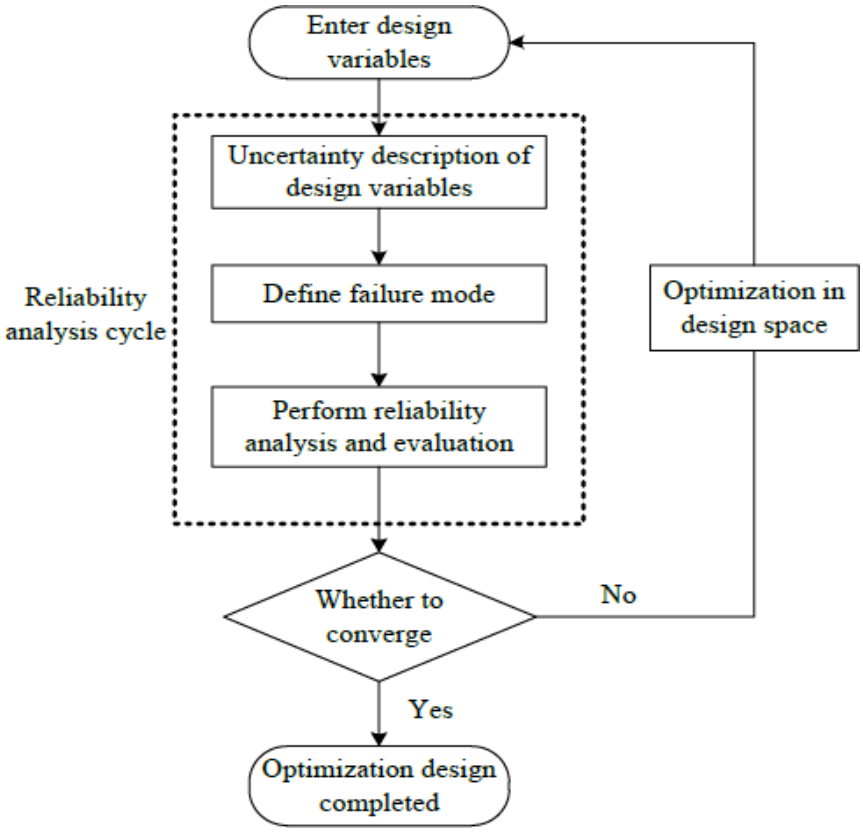

. **Figure 3.7:** Optimization flow chart of the double-loop method (Dawei et al., 2021).

A. Approach Reliability Indicator Approach (RIA)

The method is referred to as the Reliability Index Approach (RIA) introduced by Tu et al. (1999). Kwak and Lee (1987) described a procedure for minimum weight under many probability constraints. This approach utilizes a sensitivity estimation technique to address optimization and reliability challenges. The reliability index was successfully calculated using a Lagrange multiplier in this method. This approach specifies the probability constraint in terms of the target reliability index. The target reliability index indicates the required level of reliability that the system is expected to attain.

The mathematical representation of the RBDO double-loop algorithm utilizing RIA is outlined as follows:

$$\begin{cases} min\{f(d,\mu_{xi})\} \\ \beta_i(d,x) \le \beta^T \\ \mu_{x_{il}} \le \mu_{x_i} \le \mu_{x_{iu}} \\ d_l \le d \le d_u \end{cases} \tag{3.46}$$

where

$$\begin{cases} min\ \beta_i = \|u\| \\ under\ the\ constraint\ \ H(u_i) = 0 \end{cases} \tag{3.47}$$

β_i represents the reliability index associated with the design vector, and β^T denotes the target reliability index.

B. Performance Measure Approach (PMA)

A novel methodology was introduced by Der Kiureghian et al. (1994), referred to as inverse FORM (iFORM). In their 2001 study, Tu et al. (1999) designated this method as the Performance Measure Approach (PMA). This method closely resembles RIA; however, the minimum acceptable reliability index is set to the norm, which is based on the uncertain parameters obtained from the iFORM (Lee et al., 2002). The Performance Measure Approach (PMA) formulates probability constraints in terms of performance measures instead of the reliability index.

The RBDO problem utilizing the PMA method, as developed by Liang et al. (2004), is expressed as follows:

$$\begin{cases} min\{f(d,\mu_x)\} \\ G_p(d,\mu_x) \geq 0 \\ d_l \leq d \leq d_u \\ \mu_{x_{il}} \leq \mu_{x_i} \leq \mu_{x_{iu}} \end{cases} \tag{3.48}$$

The performance measure G_p is derived from the subsequent reliability minimization problem:

$$\begin{cases} G_p = min\ H(u) \\ \|U\| = \beta^T \end{cases} \tag{3.49}$$

C. Decoupled method: Sequential optimization and reliability assessment (SORA)

The SORA method utilizes a decoupled approach consisting of multiple cycles of deterministic optimization followed by reliability assessment. In each cycle, optimization and reliability assessment are treated as separate processes; the reliability assessment is performed solely after the deterministic optimization to confirm the feasibility of constraints (**Fig 3.9).** The essential aspect of this method involves adjusting the limits of violated constraints towards the feasible direction, utilizing the reliability information acquired in the preceding cycle. The design undergoes rapid enhancements from one cycle to the next, resulting in a significant improvement in computational efficiency (Du and Chen 2004). The following provides an overview of the SORA process:

1) Design Initialization: SORA begins with an initial design

2) Optimization: The optimization phase aims to improve the design by searching for the optimal values

3) Reliability Assessment: Once the optimization phase provides a new design, reliability analysis is performed to evaluate the reliability of the system. This involves considering uncertainties in design variables

4) Reliability-Based Adjustment: Design variables are modified according to reliability assessment results to meet reliability constraints.

5) Iteration: The optimization and reliability assessment steps are repeated iteratively until a satisfactory design is achieved.

The RBDO problem can be formulated using the SORA method as follows:

$$\begin{cases} \min f(d^k, {\mu_x}^k) \\ G(d^k, \mu_x^k - s_i^{k+1}, P_{MPP}^{k+1}) \geq 0 \\ d_k^l \leq d_k \leq d_k^u \, , \mu_k^l \leq \mu_k \leq \mu_k^u \end{cases} \tag{3.50}$$

The constraint boundary is shifted towards the feasible region using the shifting vector s_i^{k+1}, where:

$$s_i^{k+1} = \mu_x^k - x_{iIMPP}^K \tag{3.51}$$

x_{iIMPP}^K presents the inverse MPP estimated by the reliability assessment loop; for this, a PMA is used to involve the inverse reliability problem.

The performance measure and the MPP u^{*T} corresponding to the desired reliability index (β^T) are calculated after solving the inverse reliability problem defined as:

$$\begin{cases} \min G(U) \\ \text{subject to: } \|u\| = \beta^T \end{cases} \tag{3.52}$$

As indicated in equation (3.50), the newly acquired MPP from the reliability assessment phase is utilized in the subsequent deterministic optimization phase. This optimization process aims to minimize the objective function while considering the lower and upper bounds of the design variables and the design constraints.

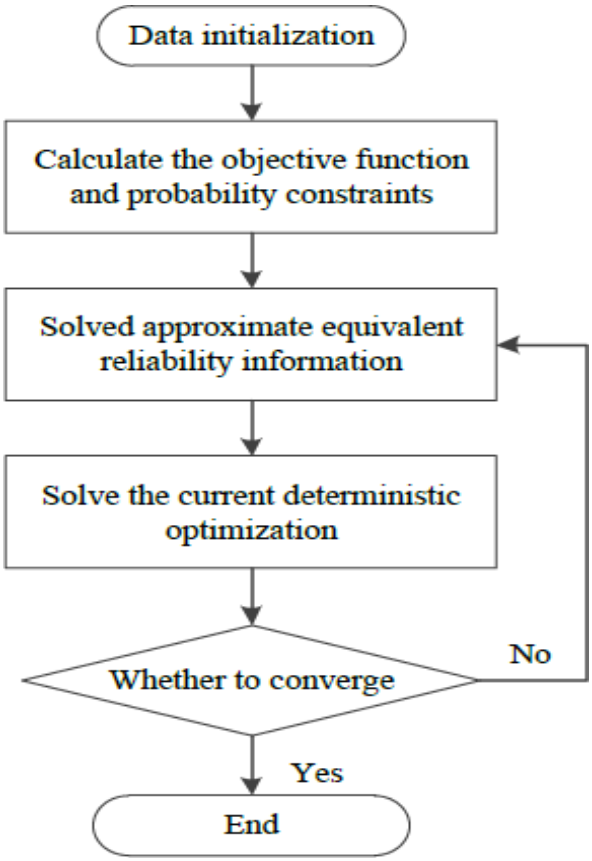

Figure 3. 8: Optimization flow chart of decoupling method (Dawei et al., 2021).

It's important to note that the choice between these RBDO methods depends on the system's characteristics, objectives, and the level of complexity involved.

3.4 Structural System Reliability Method

In two major classifications, structural systems and their sub-systems may be categorized as series systems and parallel systems. A series system meant to operate with components whose reliability is interdependent becomes less reliable in contrast to the parallel system, which allows operation as long as one of its components is functional and thus more reliable. Some special cases can be classified as hybrid, where structures would operate under a combination of series and parallel configurations. In more complicated systems, conditional dependencies may prevail, whereby failure or performance is contingent upon certain conditions. The subsequent sections will explore the above idealizations and present some fundamental results regarding the behavior.

3.4.1 Series system probability of failure

A series system, also known as a "weakest link" system, is one in which the components are arranged such that the failure of one component causes the failure of the entire system. Hence, system reliability is inferior to the reliability of the single components.

Figure 3. 9: A series system reliability model

Let $E_i(i = 1 - n)$ denote failure events with probabilities $P(E_i)$. A system classifies as a series system if the occurrence of any single failure event leads to system failure.

Thus, the probability of system failure, P_{f-sys}, is given by the probability of the union of all failure events.

Thus, the probability of system failure, P_{f-sys}, is given by the probability of the union of all failure events.

$$P_{f-sys} = prob(\cup E_i) \tag{3.53}$$

For two events: $\text{Prob}(E_1 \cup E_2) = P(E_1) + P(E_2) - P(E_1 \cap E_2)$ (3.54)

This formula can be extended for any number of events. This is then the Poincar´e formula:

$$\text{Prob}(\cup_{i=1}^{n} E_i) = \sum_{i=1}^{n} P(E_i) - \sum_{j=2}^{n} \sum_{i=1}^{j-1} P(E_i \cap E_j) + \cdots . + (-1)^n P(E_1 \cap E_2 \cap \ldots . \cap E_n) \tag{3.55}$$

3.4.2 Parallel system probability of failure

The parallel configuration is a simple system setup in which independent functional components are organized in parallel. This configuration provides redundancy, as the system is deemed to fail only when all parallel elements fail at the same time.

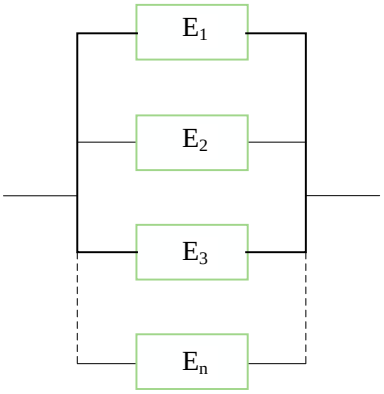

Figure 3.10. A parallel system reliability model

Let $E_i(i = 1 - n)$ denote failure events with probabilities $P(E_i)$. A system classified as a parallel system will fail only if all events occur simultaneously. The system's probability of failure $P_{f-system}$ is defined as the probability of the intersection of the failure events.

$$P_{f-syst} = Prob(\cap E_i) \tag{3.56}$$

$$P(E_1 \cap E_2) = P(E_1)P(E_2|E_1) = P(E_2)P(E_1|E_2) \tag{3.57}$$

Where $P(E_2|E_1)$ signifies 'probability of E_2 when E_1 is realized. The parallel combination fundamentally indicates redundancy; however, this holds solely when the events within the intersection are independent.

3.4.3 Combined and Complex system probability of failure

Certain structural systems incorporate both series and parallel components, resulting in combined systems. These systems may be examined by deconstructing them into more manageable series and parallel components. Furthermore, certain systems integrate conditional elements, which increases their complexity and necessitates the use of more sophisticated analytical techniques.

The discussed idealizations establish a basis for comprehending the reliability and performance of structural systems.

3.4.4 Failure probability bounds of a system

The numerical evaluation of a system's probability of failure is challenging due to multi-dimensional integration over the failure domain. Many methods have been proposed to address numerical difficulties, such as wide-bound estimation (Cornell, 1969) and narrow-bound estimation (Ditlevsen, 1979). Wide bound estimation only considers the component probability of failures, making it easy to estimate, but the bounds can be very wide, resulting in a conservative system probability of failure estimation.

In the context of the narrow-bound method, Ditlevsen's first-order upper bound, which represents the summation of the probabilities of individual component failures, may be employed as the system's probability of failure. Alternatively, Ditlevsen's second-order upper bound can be utilized by taking into account the joint probability of failure.

A. First-Order Probability Of Failure Bounds

The probability of the union of two events is, at most, the sum of their probabilities. If higher-order intersections are negligible, this concept extends to n events. extends to n events.

$$P(\bigcup_i E_i) \approx min(\sum_i Prob(E_i); 1) \quad (3.58)$$

For the system reliability, the first-order lower and upper bounds probability of failure is defined as:

$$\max_{i=1,\dots n} P(F_i) \le P_{f\_sys} \le \min_{i=1,\dots,n} (\sum_{i=1}^{n} P(F_i), 1) \quad (3.59)$$

The lower bound is defined as: $P_{f\_sys}^{-} = \max_{i=1,\dots,n} P(F_i)$ (3.60)

The upper bound is defined as: $P_{f\_sys}^{+} = \min_{i=1,\dots,n} (\sum_{i=1}^{n} P(F_i), 1)$ (3.61)

B. Second-Order Probability Of Failure Bounds

Second-order bounds improve failure probability estimation by incorporating additional terms that account for the joint probability of failure events. These terms represent the likelihood of simultaneous failures, refining the accuracy beyond simple first-order approximations. The probability of intersection failure is determined using the FORM. FORM provides an efficient way to estimate failure probabilities by approximating the limit-state function with a linear model in the standard normal space, ensuring a more precise reliability assessment.

Second-order bounds are obtained by retaining terms such as $P(E_i \cap E_j)$

$$P_{f\_sys} = \sum_{i=1}^{m} P(F_i) - \sum \sum_{i<j}^{m} P(F_i \cap F_j) + \sum \sum \sum_{i<j<k}^{m} P(F_i \cap F_j \cap F_k) \dots . \quad (3.62)$$

The third order in the equation(3.61) is neglected, so the P_{f_sys} become:

$$P(F) \ge P(F_1) + \sum_{i=2}^{m} \max\{[P(F_i) - \sum_{j=1}^{i-1} P(F_i \cap F_j)], 1\} \quad (3.63)$$

According to the Ditlevsen (Ditlevsen, 1979), the second failure probability bounds are

The lower bound is defined as:

$$P_{f\_sys} \ge P(F_1) + \max\{\sum_{i=2, j<i}^{k \le m} [P(F_i) - P(F_i \cap F_j)]\} \quad (3.64)$$

The upper bound is defined as:

$$P_{f\_sys} \le \sum_{i=1}^{m} P(F_i) - \sum_{i=2}^{m} max[P(F_i \cap F_j)] \quad (3.65)$$

C. Correlation of events Ei and Ej

Let us consider events E_i and E_j whose associated hyper-planes in approximation form are respectively Z_i and Z_j. Because $\mathrm{cov}[\{u\}\{u\}^t]$ is the unit matrix. Correlation is then given by:

$$\mathrm{cor}(Z_i, Z_j) = \langle \alpha_i \rangle \{\alpha_j\} = \rho_{ij} \tag{3.66}$$

The geometric interpretation is immediate; correlation is equal to the cosine of the angle formed by the vectors normal to the two hyper-planes(θ_{ij}).

$$\theta_{ij} = \arccos(\rho_{ij}) \tag{3.67}$$

D. Probability bounds of the intersection $P(E_i \cap E_j)$

- ***Case of positive correlation***

by the dihedron limited by the two hyper-planes on the side of the failure events.

To evaluate this quantity, two new planes are introduced (Lemaire et al., 2013):

✓ Z_A is perpendicular to Z_i the associated event is $A = E_{\perp i}$

✓ Z_B is perpendicular to Z_j the associated event is $B = E_{\perp j}$

Figure.3.12. represents the two hyperplanes Zi and Zj . $P(E_i \cap E_j)$is represented.

The distances of planes Z_i, Z_j, Z_A, and Z_B from the origin are respectively β_i, β_j, a and b, and the associated probabilities are:

$$\begin{cases} P(E_i) = \Phi(-\beta_i) \\ P(E_j) = \Phi(-\beta_j) \end{cases} \tag{3.68}$$

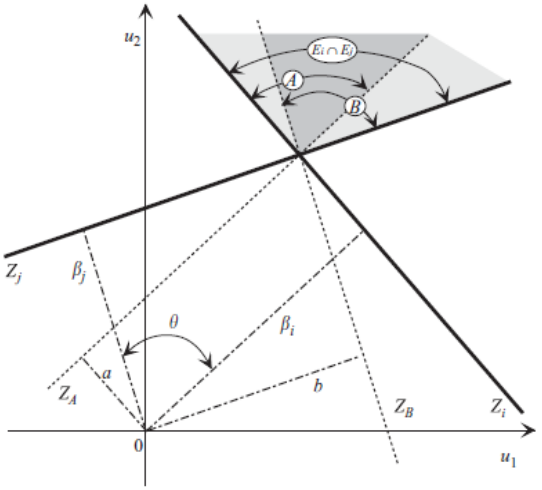

Figure 3.11: Positive correlation between events [Lemaire,(2013)]

$$\begin{cases} P(A) \le P(E_i \cap E_j) \\ P(B) \le P(E_i \cap E_j) \end{cases} \tag{3.69}$$

$$P(A) + P(B) \ge P(E_i \cap E_j) \tag{3.70}$$

Hence:

$$\max(P(A); P(B)) \le P(E_i \cap E_j) \le P(A) + P(B) \tag{3.71}$$

A calculation in the triangles gives the equations:

$$a = \frac{\beta_j - \rho_{ij}\beta_i}{\sqrt{1-\rho_{ij}{}^2}} \tag{3.72}$$

$$b = \frac{\beta_i - \rho_{ij}\beta_j}{\sqrt{1-\rho_{ij}{}^2}} \tag{3.73}$$

From the observation that P(A) is the probability of the intersection of half-spaces limited by the orthogonal hyper-planes Z_i and Z_j, it results that:

$$P(A) = \Phi(-\beta_i)\,\Phi(-a) \tag{3.74}$$

$$P(B) = \Phi(-\beta_j)\,\Phi(-b) \tag{3.75}$$

In this case, the bounds of intersection $P(G_i \cap G_j)$ are:

$$\max(P(A); P(B)) \le P(G_i \cap G_j) \le P(A) + P(B) \tag{3.76}$$

- ***Case of negative correlation***

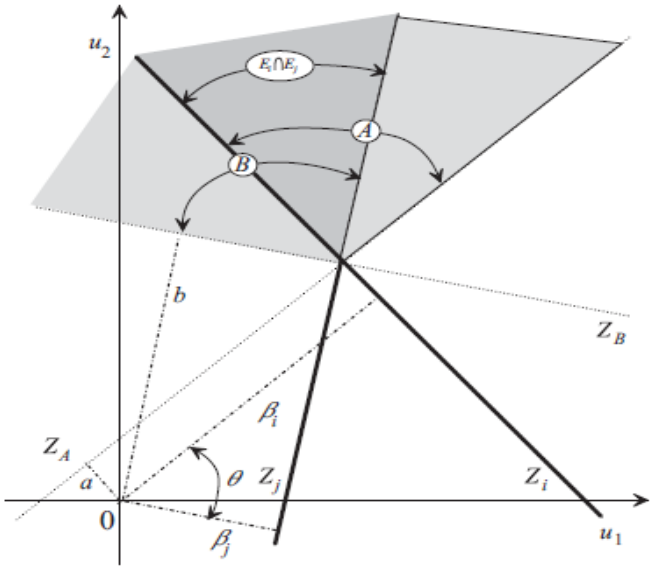

Figure 3.12: Negative correlation between events [Lemaire,(2013)]

Figure.3.13**.** shows a negative correlation.

$$P(A) \ge P(E_i \cap E_j) \tag{3.77}$$

$$P(B) \ge P(E_i \cap E_j) \tag{3.78}$$

The bounds of intersection:

$$0 \le P(E_i \cap E_j) \le \min(P(A); P(B)) \tag{3.79}$$

3.5 Conclusion

In this chapter, we have presented the main structural reliability methods used in mechanical components. These methods effectively treat the majority of problems. The first techniques based on knowledge of the design point (FORM /SORM) are the least expensive. They have been specifically developed for the study of small probabilities and offer a good balance between accuracy and efficiency.

Another advantage of these methods is the sensitivity factors analysis associated with the FORM method. Indeed, based on the random behavior of variables, these factors can determine which parameters have the most significant influence on the failure probability. Unfortunately, these methods give inaccurate results in high nonlinearity surface limit cases.

The second technique is the Monte Carlo Simulation, which has the advantage of being able to deal with the majority of problems. It can be adapted to all problems regardless of the properties of the limit state function. However, the use of a Monte Carlo Simulation is not always satisfactory. The excessive cost of the direct approach pushes us to propose alternative methods.

Furthermore, we have discussed Reliability-Based Design Optimization (RBDO) techniques, which are focused on finding the optimal design that maximizes system performance while considering uncertainties. SORA offers several advantages for solving the RBDO problem. SORA provides a systematic and efficient approach to balancing performance and reliability considerations.

Finally, this chapter describes the structural system reliability and presents two methods, which are the first and the second-order failure probability bounds. First-order bounding methods are easy computations but are often poorer estimates of failure probability. Second-order bounds are more accurate by incorporating correlation effects between failure events. Thus, using second-order bounds will definitely yield a better estimate of system reliability, especially when dependency between the components plays a significant role.

To test the quality and robustness of these methods, they are applied to analyze the reliability of speed reducer components in chapters 4, 5 and 6.

CHAPTER 4: REDUCTION DIMENSION MODEL FOR SPEED REDUCER SUBSYSTEM RELIABILITY

4.1 Introduction

Speed reducers play a vital role in many mechanical systems and are often subjected to continuous operation under harsh conditions. Due to their demanding nature, speed reducers can encounter various problems that can lead to failure and result in significant downtime losses for the system. Thus, integrating reliability analysis into the design process for these systems is essential to designing reliable products and preventing designers from repeating the same mistakes.

System reliability analysis is inherently challenging, particularly when accounting for the correlations between component failure modes. This consideration necessitates complex multidimensional integration, which is often intractable through analytical methods. Furthermore, the presence of a large number of random variables in the models increases the complexity of the analysis, rendering it computationally intensive.

To address the aforementioned limitations, dimension reduction techniques are employed in system reliability analysis. These techniques typically aim to reduce either the number of failure modes or the number of random variables, often under specific assumptions.

While such methods simplify the computational process, they can also introduce a considerable degree of uncertainty, that can significantly affect the system's reliability assessment, particularly in systems characterized by low-probability failure modes. These systems tend to be highly sensitive to small parameter variations, which can diminish the precision of the reduction techniques and potentially compromise the reliability of the estimated results.

This chapter introduces the Structural System Reliability-Based Dimension Reduction Method (SSR-DRM), a novel approach to probabilistic system failure analysis grounded in the results of the First Order Reliability Method (FORM). The SSR-DRM-FORM framework aims to enhance reliability assessments by constructing smaller, more manageable subsystem models, guided by sensitivity factors and accounting for correlations between failure modes. This method ensures that the variability of the reduced variables is accurately captured while preserving the interdependencies among all subsystem models. As a result, it maintains both the integrity of the original system and the interpretability of the results.

The failure probability of the speed reducer's components is evaluated using the First Order Reliability Method (FORM), based on the Hasofer–Lind algorithm described in

Chapter 3. The results are compared to those obtained via Monte Carlo Simulation (MCS), which is used as a reference method. Both reliability analysis approaches presented in this chapter have been implemented using MATLAB.

4.2 Structural System Reliability-Based Dimension Reduction Method SSR-DRM-FORM

The objective of the Structural System Reliability-Based Dimension Reduction Method SSR-DRM-FORM is to reduce the complexity of a high-dimensional reliability problem presenting correlated events while retaining the variability of reduced variables needed to assess the system's reliability accurately.

4.2.1 New strategy applied for Dimension reduction method

The proposed methodology is divided into two main parts. First, the reliability index of the original system model is computed to derive sensitivity factors, which are used to identify variables with lower influence on system failure. Based on the results of the sensitivity analysis and correlation analysis, equivalent variables are then constructed to reduce the dimensionality of the model. Subsequently, the reduced models are evaluated using both the First Order Reliability Method (FORM) and Monte Carlo Simulation (MCS) to validate their effectiveness in reliability assessment. The detailed steps of this methodology are presented in the following sections.

Part 1: Reliability Analysis of the Original System

In this part, the reliability analysis of the speed reducer components is conducted using the First Order Reliability Method (FORM), as detailed in Chapter 3.

- **Step 1:** Identify and describe the various subsystems of the speed reducer, and define the associated failure modes with precision.
- **Step 2:** Formulate the limit state functions corresponding to each failure mode. Identify and characterize the random variables that influence the performance of the system.
- **Step 3:** Evaluate the failure probability of the speed reducer components using FORM, treating all model variables as random. Perform a sensitivity analysis to identify the less influential random variables, which will serve as the basis for constructing a reduced-dimensional model.

Part2: Construction of Reduced Variables and Dimension Reduction Models

In this part, the results obtained from the FORM analysis are used to reduce the size of the original model by decreasing the number of random variables involved in the reliability assessment.

- **Step 1**: Identify the variables eligible for dimensional reduction based on their direction cosine values (denoted as α_i). A conservative threshold of $\alpha_i \leq 20\%$ is adopted—this falls within the typical range of 20% to 30% used in practice. Variables below this threshold are considered to have limited influence on system failure and are therefore selected for reduction. During this process, special attention is given to preserving the correlation between subsystem models.
- **Step 2:** Construct new equivalent variables $\boldsymbol{x_{eq_i}}(\mu_{\boldsymbol{eq\_i}}, \boldsymbol{\sigma_{eq\_i}})$ to replace the reduced ones. These equivalent variables are defined in a manner that maintains the statistical characteristics of the original system $\boldsymbol{x_{red\_i}}(\mu_{\boldsymbol{red\_i}}\ , \boldsymbol{\sigma_{red\_i}})$. Specifically, their means and standard deviations are computed to reflect the influence of the eliminated variables.

  A. The mean of equivalent variables $\boldsymbol{\mu}_{\boldsymbol{eq\_i}}$ are defined by:

$$\boldsymbol{\mu}_{\boldsymbol{eq\_i}} = \boldsymbol{F}(\mu_{\boldsymbol{red\_i}}) \tag{4.1}$$

  $\mu_{\boldsymbol{red\_i}}$: The mean values of the reduced variables

  ✓ The standard deviation of equivalent variables $\boldsymbol{\sigma_{eq\_i}}$ are defined by:

$$\boldsymbol{\sigma_{eq\_i}} = \left[\sum_{\boldsymbol{i=1}}^{\boldsymbol{n}} \left(\left(\frac{\boldsymbol{dF(x_{eq\_i}}}{\boldsymbol{dx_{red\_i}}}\right)^{\boldsymbol{2}} . \boldsymbol{\sigma_{red\_i}}^{\boldsymbol{2}}\right)\right]^{\frac{\boldsymbol{1}}{\boldsymbol{2}}} \tag{4.2}$$

  $\boldsymbol{x_{red\_i}}$: Are the reduced variables

  $\boldsymbol{\sigma_{red\_i}}$**:** are the standard deviation of the reduced variables

- **Step 3:** Construct the dimension-reduction models by incorporating the newly defined equivalent variables. Perform a new reliability analysis using FORM to compute the reliability index and the corresponding failure probability for each model.
- **Step 4:** Compare the results obtained from the dimension-reduced models with those from the original full-dimensional reliability analysis, as well as with a deterministic model in which the reduced variables are treated as fixed (non-random). This comparison provides insight into the impact of dimensional reduction on the accuracy of reliability predictions.
- **Step 5:** Validate the reliability results of all models by performing Monte Carlo

Simulation (MCS). The outcomes from MCS are compared with those obtained using FORM to evaluate the robustness and accuracy of the FORM-based dimension reduction approach.

The procedure described above is illustrated in the flowchart shown in **Figure 4.1**

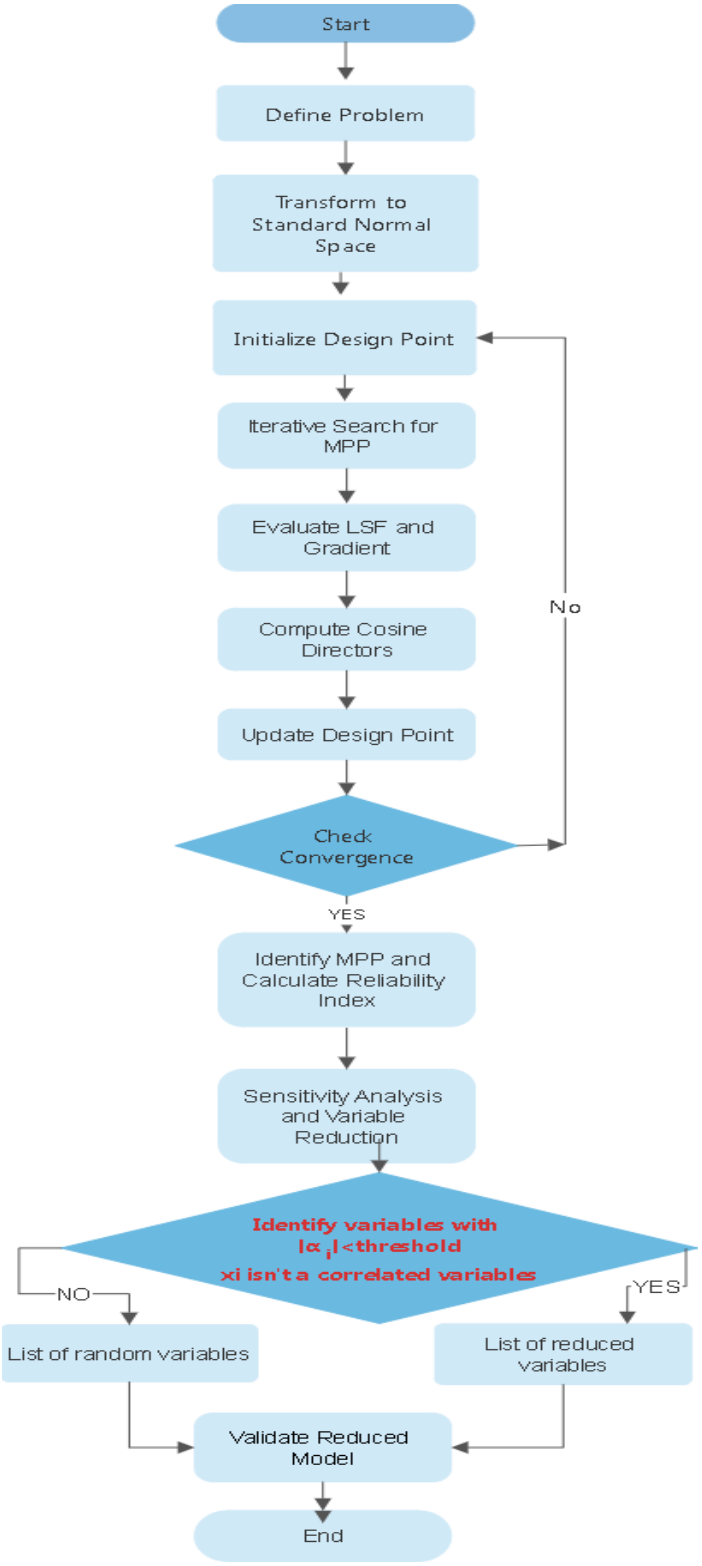

Figure 4.1: Flowchart of the proposed Structural System Reliability-Based Dimension Reduction Method (SSR-DRM- FORM)

4.3 Structural system Reliability-Based Dimension Reduction Method for the speed reducer system

To evaluate the structural reliability of each component within the speed reducer, three distinct types of models must be developed:

1) ***Mechanical model:*** Describe the mechanical behavior of the component, particularly the stress and load distribution under operational conditions.

2) ***Probabilistic model:*** This model captures the uncertainties and inherent randomness associated with material properties, geometric dimensions, loads, and other influencing factors.

3) ***Performance model:*** represented by a limit stat function for each failure mode; the limit state function should be governed by the physical cause of failure in order to ensure a realistic representation.

4.3.1 Presentation of the speed reducer system

It is important to emphasize that conducting a comprehensive reliability analysis necessitates detailed information regarding the specific design and operating conditions of the speed reducer. In this study, the example analyzed is based on a gear speed reducer design sourced from the literature, specifically from [Zhang et al.(2003)], Yang et al. (2012), Ziat (2022)]. The components of this reducer are the following:

- Cylindrical gear pairs
- A transmission shaft (input shaft and output shaft)
- Bearings (input bearing, output bearing).

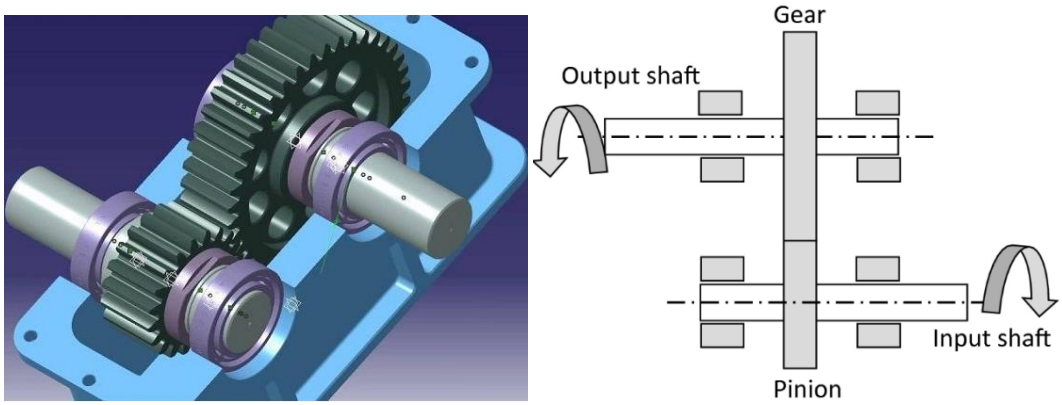

Figure 4.1: Speed reducer system (pinterest 2026)

4.3.2 Structural Reliability-Based Dimension Reduction Model of the gear pair subsystem

This section focuses on the application of the SSR-DRM-FORM to the gear pair component of the speed reducer. The objective is to develop a dimension-reduced model that captures the essential uncertainties and interactions affecting gear performance.

4.3.2.1 Reliability analysis of the original gear pair subsystem

The reliability analysis is conducted by integrating three essential models: the mechanical model; the probabilistic model; and the performance model of the original gear pair subsystem.

A. Mechanical model for the original gear pair

The bending and contact strength of the gear tooth are considered to be the main causes of gear failure in a gear pair.

Table 4. 1: The original physical model for the gear pair subsystem

A standard tooth system of 20° full-depth involutes has been selected. Gear's material 20CrMnMo	
The original model of contact strength is ISO3663 Standard (ISO 6336-2:2006)	
$\sigma_H = Z_H Z_E Z_B Z_\varepsilon \sqrt{\frac{K_A K_V K_{H\beta} K_{H\alpha} F_t (u+1)}{b.m.z_1\, u}} \leq \sigma_{HP}$	(4.3)
$\sigma_{HP} = \sigma_{Hlim}.Z_N Z_L Z_V Z_R Z_W Z_X$	(4.4)
The original model of bending strength is ISO3663 Standard (ISO 6336-3:2006)	
$\sigma_F = Y_F Y_S Y_\beta Y_\varepsilon . \frac{K_A K_V K_{F\beta} K_{F\alpha} F_t}{b.m} \leq \sigma_{FP}$	(4.5)
$\sigma_{FP} = \sigma_{Flim} Y_{ST} Y_{NT} Y_{\delta relT} Y_{RrelT} Y_X$	(4.6)
$T_i = \frac{F_t d_1}{2} = \frac{30.P}{\pi.N_i}$	(4.7)
$d_i = m.z_i$	(4.8)

A. Probabilistic model for the original gear pair

The statistical characteristics of the original random parameters are obtained from bibliographic sources [(Zhang *et al.*, (2003), Ziat (2022)].

Table 4. 2: The statistical parameters of original random variables

Random variables	***(COV)Coefficient of variation***
Mechanical property	0.05
Geometry parameters	0.005
Loads	Determined by the experiment
Material strength	The experiment or the material handbook
Other values	0.033

The standard deviation of each random variable can be calculated using its mean value multiplied by its coefficient of variation from **Tab(4.2)**. We assume that all random variables have a normal distribution($\mathcal{N}$) and are uncorrelated. The probabilistic model is given in **Tab(4.3)**.

Table 4. 3: Random variables statistic of the original gear pair subsystem

Random variables of Pinion Bending stress	***Symbol***	***variables of pinion bending***	***variables of gear bending***	***Random variables of gear pair Contact stress***	***Symbol***	***Mean values and standard deviations***
Normal module	*m(mm)*	$\mathcal{N}$ (3.5 , 0.0175)		***Normal module***	*m(mm)*	$\mathcal{N}$ (3.5 ,0.0175)
Active face width	*b(mm)*	$\mathcal{N}$ *(37.5, 0.1875)*		***Work harden factor***	Z_W	$\mathcal{N}$ *(1,0.033)*
Rotational Speed	N_1 *(N)*	$\mathcal{N}$ *(1500, 150)*	$\mathcal{N}$ *(375, 37.5)*	***Gear Ratio***	u	$\mathcal{N}$ *(4, 0.02)*
Pignon Tooth number	z_p	*18*	*72*	***Power***	*P(watt)*	*N(7500, 750)*
Experimental gear bending fatigue strength	σ_{Flim} N/mm^2	$\mathcal{N}$ *(310 , 62)*		***Experimental flank contact fatigue strength***	σ_{Hlim} N/mm^2	$\mathcal{N}$ *(1300,156)*
Tooth form factor	Y_F	$\mathcal{N}$ *(2.36,0.07788)*	$\mathcal{N}$ *(2.14,0.07062)*	***Contact ratio factor***	Z_ε	$\mathcal{N}$ *(0.81,0.00405)*
Dedendum stress concentration factor	Y_s	$\mathcal{N}$ *(1.75,0.05775)*	$\mathcal{N}$ *(1.94,0.06402)*	***Nodal field factor***	Z_H	$\mathcal{N}$*(2.32, 0.0116)*
Contact ratio factor	Y_ε	$\mathcal{N}$*(0.715, 0.003575)*		***Elastic factor***	$\frac{Z_E}{\sqrt{N/mm^2}}$	$\mathcal{N}$ *(189.8, 9.49))*
Helix angle factor	Y_β	$\mathcal{N}$ *(0.8,0.004)*		***Helix angle factor***	Z_β	$\mathcal{N}$ *(0.957,0.004785)*
Experimental gear dedendum stress concentration factor	Y_{ST}	$\mathcal{N}$ *(2.1 , 0.0693)*		***Lubricant factor***	Z_L	$\mathcal{N}$ *(0.92, 0.03036)*
Life factor	Y_{NT}	$\mathcal{N}$ *(1 , 0.033)*		***Life factor***	Z_{NT}	$\mathcal{N}$ *(1, 0.033)*
Relative sensitive factor	$Y_{\delta relT}$	$\mathcal{N}$ *(0.99,0.03267)*	$\mathcal{N}$ *(1.01,0.03333)*	***Tooth fineness factor***	Z_R	$\mathcal{N}$ *(1.03, 0.03399)*
Relative surface condition factor	Y_{RrelT}	$\mathcal{N}$ *(1.065, 0.035145)*		***Velocity factor***	Z_V	$\mathcal{N}$ *(1.04, 0.03432)*
Size factor	Y_X	$\mathcal{N}$ *(1, 0.033)*		***Size factor***	Z_X	$\mathcal{N}$ *(1, 0.033)*
Work condition factor	K_A	$\mathcal{N}$ *(1, 0.033)*		***Work condition factor***	K_A	$\mathcal{N}$ *(1, 0.033)*
Dynamic load factor	K_V	$\mathcal{N}$ *(1.484 , 0.1613)*		***Dynamic load factor***	K_V	$\mathcal{N}$ *(1.484, 0.1613)*
Longitudinal load distribution factor	$K_{F\alpha}$	$\mathcal{N}$ *(1.16 , 0.03828)*		***Transverse load distribution factor***	$K_{H\beta}$	$\mathcal{N}$ *(1.68, 0.05544)*
Transverse load distribution factor	$K_{F\beta}$	$\mathcal{N}$ *(1.603 , 0.052899)*		***Longitudinal load distribution factor***	$K_{H\alpha}$	$\mathcal{N}$ *(1.16, 0.03828)*

B. Performance models for the original gear pair

The contact gear performance model is: $\boldsymbol{g_1(x) = \sigma_{HP} - \sigma_H}$ (4.9)

The pinion bending performance model is; $\boldsymbol{g_2(x) = \sigma_{FP-p} - \sigma_{F-p}}$ (4.10)

The gear bending performance model is: $\boldsymbol{g_3(x) = \sigma_{FP-g} - \sigma_{F-g}}$ (4.11)

C. Sensitivity factors analysis of the original gear pair subsystem

In order to perform a dimensional reduction model, a sensitivity-based analysis is performed using the direction cosines factors. This approach identifies which random variables have a minor influence on system reliability and are therefore concerned by the reduction process.

The sensitivity of the reliability index with respect to standard normal variables, commonly referred to as direction cosines, offers two key advantages. First, it helps determine the relative importance of each random variable in influencing the overall system reliability. Second, the sign of the sensitivity factor provides valuable insight into the relationship between the performance function and the physical variables.

A positive sensitivity factor $\boldsymbol{\alpha_i(+)}$ implies that as the corresponding random variable increases, the reliability index decreases, or equivalently, the probability of failure increases. This indicates that the variable functions as a ***stress variable***, meaning that lower values of this variable enhance system reliability. Conversely, a negative sensitivity factor $\boldsymbol{\alpha_i(-)}$ suggests that as the random variable increases, the reliability index also increases, or the failure probability decreases. In this case, the variable acts as a ***resistance variable***, indicating that higher values improve the system's reliability and make it less susceptible to failure.

The variables that have the lower direction cosines are the variables reduced. Cosines directions are calculated using equation (3.29):

$$\alpha_i = -\frac{\partial \beta}{\partial u_i}\Big|_{u_i^*}$$

The direction cosines results are shown in **Table4.4**

Table 4. 4: Direction cosines of the original gear pairs model

Variables of bending stress	***Pinion Bending direction cosines***	***Gear Bending direction cosines***	***variables of contact stress***	***Contact direction cosines***
$\boldsymbol{b}(\boldsymbol{mm})$	***-0.0031***	**-0,003**1	***b(mm)***	***-0.0098***
$\boldsymbol{m}(\boldsymbol{mm})$	***-0.0610***	***-0.060***2	m***(mm)***	***-0.0098***
$\boldsymbol{\sigma_{Flim}}$	***-0.992****1*	***-0,9920***	$\boldsymbol{\sigma_{Hlim}}$	***-0.8539***
P(watt)	***0.0595***	***0.058****4*	***P(watt)***	***0.181****3*
$\boldsymbol{N}$ $(\boldsymbol{rpm})$	***-0.0634***	***0.0617***	***N (rpm)***	***-0.216****4*
Y_F	*0.0201*	0,0198	Z_W	*0.0640*
Y_S	*0.0201*	0,0210	Z_ε	*0.019****6***
Y_ε	*0.00296*	0,0031	Z_H	*0.019****6***
Y_β	*0.00296*	0,0032	Z_E	*0.1880*
Y_{ST}	*-0.0202*	-0,0200	Z_β	*0.019****5***
Y_{NT}	*-0.0202*	-0,0200	Z_L	*-0.1316*
$Y_{\delta relT}$	*-0.0202*	-0,0200	Z_{NT}	*-0.1314*
Y_{RrelT}	*-0.0202*	-0,0200	Z_R	*-0.1296*
Y_X	*-0.0203*	-0,0200	Z_V	*-0.1317*
K_A	*0.0202*	0,0198	Z_X	*-0.1317*
K_V	*0.0643*	0.063*4*	K_A	*-0.1317*
$K_{F\alpha}$	*0.0202*	0,019*6*	K_V	*0.1946*
$K_{F\beta}$	*0.0202*	0,0030	$K_{H\beta}$	*0.0640*
u	*0.0096*	*0.0096*	$K_{H\alpha}$	*0.0640*

The analysis of direction cosines reveals that in the bending stress model, the variable, $\boldsymbol{\sigma_{Flim}}$ exhibits the highest direction cosine, indicating a strong influence on system reliability and acting as a resistance variable. Similarly, in the contact stress model, $\boldsymbol{\sigma_{Hlim}}$ demonstrates significant sensitivity, also contributing with a resistance effect. These results confirm that $\boldsymbol{\sigma_{Flim}}$ and $\boldsymbol{\sigma_{Hlim}}$ are critical parameters in their respective models. Consequently, due to their substantial impact on reliability, these variables are excluded from the dimensional reduction process.

Both the bending stress (gear and pinion) model and the contact stress model share several common variables, the face width $\boldsymbol{b}, \boldsymbol{m}$, and pinion teeth number $\boldsymbol{z_p}$, all of which exhibit low direction cosine values, indicating minimal influence on reliability.

Power and rotational speed $(\boldsymbol{N}, \boldsymbol{P})$ also have limited impact on the bending stress model; however, they play a more substantial role in the contact stress model, which is consistent with

physical expectations. These two variables directly influence the transmitted torque, defined as ($\boldsymbol{T_i = \frac{30.P}{\pi.N_i}}$), In this relationship, power shows positive sensitivity in the contact model, as it increases the applied torque and consequently enhances contact stress. In contrast, rotational speed shows negative sensitivity, as higher speeds reduce the transmitted torque, thus lowering the associated contact forces. In bending models, stress distribution is primarily governed by bending loads, making torque a less influential factor. Conversely, in contact models, torque directly affects the contact interface by modifying both frictional and normal contact forces, making it a critical variable in the evaluation of reliability.

All these variables contribute to the correlation between both failure mode models. Consequently, excluding them from the reduction dimension process is evident in order to observe their effects on the system reliability assessment.

The remaining variables, having only a minor influence on both models, can be reduced. To ensure consistency and maintain interpretability, these variables are preferably grouped into logically equivalent sets that preserve the functional characteristics of each group and facilitate the interpretation of the results.

For instance, in the bending strength model, all working condition factors can be combined into a single equivalent variable: $\boldsymbol{K_1 = K_A K_V K_{F\beta} K_{F\alpha}}$. For contact stress, a similar reduction is performed for working conditions factors in $\boldsymbol{K_2 = K_A K_V K_{H\beta} K_{H\alpha}}$,

Similarly, the tooth root stress correction factors in the pinion bending model can be grouped as: $\mathbf{Y_{1p} = Y_{Fp} Y_{Sp} Y_\beta Y_\varepsilon}$, and for the gear bending model: $\mathbf{Y_{1g} = Y_{Fg} Y_{Sg} Y_\beta Y_\varepsilon}$.

Tooth root strength adjustment factors can also be consolidated as: $\mathbf{Y_{2p}} = \boldsymbol{Y_{ST} Y_{NT} Y_{\delta relTp} Y_{RrelT} Y_X}$ for pinion, and $\mathbf{Y_{2g}} = \boldsymbol{Y_{ST} Y_{NT} Y_{\delta relTg} Y_{RrelT} Y_X}$ for gear model.

The equivalent tooth contact stress correction factors is $\boldsymbol{Z_1 = Z_H Z_E Z_\beta Z_\varepsilon}$, and the equivalent tooth contact strength adjustment factors is: $\boldsymbol{Z_2 = Z_N Z_L Z_V Z_R Z_W Z_X}$.

4.3.2.2 Dimension Reduction Models for the Gear Pair Subsystem

To preserve the variability of the reduced variables in model reduction, the reduced variables are consolidated into a singular equivalent variable characterized by an equivalent mean and an equivalent standard deviation.

A. Mechanical dimension reduction model for the bending pinion and gear models

The equivalent variables parameters for bending pinion and gear models are in **Tab**(4.5)

Table 4. 5: Physical dimension reduction model for the Bending pinion model

The original model of bending strength is ISO 6336 Standard (ISO 6336-3:2006)

$$\sigma_F = Y_F Y_S Y_\beta Y_\varepsilon . \frac{K_A K_V K_{F\beta} K_{F\alpha} F_t}{b.m} \leq \sigma_{FP} \quad ; \quad \sigma_{FP} = \sigma_{Flim} Y_{ST} Y_{NT} Y_{\delta relT} Y_{RrelT} Y_X$$

The first equivalent variable Tooth Root Stress Correction Factor is:

$$Y_{1p} = Y_{Fp} Y_{Sp} Y_\beta Y_\varepsilon \quad (4.12)$$

$$Y_{1g} = Y_{Fg} Y_{Sg} Y_\beta Y_\varepsilon \quad (4.13)$$

The second equivalent variable, Tooth Root Strength Adjustment Factor, is:

$$Y_{2p} = Y_{ST} Y_{NT} Y_{\delta relTp} Y_{RrelT} Y_X \quad (4.14)$$

$$Y_{2g} = Y_{ST} Y_{NT} Y_{\delta relTg} Y_{RrelT} Y_X \quad (4.15)$$

The third equivalent variable Operating Work condition coefficient for bending, is:

$$K_1 = K_A K_V K_{F\beta} K_{F\alpha} \quad (4.16)$$

In this case, ***the reduction dimension model becomes:***

The pinion bending stress $\sigma_{Fp} = Y_{1p} . \frac{60 K_1 . P}{\pi . N_p b . m .^2 . z_p} \leq \sigma_{Flim} Y_{2p}$ (4.17)

The gear bending stress $\sigma_{Fg} = Y_{1g} . \frac{60 K_1 . P}{\pi . N_g b . m .^2 . z_g} \leq \sigma_{Flim} Y_{2g}$ (4.18)

B. Mechanical dimension reduction model for the gear pair contact model

The equivalent variables parameters for bending pinion and gear models are in Tab(4.6)

Table 4. 6: Physical dimension reduction model for contact model

The original model of contact strength is ISO 6336 Standard (ISO 6336-2:2006)

$$\sigma_H = Z_H Z_E Z_\beta Z_\varepsilon \sqrt{\frac{K_A K_V K_{H\beta} K_{H\alpha} F_t (u+1)}{b.m.z_p\, u}} \leq \sigma_{HP} \quad ; \quad \sigma_{HP} = \sigma_{Hlim} . Z_N Z_L Z_V Z_R Z_W Z_X$$

The equivalent variable $Z_1 = Z_H Z_E Z_\beta Z_\varepsilon$ (4.19)

$$Z_2 = Z_N Z_L Z_V Z_R Z_W Z_X \quad (4.20)$$

The equivalent variable K_2:

$$K_2 = \frac{u}{(u+1)} (K_A K_V K_{H\beta} K_{H\alpha}) \quad (4.21)$$

In this case, the reduction dimension model is:

$$\sigma_H = Z_1 \sqrt{\frac{60 . K_2 . P}{\pi . N_P b . (m .. z_p)^2}} \leq Z_2 \sigma_{Hlim} \quad (4.22)$$

C. Probabilistic model for the dimension reduction model of the gear pair subsystems

Table (4.7) shows the statistics variables of reduced models for gear pair subsystems. All variables are a standard normal distribution designed with N(mean, SD).

Table 4. 7: Random variables statistics for the gear pair models

Random variables	***Symbol***	***Reduced model parameters***	***Deterministic model parameters***
Transmission rapport	u	$\mathcal{N}$ (4, 0.02)	4
Standard module	$m\ (mm)$	$\mathcal{N}$ (3.5, 0.0175)	$\mathcal{N}$ (3.5, 0.0175)
Face width	$b(mm)$	$\mathcal{N}$ (37.5, 0.1875)	$\mathcal{N}$ (37.5, 0.1875)
Allowable contact stress	$\sigma_{Hlim}\left(N/_{mm^2}\right)$	$\mathcal{N}$ (1300, 156)	$\mathcal{N}$ (1300, 156)
Allowable bending stress	$\sigma_{Flim}\left(N/_{mm^2}\right)$	$\mathcal{N}$ (310, 62)	$\mathcal{N}$ (310, 62)
Rotational pinion speed	*N(rpm)*	$\mathcal{N}$ (1500. 150)	$\mathcal{N}$ (1500. 150)
Power	$P(watt)$	$\mathcal{N}$ (7500, 750)	$\mathcal{N}$ (7500, 750)
Number of Pignon teeth	z_p	18	18
Tooth root stress correction factor for pinion	Y_{1p}	$\mathcal{N}$ (2.362, 0.1115)	2.362
Tooth root stress correction factor for gear	Y_{1g}	$\mathcal{N}$ (2.375, 0.1121)	2.375
Tooth Root Strength Adjustment Factor for pinion	Y_{2p}	$\mathcal{N}$ (2.214, 0.1634)	2.214
Tooth Root Strength Adjustment Factor for gear	Y_{2g}	$\mathcal{N}$ (2.259, 0.1667)	2.259
Operating Work condition coefficient for bending	K_1	$\mathcal{N}$ (2.759, 0.3389)	2.759
Operating Work condition coefficient for contact	K_2	$\mathcal{N}$ (3.615, 0.3985)	3.615
Equivalent of reduced variables	Z_1	$\mathcal{N}$ (341.335, 17.321)	341.335
Equivalent of reduced variables	Z_2	$\mathcal{N}$ (0.9855, 0.0796)	0.9855

D. Performance model

- ***The bending reduced models:***

To prevent gear tooth failure from bending, the bending performance models are established as the tooth root stress for both the pinion and the gear:

$$G_{1P}(x) = \sigma_{FP}\text{-}\sigma_F \tag{4.23}$$

$$G_{2G}(x) = \sigma_{FP} - \sigma_F \tag{4.24}$$

$$\text{Gear Bending limit stat}\begin{cases} G_1 = \sigma_{\text{Flim}} Y_{2P} - Y_{1P}.\frac{60K_1.P}{\pi.N_p b m^2.z_p} \\ G_2 = \sigma_{\text{Flim}} Y_{2g} - Y_{1g}.\frac{60K_1.P}{\pi.N_g b m^2.z_g} \end{cases} \quad (4.25)$$

- ***The contact reduced performance model.***

The gear pairs contact failure scenario presents the limit state function of the contact stress as follows:

$$G_3(x) = \sigma_{HP} - \sigma_H \quad (4.26)$$

$$\text{Gear Contact limit stat}\begin{cases} \sigma_H = Z\sqrt{\frac{60.K_2.P}{\pi.N_P b.(m.z_p)^2}} \le \sigma_{\text{Hlim}} \\ G_3 = Z_2.\sigma_{\text{Hlim}} - \frac{Z_1}{m.z_p}\sqrt{\frac{60.K_2.P}{\pi.N_P b}} \end{cases} \quad (4.27)$$

E. Results of the gear pair probability of failure

The results of the gear pair reliability analysis are presented for three model variants: the original, dimension-reduced, and deterministic models. Each failure scenario includes the estimated failure probability and the corresponding reliability index obtained using both FORM and MCS. While MCS is relatively straightforward to implement, it is computationally intensive and time-consuming. Moreover, for low failure probabilities, MCS results may exhibit significant variability. To ensure the robustness of the estimates, multiple simulation runs are recommended. Accordingly, the margin of error for the MCS results has been determined from 10 repeated simulations, with a 95% confidence interval (CI) used to evaluate the accuracy of the findings. The results of both techniques are shown and in Tables (4.8) and (4.9).

1) Reduced bending model reliability results

Table 4. 8: Pinion bending failure probability results

Bending Pinion	***Reliability index β***	***Failure probability P_f***	***Reliability R***	***Error ε(R) %***
MCS Original model C0V 0.078	4.423761	4.850000e-06 [4.49e-06, 5.21e-06]	0.99999515	0
FORM Original model	4.420054	4.9338094e-06	0.999995066	8.43e-06
MCS reduced model C0V 0.082	4.4220922	4.88790e-06 [4.54e-06, 5.24e-06]	0.999995122	3.75e-06
FORM reduced model	4.4201611	4.93152e-06	0.999995067	8.15e-06
MCS deterministic model C0V 0.097	4.4515570	4.26250e-06 [3.77e-06, 4.76e-06]	0.999995738	5.9e-06
FORM deterministic model	4.4458715	4.376813e-06	0.9999956232	4.73e-06

Table 4. 9 : Gear bending failure probability results

Gear Bending	***Reliability index β***	***Failure probability*** P_f	***Reliability R***	***Error ε(R) %***
MCS Original model C0V 0.125	4.42154	4.900e-06 [4.64e-06, 5.36e-06]	0.99999510	0
FORM Original model	4.42921	4.733992e-06	0.999995267	1.2e-05
MCS reduced model C0V 0.1314	4.427497	4.7666667e-06 [4.29e-06, 5.25e-06]	0.999995234	8.3e-06
FORM reduced model	4.429062	4.732252e-06	0.99999527	1.2e-05
MCS deterministic model C0V 0.11	4.458761	4.3120e-06 [3.87e-06, 4.73e-06]	0.99999572	5.5e-05
FORM deterministic model	4.445862	4.377256 e-06	0.999995636	4.7e-05

Compared to the original model, the results obtained from the reduced-dimension model for bending strength closely align with those from both the MCS and FORM methods. This highlights the effectiveness of the dimensionality reduction technique for bending strength analysis. In contrast, treating the input variables as deterministic yields less accurate results for the same models. An error percentage is extremely low (ranging from 10^{-5} to 10^{-6}), suggesting that the approximations or model reductions does not introduce significant discrepancies in the reliability assessment.

The estimated failure probabilities P_f are on the order of (10^{-6}); indicating a very low likelihood of failure due to random fluctuations. The confidence intervals associated with the MCS results reflect the inherent uncertainty in the simulation-based estimates. Notably, the failure probabilities obtained using FORM for the original model fall within the MCS confidence bounds, demonstrating that FORM provides a reliable and accurate approximation of the gear bending strength model.

The following figures illustrate the values of the dimension-reduced function in comparison to those of the original function, evaluated at the most probable point $(\mathrm{MPP}_{\_\,\mathrm{original}})$.

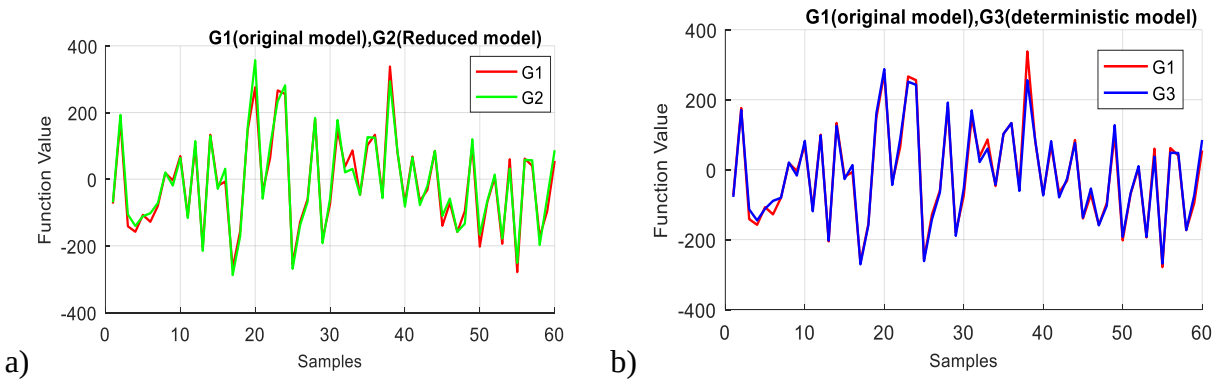

a) b)

Figure 4.3. Bending pinion Functions values at $(\mathrm{MPP}_{\_\,\mathrm{original}})$; a) the original model against the reduced model; b) the original model against the deterministic model

Figure 4.3 illustrates that the function values G1, G2, and G3 at the original Most Probable Point $(\mathrm{MPP}_{\_\,\mathrm{original}})$ are nearly identical across the three models: original, reduced, and deterministic. These findings are consistent with the failure probabilities reported in **Tab 4.8**, **Tab 4.9** which indicate a negligible difference of 10^{-6} and 10^{-6} among the models. This confirms that the models yield comparable reliability estimates. Furthermore, the results closely match those obtained via Monte Carlo Simulation (MCS), demonstrating that the slight nonlinearity present in the limit state function does not significantly affect the accuracy of the FORM approximation.

The subsequent figures compare the function values obtained through the dimension-reduced models to those of the original function, evaluated at the $(\mathrm{MPP}_{\_\,\mathrm{original}})$ without dispersions in variables (standard deviations=0).

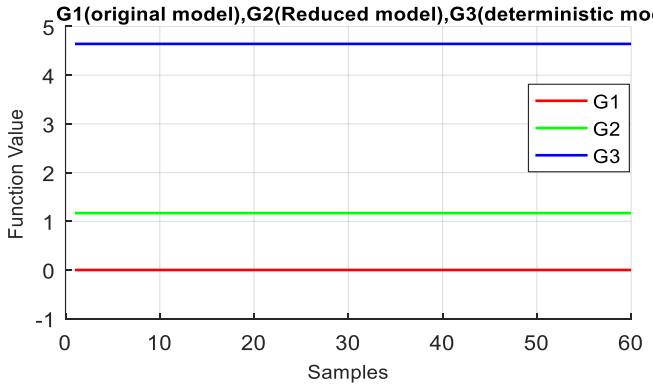

Figure 4.4. Bending pinion Functions values at $(\mathrm{MPP}_{\_\,\mathrm{original}})$ without variables dispersions

The graphs of **Fig 4.4** display the function values obtained from two models: the deterministic model (G3 function value = 4.64) and the reduced model (G2 function value =

1.17). These are compared against the original function G1 value of (-1.31e^{-06}) at the $(\text{MPP}_{\_\text{original}})$. The discrepancy between the original and reduced models is considerably smaller than that between the original and deterministic models. This observation supports the validity of the selected reduced variables, as they preserve the essential characteristics of the original model without introducing significant deviation.

2) Gear pair contact reliability results

Table 4. 10: Gear pair contact failure probability results

Gear Pairs Contact	***Reliability index β***	***Failure Probability*** P_f	***Reliability R***	***Error ε(R) %***
MCS Original model C0V 0.094	4.3435999	7.0083333e-06 [6.59e-06, 7.43e-06]	0.9999929917	-
FORM Original model	4.390794	5.646868900e-06	0.999994353	1.34e-04
MCS reduced model C0V 0.106	4.344103	6.99231e-06 [6.55e-06, 7.44e-06]	0.9999930	1.6e-06
FORM reduced model	4.388751	5.7002 e-06	0.999994299	1.31e-04
MCS deterministic model C0V 0.283	4.795834	8.10002e-07 [6.43e-07, 9.77e-07]	0.99999917	6.2e-04
FORM deterministic model	4.8019704	7.85559587e-07	0.9999992144	6.22e-04

The contact gear demonstrates a very low failure probability, indicating a high level of reliability. In this case, the failure probability can be classified as a rare event, as P_f is lies in the order of 10^{-6}. However, for such rare events, especially in the context of nonlinear limit state functions—such as the contact strength model—the estimated failure probability tends to be unstable.

Despite this, the reliability values obtained using FORM and MCS across the three models are in close agreement, with error percentages falling within the range of (10^{-4}%) This consistency suggests that the influence of nonlinearity in the limit state function is minimal in this context.

A second important observation is that the newly proposed reduction model for contact strength yields results that are very similar to those obtained from both MCS and FORM when applied to the original model. This confirms the effectiveness of the reduction approach for this type of nonlinear model. In contrast, the deterministic model provides less accurate results when

the input variables are treated deterministically, underscoring the importance of accounting for uncertainties in reliability analysis.

Figure 4.5 presents a comparison of the function values obtained from the reduced model and the deterministic model against those of the original model.

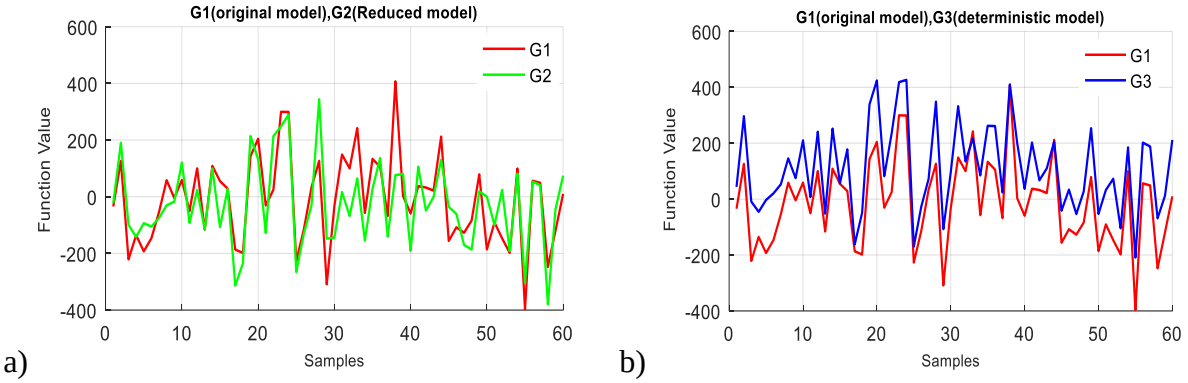

a) b)

Figure 4.5. Contact gear Functions values at $(\mathrm{MPP}_{\_\,\mathrm{original}})$; a) the original model against the reduced model; b) the original model against the deterministic model

Another observation from **Figure 4.5** indicates that the values of the reduced model at the original Most Probable Point $\mathrm{MPP}_{\_\,\mathrm{original}}$, are more accurate than those of the deterministic model.

Figure 4.6. Contact gear Functions values at $(\mathrm{MPP}_{\_\,\mathrm{original}})$ without dispersions

Figure 4.6 illustrates the deviation of both the reduced and deterministic models compared to the original model at the original Most Probable Point $(\mathrm{MPP}_{\_\,\mathrm{original}})$. The reduced-dimension model shows a minimal deviation from the original model, within the order of (range of 10^{-5} whereas the deterministic model exhibits a significantly larger deviation (approximately 130). These results confirm that the reduced-dimension model provides a more accurate and reliable representation of the original model, particularly for evaluating the contact strength of gear pair.

4.3.3 Structural Reliability-Based Dimension Reduction of the Bearings Subsystem

This section presents the application of structural reliability-based dimension reduction to the bearings subsystem **,** aiming to simplify the reliability analysis while preserving the essential characteristics of the original model.

4.3.3.1 Reliability analysis of the original Bearings subsystem

The selection of bearings is primarily guided by fatigue analysis, which accounts for operational conditions and the expected service life. This process is carried out in accordance with the specifications of the gears and the input and output shafts of the speed reducer, as outlined in previous references. Consequently, the choice of bearings is closely linked to this dimensioning process, which considers factors such as radial and axial loads, rotational speed, and input power.

A. Mechanical model for the original bearings

The service life of a ball bearing is restricted by fatigue failure at the surfaces of the balls and races; hence, the dynamic load-carrying capacity of the bearing is contingent upon its fatigue life.

Table 4. 11: Physical model for original bearings

Transmitted Torque	$T_i = \frac{F_t d_i}{2} = \frac{30.P}{\pi.N_i}$	
The tangential force	$F_t = \frac{2T_i}{d_i} = \frac{2T_i}{m.z_i} = \frac{60.P}{\pi.m.z_i N_i}$	(4.28)
Radial force	$F_r = F_t.\tan\alpha$	(4.29)
The equivalent dynamic load	$P_{br} = X.F_r + Y.F_a$	(4.30)
Bearing Life	$L_{10} = \frac{60.N_i.L_{10h}}{10^6}$	(4.31)
Dynamic load capacity	$C = P.(L_{10})^{1/3}$	(4.32)
	$C = \frac{60.P}{\pi.m.z_i N_i}.\tan\alpha.\left(\frac{60.N_i.L_{10h}}{10^6}\right)^{1/3}$	(4.33)
	$C = \frac{60.P.(N_i)^{1/3}}{\pi.m.z_i N_i}.\tan\alpha.\left(\frac{60.L_{10h}}{10^6}\right)^{1/3} = \frac{60.P}{\pi.m.z_i (N_i)^{2/3}}.\tan\alpha.\left(\frac{60.L_{10h}}{10^6}\right)^{1/3}$	(4.34)

B. Probabilistic model for the original bearing model

Assuming the machine operates for 8 hours per day, the estimated service life of the bearings is approximately 12,000 hours.

- The ball bearing SKF No. 6004 is selected for the pinion shaft , which has a diameter of 20 mm.
- The ball bearing **SKF No.** 16006 is selected for gear, which has a diameter of 32 mm.

The statistics parameters of the original bearing subsystems are mentioned in **Tab** (4.12)

Table 4. 12: Random variables statistics for the original ball bearings variables

Random variables	***Symbol units***	***Mean values and standard deviations***
Standard module	$m(mm)$	$\mathcal{N}$ (3.5, 0.0175)
Pinion teeth numbers	z_p	18
bearing life for general gears	$\mathrm{L}_{10\mathrm{h}}(hrs)$	$\mathcal{N}$ (12000, 1200)
Dynamic load capacity limit selected from SKF for bearing1 No. 6004	$\mathrm{C}_{\mathrm{lim1}}(N)$	$\mathcal{N}$ (9360, 936)
Dynamic load capacity limit selected from SKF for bearing2 No. 16006	$\mathrm{C}_{\mathrm{lim2}}(N)$	$\mathcal{N}$ (11200, 1120)
Power	$P(watt)$	$\mathcal{N}$ (7500, 750)
Pinion Shaft speed	$N_p(rpm)$	$\mathcal{N}$ (1500. 150)
Pressure angle	tanα	$\mathcal{N}$ (0.364, 0.00182)

Table 4.13 presents the direction cosines obtained from the original ball bearing models, illustrating the orientation of key variables within the reliability analysis framework.

Table 4. 13: direction cosines results of the original ball bearings models

Bearing variables	***Random variables means***	***direction cosines***	***Gear shaft Bearing variables***	***direction cosines***
m	3.5	-0.0285	3.5	-0.0203
$\mathbf{L_{10h}}$	12000	0.1793	12000	0.1244
$\mathbf{C_{lim}}$	**9360**	**-0.7287**	**11200**	**-0.8692**
P	7500	**0.4945**	4*7500	**0.3334**
$\mathbf{\tan\alpha}$	0.364	0.0283	0.364	0.0203
$\mathbf{N_1}$	1500	**-0.4365**	1500/4	**-0.3425**

The variable exerting the greatest influence on the probability of failure in both bearing subsystems is the dynamic load capacity $\mathbf{C_{lim}}$. The negative sign associated with this variable indicates that an increase in $\mathbf{C_{lim}}$ leads to improved reliability; therefore, this variable is excluded from the dimension reduction process.

Both the transmission power **P** and the pinion shaft speed $\mathbf{N_1}$ have similar significance in the two bearing models, with **P** acting as a constraint and $\mathbf{N_1}$ serving as a resistance. This relationship arises because power is linked to the tangential effort, which directly impacts the dynamic load capacity ($\boldsymbol{C}$). An increase in either P or N results in an inversely proportional effect on the overall performance of the bearing subsystem.

Several variables, such as the normal module, $\boldsymbol{m, z_p}$, and $\boldsymbol{N, P}$ are common to both the bearing and gear pair models. Due to their correlated nature, these variables are also excluded from the reduction process.

Additionally, the variables $\mathbf{L_{10h}}$ (bearing rated life) and the pressure angle $\mathbf{\tan \alpha}$ which are shared exclusively between the bearing models, exhibit very small direction cosines. As a result, they can be effectively combined into a single equivalent random variable for dimension reduction purposes.

4.3.3.2 Dimension Reduction Models for the ball bearing subsystems

The equivalent variable parameters for ball bearing models is in Tab(4.14)

Table 4. 14: Bearing model equivalent variables parameters

Equivalent variable	Mean value	Standard deviation
$\mathrm{L} = \tan \alpha . \left(\frac{60.\,\mathrm{L_{10h}}}{10^6}\right)^{1/3}$	0.326246265	0.010996537

A. Performance Reduction model for ball bearing subsystems

The limit state function is therefore defined as the difference between the dynamic load capacity limit and the dynamic load capacity calculated using equation (4.39).

$$G_{br}(x) = \mathrm{C_{limi}} - C_i \tag{4.35}$$

$$\text{Bearings limit stats functions} \begin{cases} G_{br1} = \mathrm{C_{lim1}} - \frac{60.P}{\pi.m.z_i(\mathrm{N_i})^{2/3}}.\mathrm{L} \\ G_{br2} = \mathrm{C_{lim2}} - \frac{60.P}{\pi.m.z_i(\mathrm{N_i})^{2/3}}.\mathrm{L} \end{cases} \tag{4.36}$$

B. Results of failure Probability of the ball bearings subsystem

The reliability results of the pinion shaft bearings are presented **Tab** (4.15)

Table 4. 15: pinion shaft ball bearing failure probability results

Ball bearing pinion shaft	*Reliability index β*	*FailuProbability P_f*	*Reliability R*	*Error ε(R) %*
MCS Original model C0V 0.0316	3.016632	1.27810e-03 [1.26e-03, 1.30e-03]	0.998721931	0
FORM Original model	3.032610	1.212312736e-03	0.9987876872	6.6e-03
MCS reduced model C0V 0.033	3.006050	1.32339658e-03 [1.30e-03, 1.35e-03]	0.998676603	4.5e-03
FORM reduced model	3.030830	1.219481761e-03	0.998780518	5.9e-03
MCS deterministic model C0V 0.0238	3.056051	1.121434441e-03 [1.11e-03, 1.14e-03]	0.9988785655	1.57e-02
FORM deterministic model	3.086281	1.013454287e-03	0.9989865457	2.65e-02

All bearings of the pinion shaft exhibit a failure probability of approximately (5.10^{-3}), indicating a moderate level of reliability. Furthermore, the reliability values calculated by the FORM for each model closely match the reference results obtained through MCS, thereby confirming the robustness of the FORM approach in this context. The results of the dimension reduction model closely resemble those of the original model, whereas the deterministic model results show somewhat greater deviation from the original.

The comparison of reliability indices reveals that the FORM approximation results differ slightly more from those of the MCS method, reflecting the pronounced nonlinearity present in the limit state function of the ball bearing model.

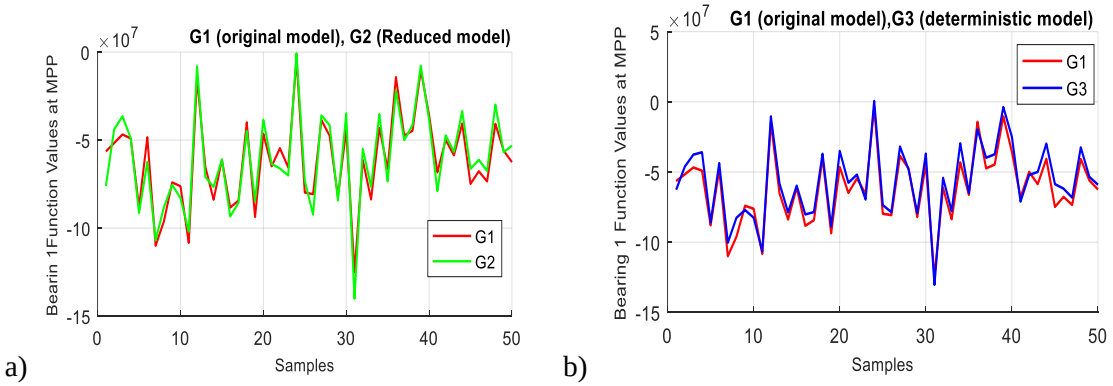

a) b)

Figure 4.7. Functions values at $(\mathrm{MPP}_{_\,\mathrm{original}})$model for Bearing 1: a) the original model against the reduced model; b) the original model against the deterministic model

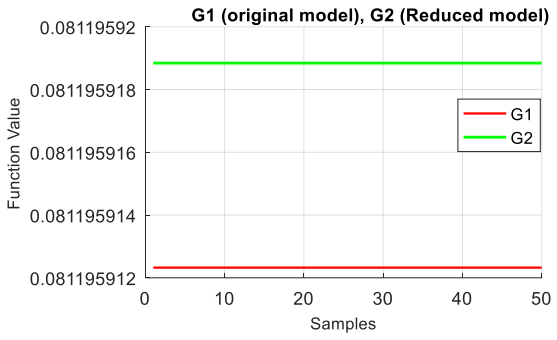

c)

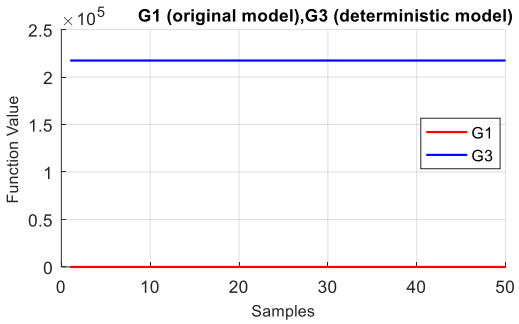

d)

Figure 4.8. Functions values at $(\mathrm{MPP}_{\_\,\mathrm{original}})$ model without dispersions for pinion shaft bearings

Fig (4.7) and **Fig (4.8)** show the deviation of reduced and deterministic model compared with the original one at the most probable point $(\mathrm{MPP}_{\_\,\mathrm{original}})$. It is clear that the reduced dimension model exhibits a minimal deviation from the original model (range of 10^{-8}), whereas the deterministic model shows a significantly larger deviation, approximately (range of 10^{5}). This supports the appropriateness of selecting the reduced model as a reliable representation of the original system.

The reliability results for the gear shaft bearings are presented in **Tab**(4.16)

Table 4. 16: Gear shaft bearings failure probability results

Gear shaft bearings	***Reliability index β***	***Failure Probability*** P_f	***Reliability R***	***Error ε(R) %***
MCS Original model	-	0	1	-
FORM Original model	6.18982156	3.011045857e-10	0.9999999996989	-
MCS reduced model C0V 0.0108	-	0	1	
FORM reduced model	6.186015	3.01002e-10	0.999999999696	-
MCS deterministic model C0V 0.0147	-	0	1	-
FORM deterministic model	6.2413560	2.178547e-10	0.999999999782	-

Gear shaft bearings shows an exceptionally low failure probability on the order of (10^{-10}). indicating an extremely high level of reliability under standard operating conditions. This degree of reliability classifies the failure event as rare.

However, for such rare events, the failure probability estimates tend to be highly variable, particularly when dealing with nonlinear limit state functions, such as the bearing fatigue model.

Furthermore, the reliability values obtained via the FORM for each model closely correspond to the reference results derived from MCS. The dimension reduction model results align well with those of the original model, while the deterministic model results also show notable similarity to the original model.

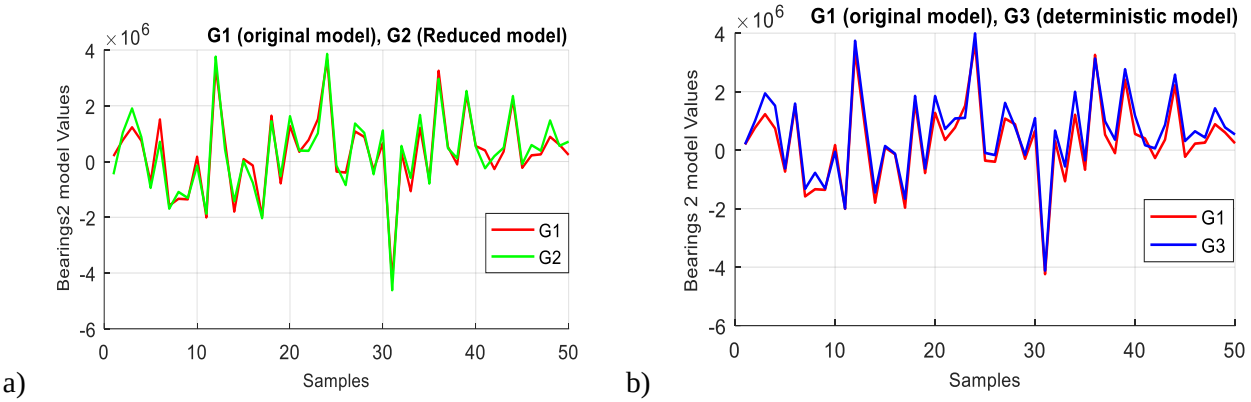

a) b)

Figure 4.9. Functions values at $(MPP_original)$model for Bearing 1; a) the original model against the reduced model; b) the original model against the deterministic model

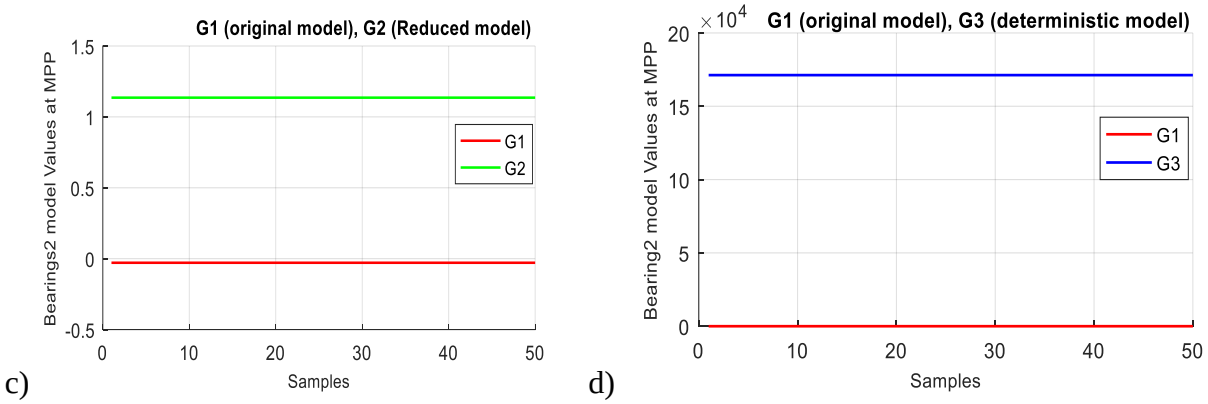

c) d)

Figure 4.10. Bearings Functions values at $(MPP_original)$without dispersions for gear shaft bearings

The Figures **(4.9), (4.10)** illustrate the deviations of the reduced and deterministic models relative to the original model at the original Most Probable Point $(MPP\_original)$. The reduced-dimension model exhibits a minimal variation from the original model, whereas the deterministic model shows a substantially larger deviation of (17.10^4). These results further validate the suitability of the reduced model as an accurate representation of the original system.

4.3.4 Structural Reliability-Based Dimension Reduction of the shafts Subsystem

This section focuses on applying structural reliability-based dimension reduction techniques to the shafts subsystem.

4.3.4.1 Reliability analysis of the original shafts subsystem

The reliability analysis of a shaft subjected to constant torque integrates probabilistic methods to account for uncertainties in loading conditions, material properties, and geometric parameters. The dimensions of the pinion and gear shafts are adopted from the study by Ziat et al. (2022).

A. Mechanical model for the transmission shafts

The gear and pinion shafts are constructed from plain SAE1045 (45C8), with a tensile yield strength Syt=[310- 450] MPa. According to the maximum shear stress theory, which is the most appropriate criterion for ductile materials subjected to combined bending and torsional moments without axial force Bhandari,. (2020), the physical model parameters are summarized in **Tab(4.17).**

Table 4. 17: Physical original model for the shafts subsystem

The tangential force $$F_t = \frac{2T_i}{d_p} = \frac{2T_i}{m.z_i} = \frac{60.P}{\pi.m.z_i N_i}$$

The radial force $$F_r = F_t.\tan\alpha$$

The bending moment

$$M_b = \frac{F_r.L_{sh}}{4} \quad (4.38)$$

$\mathbf{L_{sh}}$ is the shaft length(space between bearings): $L_{sh} = b + 2e$ (4.39)

$\boldsymbol{b}$: teeth gear width (b=37.5mm)

$\boldsymbol{e}$: is the space for bearings and mounting (generally between **20 and 50 mm** on each side).

If we take a value of **e=30mm**, we get: $L_{sh} = b + 2e = 97.5mm$ so we keep $\mathbf{L_{sh}} = \boldsymbol{100mm}$

According to maximum shear stress, the principal shear stress τ_{max} is:

$$\tau_{max} = \sqrt{\left(\frac{\sigma_b}{2}\right)^2 + \tau^2} \quad (4.40)$$

The bending moment $$\sigma_b = \frac{32M_{bi}}{\pi {d_i}^3} \quad (4.41)$$

The tensional moment is: $$\tau = \frac{16T_i}{\pi {d_i}^3} \quad (4.42)$$

$$\tau_{max} = \sqrt{\left(\frac{16M_b}{\pi {d_i}^3}\right)^2 + \left(\frac{16T_i}{\pi {d_i}^3}\right)^2} = \frac{16}{\pi {d_i}^3}\sqrt{{M_b}^2 + {T_i}^2} \quad (4.43)$$

The permissible value of maximum shear stress is:

$$\tau_{per-max} = \frac{0.5\,S_{yt}}{fs} \quad (4.44)$$

S_{yt} is the yield strength of shafts material, we adopt the smaller value $\boldsymbol{S_{yt} = 310N/mm^2}$

f_s is rhe security factor for transmission shaft $f_s = [2, 3]$, in the case of moderate loads, the value $\boldsymbol{f_s = 2}$ is adopted.

B. Probabilistic model of the original for the transmission shafts model

The statistical parameters of the variables in the original shafts subsystem model are presented in Tab (4.18).

Table 4. 18: Random variables statistics for pinion and gear shafts variables

Random variables	*Symbol*	*Mean values and standard deviations*	*units*
Standard module	m	$\mathcal{N}$ (3.5, 0.0175)	*mm*
Power	P	$\mathcal{N}$ (7500,750)	*watt*
Pignon Shaft speed	N_p	$\mathcal{N}$ (1500, 150)	*rpm*
Maximum permissible shear	$\tau_{\text{per}-\max}$	$\mathcal{N}$ (78, 11.7)	N/mm^2
Pignon Shaft diameter	d_s	$\mathcal{N}$ (20, 0.1)	*mm*
Gear Shaft diameter	d_g	$\mathcal{N}$ (32, 0.16)	*mm*
Shaft length	L_{sh}	$\mathcal{N}$ (100, 0.5)	*mm*
Pressure angle	tanα	$\mathcal{N}$ (0.364, 0.00182)	

C. Performance model of the original shafts model

Based on the maximum shear theory, the limit stat function is given by:

$$\begin{cases} \text{Pinion shaft} : G_{sh\_p} = \tau_{per-max} - \frac{16}{\pi {d_{sh1}}^3}\sqrt{\left(\frac{60.P.L_{sh}.tan\alpha}{4.\pi.m.z_p N_p}\right)^2 + \left(\frac{30.P}{\pi.N_p}\right)^2} \\ \text{Gear shaft 2:} G_{sh\_g} = \tau_{per-max} - \frac{16}{\pi {d_g}^3}\sqrt{\left(\frac{60.P.L_{sh}.tan\alpha}{4.\pi.m.z_g N_g}\right)^2 + \left(\frac{30.P}{\pi.N_g}\right)^2} \end{cases} \quad (4.45)$$

D. Sensitivity factors analysis of the transmission shaft subsystem

The **Tab 4. 19** presents the sensitivity factor analysis conducted on the transmission shaft subsystem to identify the most influential variables affecting its reliability performance.

Table 4. 19: Shafts direction cosines results

Pinion shaft variables	*Random variables means*	*Direction cosines*	*Gear shaft variables*	*direction cosines*
$\boldsymbol{m}$	3.5	-0.0013	3.5	-7.67e-05
P	**7500**	**0.2778**	**7500**	**0.2654**
$\boldsymbol{L_{sh}}$	100	-0.0013	100	-7.67e-05
$\boldsymbol{\tau_{max}}$	**78**	**-0.8932**	**78**	**-0.9038**
$\boldsymbol{d_s}$	20	-0.0461	-	-
$\boldsymbol{d_g}$	32	-	32	-0.0439
$\mathbf{N_p}$	**1500**	**-0.3513**	**1500/4**	**-0.3345**
tanα	0.364	-0.0013	0.364	-7.67e-05

n

The sensitivity analysis results for the shafts indicate that the maximum permissible shear stress exerts the most significant influence on the probability of failure in both shaft subsystems. As a result, this variable is excluded from the dimensionality reduction process. Similarly, the correlated variables $\boldsymbol{m, z_p}$, and $\boldsymbol{N, P}$ which are common across all failure models, are also excluded from the reduction procedure.

The transmission power $\boldsymbol{P}$ and pinion shaft speed $\boldsymbol{N}$ exhibit equivalent influence in both shaft models, with $\boldsymbol{P}$ acting as a load (constraint) and $\boldsymbol{N}$ as a resistance variable. This is because both variables are linked to tangential forces, which directly affect the bending and torsional moments. An increase in either $\boldsymbol{P}$ or $\boldsymbol{N}$ results in an inversely proportional variation in the overall performance of the shaft subsystem.

Additionally, the variables $\boldsymbol{L_{sh}}$ and $\boldsymbol{\tan \alpha}$ which are shared exclusively between the shaft models, have very small direction cosines. Therefore, they can be combined into a single equivalent random variable for the purposes of dimensionality reduction.

4.3.4.2 Dimension Reduction Models for transmission shafts subsystem

The parameters of the equivalent variables for the shaft models are presented in Tab(4.20)

Table 4. 20: Shafts model equivalent variable parameters

Equivalent variable	Mean value	Standard deviation
$L_{eq} = \frac{\tan \alpha . L_{sh}}{2}$	36.4	0.12869

C. Performance model of the dimension reduction model for transmission shafts

The new limit state functions for the reduced models is therefore expressed as follows:

$$\begin{cases} \text{Pinion shaft: } G_{sh\_p} = \tau_{per-max} - (48.634).\left(\frac{P}{d_s N_p}\right)\sqrt{\frac{Leq^2}{(m.z_p)^2}+1} \\ \text{Gear shaft 2: } G_{sh\_g} = \tau_{per-max} - (48.634).\left(\frac{P}{d_g N_g}\right)\sqrt{\frac{Leq}{(m.z_g)^2}+1} \end{cases} \quad (4.46)$$

D. Probability of failure results for transmission shafts

The reliability analysis results for the gear and pinion shafts, obtained using both the Monte Carlo Simulation (MCS) and First-Order Reliability Method (FORM), are presented in the following tables.

Table 4. 21: Pinion shaft probability of failure

Shaft of Pinion	*Reliability index β*	*probability of failure P_f*	*Reliability R*	*Error ε(R)%*
MCS Original model COV=0.028	3.59577911	1. 61748495e-04 [1.58e-04, 1.66e-04]	0. 99983825	-
FORM Original model	3.63428909	1.39374085e-04	0.999860626	2.2 e-03
MCS reduced model C0V 0.034	3.59307625	1. 63436062e-04 [1.58e-04, 1.68e-04]	9998365639	2.0 e-04
FORM reduced model	3.63429262	1. 39406935e-04	0. 999860593	2.2 e-03
MCS deterministic C0V 0.018	3.59589320	1. 61677621e-04 [1.59e-04, 1.64e-04]	0. 999838322	2.0e-03
FORM deterministic	3.63429510	1. 39405594e-04	0. 999860594	2.2 e-03

Table 4. 22: Probability of failure results of gear shaft

Shaft of Gear	*Reliability index*	*Failure probability Pf*	*Reliability R*	*Error ε(R) %*
MCS Original model COV==0.037	3.7759321	7. 9730976e-05 [7.73e-05, 8.22e-05]	0. 999920269	-
FORM Original model	3.8167457	6. 7635165e-05	0. 9999323648	1.2e-03
MCS reduced model C0V 0.045	3.7791322	7. 8713513e-05 [7.60e-05, 8.14e-05]	0. 9999212864	1.0e-04
FORM reduced	3.81674631	6. 7634998e-05	0. 999932365	1.2e-03
MCS deterministic model C0V 0.084	3.7825242	7. 7648384e-05 [7.22e-05, 8.31e-05]	0. 9999223516	2.0e-04
FORM deterministic	3.8167456	6. 7635193e-05	0. 9999323648	1.2e-03

The first notable observation is that all models yield very similar results when evaluated using MCS, with a relative error on the order of 10^{-4} % and similarly consistent results when using the First-Order Reliability Method (FORM), with an error on the order of 10^{-3} %; These small discrepancies are primarily due to the reduced variables having very low sensitivity factors, meaning their influence on the failure probability is minimal. As a result, these variables can be treated as deterministic without significantly compromising the accuracy of the failure probability estimation. Both shafts demonstrate high reliability, with failure probabilities below 10^{-4}. The reliability indices derived from both MCS and FORM exceed 99.9%, confirming the robustness of the system.

Although FORM slightly overestimates the reliability compared to MCS, the deviation is marginal—approximately 10^{-3}%. This close agreement indicates that FORM provides a reliable and efficient alternative to MCS for evaluating this type of failure model.

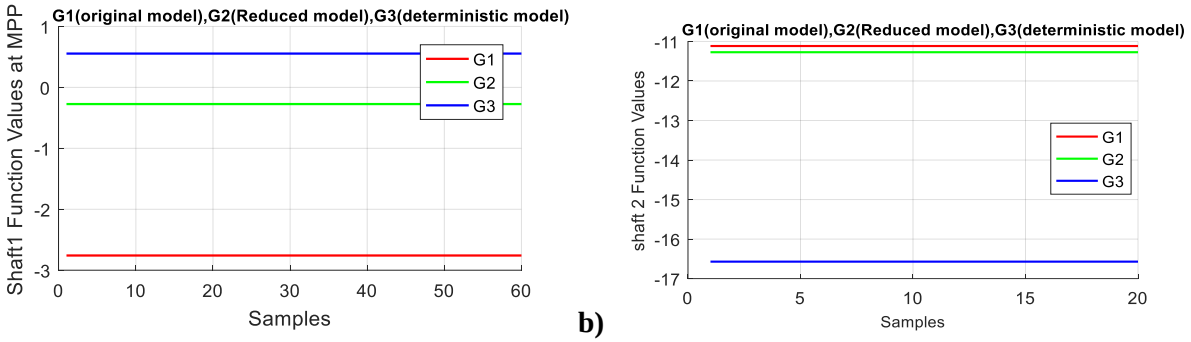

Figure 4.11. Shafts Functions values at $(\mathrm{MPP}_{_\,\mathrm{original}})$without dispersions; a) pinion shaft model; b) gear shaft model

The Fig (**4.11**) illustrates the variation of the reduced and deterministic models relative to the original model at the most probable point ($(\mathrm{MPP}_{\_\,\mathrm{original}})$. Both models exhibit small deviations from the original model; however, the reduced dimension model demonstrates greater accuracy compared to the deterministic model. This supports the suitability of the reduced model for accurately representing the original model.

4. 4 Conclusion

This chapter introduced the Structural System Reliability-Based Dimension Reduction Method (SSR-DRM) based on FORM approximation**,** as an innovative approach for probabilistic system failure analysis. SSR-DRM aims to simplify reliability assessments by decomposing complex systems into smaller subsystems while maintaining the variability of parameters and the effects of their correlations.

The First-Order Reliability Method (FORM) is initially employed to calculate direction cosines, which serve to identify variables suitable for dimensionality reduction.

The proposed method is validated through three modeling approaches for each failure type: the reduced dimension model, the deterministic model in which the reduced variables are considered deterministic. These models are compared to the original system design using both Monte Carlo Simulation (MCS) and the FORM approximation.

The initial results highlight the ease of interpreting the equivalent variables within the reduced-dimension models. The findings demonstrate a strong agreement between the FORM and MCS results for most of the evaluated models, confirming that the reduced-dimension model provides the closest representation of the original system. This observation holds true for both linear and nonlinear limit state functions, including those related to gear pair contact, the fatigue life equation of bearings, and the torsional bending equation of shafts.

Reliability analysis results for the gear pair, transmission shafts, and bearing subsystems reveal critical insights, with some subsystems demonstrating higher failure probabilities. The SSR-DRM-FORM framework achieves an effective balance between computational efficiency and predictive accuracy by properly reflecting the variability of reduced variables while preserving interdependencies among subsystems.

In the following chapter, the focus will shift to applying the direction-based dimension reduction model to estimate the failure probability of the overall system based on its components. This will involve using first and second-order failure probability bounds. Subsequently, a Reliability-Based Design Optimization (RBDO) procedure will be conducted to enhance the reliability of the weakest subsystem.

CHAPTER 5: SYSTEM PROBABILITY OF FAILURE BOUNDS BASED ON DIMENSION REDUCTION MODEL OF A SPEED REDUCER

5.1 Introduction

A series system—often referred to as a weakest link or chain system—fails when any one of its components fails. The presence of correlations between subsystem models complicates the assessment of the system's failure probability. This complexity arises primarily from the multidimensional integration required to evaluate the joint probability of failure.

Rather than performing direct integration of the failure probability expression, an alternative approach involves establishing upper and lower bounds for the structural system's failure probability. In practice, a structural system is subjected to a sequence of loadings, during which failure can occur due to one or more failure modes at any stage. By evaluating the probabilities associated with individual failure modes, the overall system failure probability can be estimated within defined bounds, thereby providing a more tractable and realistic framework for reliability analysis

The objective of this chapter is to apply a probabilistic approach to establish bounds on the failure probability of series systems. The analysis is conducted using the dimensionally reduced models of the speed reducer components developed in Chapter 4. The primary aim is to assess the robustness of these reduced models within the framework of multi-component system reliability analysis, particularly in the presence of correlated failure modes.

The failure probability bounds of the series system—namely, the speed reducer—are evaluated using the **First-Order Probability of Failure Bounds** (providing the widest upper and lower bounds), and the **Second-Order Upper Bound Method** (yielding narrower bounds) based on the FORM approximation described in Chapter 3. The results obtained from these methods, applied to both the original and the dimensionally reduced models, are compared with those derived from Monte Carlo Simulation (MCS).

All techniques presented in this chapter are implemented using MATLAB.

5.2 Strategy Adopted for Calculating the failure probability bounds of the Speed Reducer System

This section presents a probabilistic methodology for establishing failure probability bounds in series systems, taking into account both model dimensionality and the correlation between failure modes. The adopted strategy is structured in two main parts:

Part 1: First Order Probability Of Failure Bounds (largest upper and lower bounds)

This part focuses on computing the largest upper and lower bounds for the probability of failure in a multi-component system. This part is divided into two steps:

- **Step 1**: Perform reliability analysis for each failure mode using the Reduced-Dimensional model for each failure mode using FORM and Monte Carlo Simulation (MCS).
- **Step 2:** Use the results from Step 1 to evaluate the First-Order Probability of Failure Bounds, based on the approximation proposed by Kounias (1968), for each subsystem. These bounds are then aggregated to estimate the overall failure probability bounds of the speed reducer system. The results are compared with those obtained via MCS for both the original and reduced models.

Part 2: This part applies Ditlevsen's Second-Order Upper Bound Method (Narrow Bounds) to obtain tighter bounds on the system's failure probability. It is divided into two steps:

- **Step 1**: Compute the direction cosines of all random variables, followed by the evaluation of the correlation matrix among the failure modes of the speed reducer system.
- **Step 2:** Calculate the second-order failure probability bounds for each subsystem. These are then used to estimate the overall system bounds using Ditlevsen's second-order upper bound method (Ditlevsen, 1979). The results are compared with those obtained from MCS applied to both the original and reduced models.

5.3 First-Order failure probability bounds of the speed reducer

The system is initially decomposed into several simple subsystems, each exhibiting multiple failure modes. The first-order failure probability bounds, the widest upper and lower bounds, are then calculated using equations (3.58), (3.59), and (3.60):

$$\max_{i=1,\dots n} P(F_i) \le P_{fsys} \le \min_{i=1,\dots,n}\left(\sum_{i=1}^{n} P(F_i), 1\right)$$

The lower bound is defined as: $P_{fsys}^{-} = \max_{i=1,\dots,n} P(F_i)$

The upper bound is defined as: $P_{fsys}^{+} = \min_{i=1,\dots,n} (\sum_{i=1}^{n} P(F_i), 1)$

This section presents a reliability analysis of a speed reducer system, accounting for multiple failure modes typically encountered during operation. The analysis focuses on the system's main components: the gear pair subsystem, the transmission shaft subsystem, and the bearing subsystem, which together comprise seven failure modes.

First, the lower and upper failure probability bounds for each component are determined using the results obtained from the dimensionally reduced models developed in Chapter 4. These component-level bounds are then used to estimate the overall system failure bounds using Kounias's (1968) first-order approximation (equations 3.58–3.60). The results are compared with those obtained from Monte Carlo Simulation (MCS) for both the reduced and original models.

This comparison serves a dual purpose: to assess the robustness of the reduced-dimensional models and to evaluate the accuracy and effectiveness of the first-order failure probability bound approximation.

5.3.1 First Order Failure Probability Bounds of the gear pair subsystem

The calculation of the first-order failure probability bounds for the gear pair subsystem considers three failure modes: pinion bending, gear bending, and gear pair contact failure. The dimensionally reduced models corresponding to these failure modes are as follows:

$$\text{Gear Bending limit stat}\begin{cases} g_1 = \sigma_{\text{Flim}} Y_{2P} - Y_{1P}.\dfrac{60K_1.P}{\pi.N_p b m^2.z_p} \\ g_2 = \sigma_{\text{Flim}} Y_{2g} - Y_{1g}.\dfrac{60K_1.P}{\pi.N_g b m^2.z_g} \end{cases}$$

$$\text{Gear Contact limit stat}\begin{cases} g_3 = Z_2.\sigma_{Hlim} - \dfrac{Z_1}{m.z_p}\sqrt{\dfrac{60.K_2.P}{\pi.N_P b}} \end{cases}$$

Table 5.1. First-order failure probability bounds of the gear pair subsystem

Gear pair subsystem	*Bending pinion*	*Bending gear*	*Contact gear pair*
Reliability index	$\beta_{\_FORM\_red}$ = 4.4201611 $\beta_{\_MCS\_or}$= 4.423761	$\beta_{\_FORM\_red}$ =4.429062 $\beta_{\_MCS\_or}$=4.42154	$\boldsymbol{\beta_{\_FORM\_red}}$ **=4.388751** $\beta_{\_MCS\_or}$= 4.3435999
Failure Probability	$P_{f\_FORM\_red}$ = 4.93e-06 $P_{f\_MCS\_or}$= 4.85e-06	$P_{f\_FORM\_red}$ =4.73e-06 $P_{f\_MCS\_or}$= 4.9e-06	$\boldsymbol{P_{f\_FORM\_red}}$ **=5.7e-06** $P_{f\_MCS\_or}$= 7.01e-06

First-order failure probability bounds of the gear pair subsystem

	Probability of failure	**Reliability index**	**Error (MCS)**
Lower bound	P_f =5.70 e-06	$\boldsymbol{\beta}$**= 4.38875**	$\varepsilon_{relative}(\%)$ =7.5e-04
Upper bound	$\boldsymbol{P_f}$ **=1.5363966e-05**	$\boldsymbol{\beta}$**=4.168007**	$\varepsilon_{relative}(\%)$ =2.1e-04
MCS reduced model	P_f =1.2367e-05 [1.17e-05, 1.30e-05]	$\boldsymbol{\beta}$**=4.21722** COV=0.08	$\varepsilon_{relative}(\%)$ =8.4e-05
MCS original model	1.3208e-05 [1.24e-05, 1.40e-05]	$\boldsymbol{\beta}$**= 4.202343** COV=0.09	0

The results presented in Table 5.1 show that the failure probability of the gear pair subsystem, as computed using all techniques, is lower than that of its weakest individual component. This outcome is consistent with expectations for components arranged in a series configuration. Moreover, the results obtained from the reduced model and the first-order upper bound approximation closely align with those from the reference simulations, demonstrating higher accuracy compared to the first-order lower bound estimation.

5.3.2 First-order Failure probability Bounds of the bearings subsystem

This subsystem consists of four ball bearings: two mounted on the pinion shaft and two on the gear shaft. The corresponding limit state functions, based on the dimensionally reduced models, are as follows:

$$\text{Reduced Bearings limit stats functions}\begin{cases} G_{br1} = C_{lim1} - \dfrac{60.P}{\pi.m.z_i(N_i)^{2/3}}.L \\ G_{br2} = C_{lim2} - \dfrac{60.P}{\pi.m.z_i(N_i)^{2/3}}.L \end{cases}$$

The results of this section are mentioned in **Tab (5.2)**

Table 5.2. First-order Probability Bounds of the ball bearings subsystem

Bearings subsystem	***Bearings of the pinion shaft***	***Bearings of the gear shaft***
Reliability index	$\boldsymbol{\beta_{\_FORM\_red}}$ **= 3.030830** $\beta_{\_MCS\_or}$= 3.016632	$\beta_{\_FORM\_red}$ =6.186015 $\beta_{\_MCS\_}or$=6.18982156
Failure Probability	$P_{f\_FORM\_red}$ = 1.21949e-03 $\boldsymbol{P_{f\_MCS\_or}}$**= 1.2781e-03**	$P_{f\_FORM\_red}$ =3.01002-10 $P_{f\_MCS\_or}$= 3.01104e-10

First-order failure probability bounds of the ball bearing subsystem

	Probability of failure	**Reliability index**	**Error (MCS)**
Lower bound	$\boldsymbol{P_f}$ **=1.21949e-03**	$\boldsymbol{\beta}$**= 3.0308110**	$\varepsilon_{relative}(\%)$ =0.14
Upper bound	P_f =2.438978e-03	β = **2.8149846**	$\varepsilon_{relative}(\%)$ =1.6e-02
MCS reduced model COV=0.01	P_f =2.6641 e-03 [2.64e-03, 2.69e-03]	β= **2.78649155**	$\varepsilon_{relative}(\%)$ =6.4e-03
MCS original model COV=0.01	P_f =2.59818304 e-03 [2.57e-03, 2.63e-03]	β= **2.794602**	-

The results for the bearing subsystem show a slight deviation from those of the individual components. This deviation is attributed to the presence of two identical bearing pairs within the subsystem, which reduces the overall failure probability more significantly than in other subsystems. Furthermore, the results obtained from the first-order upper bound and the reduced model closely match the reference values, demonstrating greater accuracy compared to the first-order lower bound estimates.

5.3.3 First-order Failure probability Bounds of the transmission Shafts Subsystem

This subsystem includes two shafts, the pinion shaft and the gear shaft. The corresponding limit state functions are defined as follows:

$$\text{Reduced Shafts limit stats} \begin{cases} \text{shaft 1: } \mathrm{G_{sh1}} = \tau_{max} - (48.634).\left(\frac{P}{d_s N_p}\right)\sqrt{\frac{Leq^2}{\left(m.\,\mathrm{z_p}\right)^2}+1} \\ \text{shaft 2: } \mathrm{G_{sh2}} = \tau_{max} - (48.634).\left(\frac{P}{d_g N_g}\right)\sqrt{\frac{Leq}{\left(m.\,\mathrm{z_g}\right)^2}+1} \end{cases}$$

Table 5.3. First-order failure probability bounds of the shafts subsystem

Shafts subsystem	***Shaft of pinion***	***Shaft of gear***
Reliability index	β_{FORM_red} = 3.63429262 $\beta_{\_MCS\_}or$= 3.59577911	β_{FORM_red} =3.81674631 $\beta_{MCS\_}or$= 3.7759321
Failure Probability	$P_{f\_FORM\_red}$ = **1.394e-04** $P_{f\_MCS\_}or$= 1.617e-04	$P_{f\_FORM\_red}$ =6.763e-05 $P_{f\_MCS\_or}$= 7. 973e-05

First-order failure probability bounds of the shafts subsystem

	Probability of failure	**Reliability index**	**Error (MCS)**
Lower bound	P_f**= 1.39373405e-04**	β**=3.6342909**	$\varepsilon_{relative}(\%)$ =1.5e-01
Upper bound	P_f= 2.069861e-04	β=**3.5310128** $\varepsilon_{relative}(\%)$ =1.4e-01	
MCS reduced model COV=0.02	P_f= 1.617416667e-04 [1.59e-04, 1.64e-04]	β =**3.595730**	$\varepsilon_{relative}(\%)$ =1.4e-03
MCS original COV=0.02	P_f= 1.6312222e-04 [1.61e-04, 1.66e-04]	β= **3.5935169**	-

Table 5.3 shows that the results obtained from the reduced model closely align with the reference values and exhibit greater accuracy compared to both the first-order lower and upper bound approximations. The second set of failure probability results obtained through Monte Carlo Simulation (MCS) of the reduced model are very close to those calculated using MCS of the original model of the shaft subsystem because the reduced variables have a very low importance factor. These results demonstrate that the weight of reduced variables significantly influence the accuracy of the reliability assessment.

5.3.4 First-order Failure probability Bounds of the speed reducer system

The speed reducer system consists of a gear pair, four roller bearings, and two shafts, and is subject to a total of seven failure modes. The results for the system-level failure probability are presented in **Tab (5.4)**

Table 5.4. First-order Probability of Failure Bounds of the speed reducer system

Speed reducer system	**Failure probability**	**Reliability index**	**Error (MCS)**
Lower bound	P_f= 1.2195e-03	β= 3.030811	$\varepsilon_{relative}(\%)$ =2.8e-01
Upper bound	P_f = 2.6613e-03	β= 2.786829	$\varepsilon_{relative}(\%)$ =1.4e-01
MCS reduced model COV=0.003	P_f =4.1598e-03 [4.15e-03, 4.17e-03]	β= 2.638816	$\varepsilon_{relative}(\%)$ =9.1e-03
MCS original COV=0.002	P_f =4.0684e-03 [4.06e-03, 4.08e-03]	β= 2.646342	-

The first observation is that the failure probability of each subsystem is lower than the failure probabilities of the individual components it comprises. This outcome is expected, as the components are arranged in a series configuration, where the weakest link predominantly influences the overall reliability of the subsystem.

The second observation is that the failure probability estimated using the upper bound is more accurate than that obtained using the lower bound. This finding supports the rationale behind second-order methods, which primarily focus on refining the upper-bound estimation.

The final observation is that the failure probability of the reduced model, as calculated through Monte Carlo Simulation (MCS), closely matches that of the original subsystem and the full system. This highlights the effectiveness and robustness of the dimensionally reduced models in preserving the accuracy of reliability assessments.

5.4 Second-Order Upper Bound Method for the speed reducer system

In a series system where components exhibit positive correlation, the failure probability is influenced by the dependencies among individual elements. Positive correlation implies that the failure of one component increases the likelihood of failure in others, thereby amplifying the overall system risk.

As noted in the previous section, the upper bound of the failure probability is more accurate than the lower bound when compared with the exact results obtained through Monte Carlo Simulation (MCS) across all subsystems, thereby ensuring a conservative estimate of reliability. However, to achieve a more precise assessment, second-order bounds incorporate the aggregated effects of dependencies by integrating pair wise correlations. These correlations are computed directly using the cosine directions vector of random variables in the failure models, effectively capturing the geometric relationships between failure probabilities. This approach enhances the estimation of system reliability by accounting for the inherent dependencies among components, leading to a more realistic evaluation of failure risk.

5.4.1 Cosines direction analysis for the speed reducer models

The values of the cosine direction factors define the relative contribution of each random variable to the probability of failure. Additionally, the sign of a cosine direction factor indicates the nature of the relationship between the performance function and the physical variables. A positive cosine direction factor suggests that the variable behaves like a stress

variable, meaning that an increase in its value leads to a higher probability of failure. Conversely, a negative cosine direction factor indicates a resistance variable, where an increase in its value results in a decrease in the probability of failure.

The following section presents the cosine direction results computed using the FORM for the seven reduced models corresponding to the failure modes defined in Chapter 4.

A. Cosines direction results for bending gear pair

Tab. (5.5) illustrates the direction cosines factors (α_i) and the most probable point **(MPP)** concerning the bending stress of pinion and gear of the gear pair subsystem.

Table 5.5. Cosines direction results for the bending gear pair

Bending Stress Variables		***Pinion***			***Gear***	
		Mean	***MPP***	α_i	***MPP***	α_i
Active face width	b	37.5	37.497	-0.003	37.497	-0.003
Normal module	m	3.5	3.499	-0.006	3.499	-0.006
Experimental gear bending fatigue strength	σ_{Flim}	**310**	**38.10**	**-0.992**	**37.48**	**-0.9924**
Tooth root stress correction Factor	$\begin{cases} Y_{1p} \\ Y_{1G} \end{cases}$	(2.362 2.375)	2.376	0.0286	2.389	0.028
Tooth Root Strength Adjustment Factor	$\begin{cases} Y_{2p} \\ Y_{2G} \end{cases}$	2.214 2.259	2.180	-0.045	2.226	-0.0457
Operating Work condition factor for bending	K_1	2.759	2.867	0.0721	2.866	0.071
Power	P	7500	7697.01	0.0594	7694.34	0.058
Pinion rotational speed	N	1500	1458.4	-0.0627	1458.995	-0.062

Table (5.5) indicates that σ_{Flim} is the dominant factor with a negative sign, which means that it is a resistance variable. This signifies that the failure probability of gear pairs due to bending strength is predominantly influenced by this variable, and a decrease in this parameter might result in a significant decrease in the reliability of gear pairs.

The Most Probable Point (MPP) values represent the variable combinations that may lead to the bending failure of gear pairs at the specified reliability level. The allowable fatigue strength of the pinion is 38.1 N/mm², while that of the gear is 37.48 N/mm². At a high reliability index of $\beta = 4.420$ for the pinion and $\beta = 4.429$ for the gear, these strength values are critical and may lead to failure. The other variables have negligible sensitivity, indicating their little impact on the reliability model.

The equivalent variable sensitivities in the dimension reduction model are quite higher than those in the original model; that means that the sensitivity value becomes more important when variables are combined. This outcome is logically consistent, as the equivalent variables are functions of multiple reduced variables. Consequently, their sensitivity factors satisfy the constraint: $\sum_{i=1}^{n} {\alpha_i}^2 = 1$.

B. Cosines direction results for gear pairs contact

The cosines direction results for the contact gear pair are shown in **Tab 5.6.**

Table 5.6. Cosines direction results for the contact gear pair

Contact Variables	***Symbol***	***Mean***	***MPP***	$\boldsymbol{\alpha_i}$
Active face width	$\boldsymbol{b}$	37.5	37.49	-0.0098
Normal module	$\boldsymbol{m}$	3.5	3.498	-0. 019
Experimental flank contact fatigue strength	$\boldsymbol{\sigma_{Hlim}}$	**1300**	**721.76**	**-0.845**
Contact stress correction factors	$\boldsymbol{Z_1}$	341.335	355.8	0.19
Tooth contact strength adjustment Factors	$\boldsymbol{Z_2}$	**0.9855**	**0.859**	**-0.36**
Working conditions factors	$\boldsymbol{K_2}$	3.615	3.959	0.197
Power	**P**	7500	8095.998	0.18
Pinion speed	$\boldsymbol{N}$	1500	1357.856	-0.22

According to Table (5.6), $\boldsymbol{\sigma_{Hlim}}$ is the primary factor affecting the failure probability of gear pairs in the contact stress model. Decreases in this parameter may lead to a considerable fall in gear pair reliability. MPP values represent variable values that may cause gear pair contact strength failure at the required reliability.

The factors($\boldsymbol{Z_1}$, $\boldsymbol{Z_2}$, $\boldsymbol{P}$, $\boldsymbol{N}$, $\boldsymbol{K_2}$, and $\mathbf{T_1}$) contribute moderately to the contact failure probability but are not dominant factors. In the dimension reduction model, equivalent variable sensitivities are much larger than in the original model, making sensitivity more significant when variables are combined.

The suggested gear material, 20CrMnMo, satisfies the design requirements for both bending and contact strength, as evidenced by the high reliability values obtained for the gear pairs.

C. Cosines direction results for ball bearings subsystem.

The cosines direction results for the bearings are shown in **Tab 5.7.**

Table 5.7. Cosines direction results for the bearings subsystem

Ball bearings Variables	***Pinion shaft Bearings***			***Gear shaft Bearings***	
	Mean	***MPP***	α_i	***MPP***	α_i
Normal module m	3.5	3.498	-0.0286	3.498	-0.02
Dynamic load capacity lim C_{lim1}, C_{lim2}	**(9360, 11200)**	**7295.19**	**-0.730**	**5192.64**	**-0.867**
Power **P**	**7500**	**8621.73**	**0.490**	**9047.1**	**0.330**
Pinion speed N	**1500**	**1301.89**	**-0.436**	**1180.073**	**-0.345**
Equivalent variable L	0.3262	0.3325	0.188	0.335	0.130

The load capacity C_{lim} the most significant influence on the probability of failure; increasing Clim leads to substantial improvements in system reliability. Additionally, both ball bearings are moderately affected by variations in power and rotational speed. The equivalent variable sensitivities in the dimension-reduced model are notably higher than those in the original model, confirming the principle that sensitivity increases when variables are combined.

D. Cosines direction results for shaft subsystem.

The cosines direction results for the shaft subsystem are shown in **Tab 5.8.**

Table 5.8. Cosines direction results for the shaft subsystem

Shafts Variables	***Pinion shaft***			***Gear shaft***	
	Mean	***MPP***	α_i	***MPP***	α_i
Normal module m	3.5	3.499	-0.0012	3.499	-0.000075
Power P	**7500**	**8548.40**	**0.278**	**8257.18**	**0.26**
Pinion speed N	**1500**	**1322.7**	**-0.351**	**1308.5**	**-0.33**
Pignon Shaft diameter d_P	20	19.984	-0.046	-	-
Gear Shaft diameter d_g	32	-	-	31.974	-0.044
Maximum permissible shear τ_{max}	**78**	**37.12**	**-0.893**	**37.65**	**-0.903**
L_{sh}	36.4	36.412	8.3e-04	36.404	0.000053

The variable with the greatest influence on the probability of failure is the maximum permissible shear stress. Both shafts exhibit a Most Probable Point (MPP) value of approximately 37 N/mm² for this variable, indicating that this threshold may lead to failure at the estimated reliability level.

Additionally, power and rotational speed have a moderate impact on the performance of both shafts. While variations in these parameters may influence performance, prioritizing more critical factors—such as shear stress—may yield more substantial improvements. Nevertheless, controlling power and rotational speed remains essential to ensure shaft balance and overall system reliability

5.4.2 Correlation matrix for the speed reducer models

Second-order bounds improve the estimation of failure probability by considering the combined effects of component dependencies. They accomplish this by incorporating pair wise correlations, which illustrate the impact of one component's failure on another. The cosines direction of random variables in failure models is explicitly used to calculate these correlations, which represent their geometric relationships.

Table 5.9. Cosines direction of the speed reducer random variables

Random Variables	$\alpha_{G1(ben-p)}$	$\alpha_{G2(ben-g)}$	$\alpha_{G3(cont-gp)}$	α_{G4-br1}	α_{G5-br2}	α_{G6-shp}	α_{G7-shg}
$\boldsymbol{b}$	-0.003	-0.003	-0.0098	0	0	0	0
$\boldsymbol{m}$	-0.006	-0.006	-0. 019	-0.0286	-0.02	-0.0012	-7.5 e-05
$\boldsymbol{\sigma_{Flim}}$	**-0.992**	**-0.9924**	0	0	0	0	0
$\boldsymbol{Y_{1p}}$	0.0286	0	0	0	0	0	0
$\boldsymbol{Y_{2p}}$	-0.045	0	0	0	0	0	0
$\boldsymbol{P}$	0.0594	0.058	0.18	**0.490**	**0.330**	0.278	0.26
$\boldsymbol{N}$	-0.0627	-0.062	-0.22	-0.436	-0.345	-0.351	-0.33
$\boldsymbol{K_1}$	0.0721	0.071	0	0	0	0	0
$\boldsymbol{Y_{2g}}$	0	0.028	0	**0**	**0**	**0**	**0**
$\boldsymbol{Y_{1g}}$	0	-0.0457	0	**0**	**0**	**0**	**0**
$\boldsymbol{\sigma_{Hlim}}$	0	0	**-0.845**	0	0	0	0
$\boldsymbol{Z_2}$	0	0	0.19	0	0	0	0
$\boldsymbol{Z_1}$	0	0	-0.36	0	0	0	0
$\boldsymbol{K_2}$	0	0	0.197	0	0	0	0
$\boldsymbol{C_{lim1}}$	0	0	0	**-0.730**	0	0	0
$\boldsymbol{L}$	0	0	0	0.188	0.130	0	0
$\boldsymbol{C_{lim2}}$	0	0	0	0	**-0.867**	0	0
$\boldsymbol{d_{sp}}$	0	0	0	0	0	-0.046	0
$\boldsymbol{\tau_{max}}$	0	0	0	0	0	-0.893	**-0.903**
$\boldsymbol{d_{sg}}$	0	0	0	0	0	0	-0.044
$\boldsymbol{L_{sh}}$	0	0	0	0	0	8.3e-04	5.3e-05

The correlation matrix is then calculated based on direction cosines in **Tab**. (5.9) using equation(3.50):

$$\mathrm{Cor}(G_i, G_j) = \langle \alpha_{Gi} \rangle \{\alpha_{Gj}\} = \rho_{ij}$$

The correlation matrix is:

1.0000	0.9971	0.0247	0.0567	0.0415	0.0385	0.0363
0.9971	1.0000	0.0243	0.0557	0.0408	0.0379	0.0356
0.0247	0.0243	1.0000	0.1852	0.1362	0.1273	0.1198
0.0567	0.0557	0.1852	1.0000	0.3381	0.2893	0.2721
0.0415	0.0408	0.1362	0.3381	1.0000	0.2132	0.2005
0.0385	0.0379	0.1273	0.2893	0.2132	1.0000	0.9975
0.0363	0.0356	0.1198	0.2721	0.2005	0.9975	1.0000

The correlation matrix shows that the bending strength of the pinion and gear are associated events, with a value exceeding (0.9971). A similar scenario exists for the shafts model, which has a correlation factor of more than (0.9975), signifying that these two events can occur concurrently. The bearing models have a moderate correlation factor of (0.3388), indicating that the failure of one may precipitate the failure of another. A similar scenario exists for the bearing models in conjunction with the shaft models ($\rho_{46} = 0.2893$), which also demonstrate a moderate correlation.

The correlation factors ρ_{ij} between the speed reducer failure modes are presented in the vector:

$$\rho_{ij} = [\rho_{12}\ \rho_{13}\ \rho_{14}\ \rho_{15}\ \rho_{16}\ \rho_{17}\ \rho_{23}\ \rho_{24}\ \rho_{25}\ \rho_{26}\ \rho_{27}\ \rho_{34}\ \rho_{35}\ \rho_{36}\ \rho_{37}\ \rho_{45}\ \rho_{46}\ \rho_{47}\ \rho_{56}\ \rho_{57}\ \rho_{67}]$$

$$\rho_{ij} = [0.9971\ \ 0.0247\ \ 0.0567\ 0.0415\ 0.0385\ 0.0363\ 0.0243\ 0.0557\ 0.0408\ 0.0379\ 0.0356$$
$$0.1852\ 0.1362\ 0.1273\ 0.1198\ 0.3381\ 0.2893\ 0.2721\ 0.2132\ 0.2005\ \ 0.9975]$$

The angles between the normal vectors of respective limit-states (θ_{ij}) planes graphically shows the correlations among failure occurrences.

θ_{ij} [6.5363 89.2666 87.9254 88.7337 88.6076 88.6362 89.4041 88.3153 88.9686 88.8712 88.8941 84.6465 86.7324 86.4339 86.5085 78.0124 79.7758 79.9912 83.7827 83.9095 4.5849

The cosine of this angle corresponds to the correlation coefficient; a value of 1(0° angle) signifies perfect alignment, indicating that the two events occur simultaneously. On the other hand, an angle of 0° (90°) indicates independence, suggesting that the two events are

likely to occur simultaneously. If the angle is 90 degrees (cosine 0), the variables are uncorrelated; if the angle is substantial (cosine approaching -1), they exhibit a negative correlation.

For example, the bending strengths of the pinion and gear represent strongly correlated events, with a correlation factor of ρ_{12} =0.9971, resulting in an angle of $\theta_{12} = 6.5363$ between the normal vectors of their respective limit-state hyper planes. Similarly, in the shafts model, the two failure events are also highly correlated, with a correlation factor of ρ_{67} =0.9975 corresponding to an angle $\theta_{67} = 4.5849$ between the normal vectors of respective limit-state hyper planes. In contrast, the correlation between the pinion bending model and the gear pair contact model is very low, with ($\rho_{13} = 0.0247$), resulting in a nearly orthogonal angle of ($\theta_{13} = 89.2666$) between their respective limit-state hyper planes.

5.4.3. Second-order of failure probability bounds for the speed reducer system

Second-order bounds are derived by including supplementary terms that reflect the joint probability of failure events $\mathbf{P}(\mathbf{E_i} \cap \mathbf{E_j})$. These terms specifically involve the probability of failure of intersection between events, thereby enhancing the accuracy of the estimation. The failure probability bounds of the intersection $\mathbf{P}(\mathbf{G_i} \cap \mathbf{G_j})$ are calculated based on the first-order approximation method (FORM). The method is explained in detail in chapter 3. The steps to calculate the term $\mathbf{P}(\mathbf{G_i} \cap \mathbf{G_j})$ are as follows:

1) Calculate: $\boldsymbol{a_{ij}} = \frac{\beta_j - \rho_{ij}\beta_i}{\sqrt{1-\rho_{ij}{}^2}}$ and $\boldsymbol{b_{ij}} = \frac{\beta_i - \rho_{ij}\beta_j}{\sqrt{1-\rho_{ij}{}^2}}$

2) Calculate: $P(A) = \Phi(-\beta_i)\Phi(-b_{ij})$

3) Calculate: $P(B) = \Phi(-\beta_j)\Phi(-a_{ij})$

4) As shown in the correlation matrix, all factors are positive. In this case, the bounds of intersection $\mathbf{P}(\mathbf{G_i} \cap \mathbf{G_j})$ are:

$$\max(P(A); P(B)) \leq P(G_i \cap G_j) \leq P(A) + P(B)$$

$$P_{ij} = [\max(P(A); P(B)), P(A) + P(B)]$$

5) It is now possible to calculate the terms $\mathbf{P}(\mathbf{G_i} \cap \mathbf{G_j})$ needed for the second-order bounds. The results are shown in **Tab 5.10**.

Table 5.10. Failure probability bounds of the intersection $\mathbf{P}(\mathbf{G_i} \cap \mathbf{G_j})$

	ρ_{ij}	a_{ij}	$P_{ij}(A)$	b_{ij}	$P_{ij}(B)$	$\mathbf{P}(\mathbf{G_i} \cap \mathbf{G_j})$
G_1G_2	0.9971	0.285	0.388	0.051	0.479	[2.3e-06 4.2e-06]
G_1G_3	0.0247	4.281	9.31e-06	4.313	8.05e-06	[4.6e-11 9.2e-11]
G_1G_4	0.0567	2.785	0.0027	4.255	1.0e-05	[1.3e-08 2.6e-08]
G_1G_5	0.0415	6.01	9.4e-10	4.167	1.5e-05	[4.7e-15 9.4e-15]
G_1G_6	0.0385	3.467	2.6e-04	4.283	9.2e-06	[1.3e-09 2.6e-09]
G_1G_7	0.0363	3.659	1.28e-04	4.285	9.1e-06	[6.2e-10 1.2e-09]
G_2G_3	0.0243	4.282	9.2e-06	4.324	7.7e-06	[4.3e-11 8.7e-11]
G_2G_4	0.0557	2.788	0.0026	4.267	9.9e-06	[1.2e-08 2.4e-08]
G_2G_5	0.0408	4.211	1.27e-05	4.180	1.4e-05	[6.0e-11 6.0e-11]
G_2G_6	0.0379	3.468	2.6e-04	4.294	8.7e-06	[1.2e-09 2.4e-09]
G_2G_7	0.0356	3.661	1.25e-04	4.296	8.7e-06	[5.9e-10 1.2e-09]
G_3G_4	0.1852	2.257	0.012	3.895	4.9e-05	[6.8e-08 1.3e-07]
G_3G_5	0.1362	5.641	8.4e-09	3.580	1.7e-04	[5.3e-14 1.0e-13]
G_3G_6	0.1273	3.101	9.6e-04	3.958	3.8e-05	[5.5e-09 1.07e-08]
G_3G_7	0.1198	3.315	4.58e-04	3.958	3.8e-05	[2.6e-09 5.1e-09]
G_4G_5	0.3381	5.484	2.07e-08	0.998	0.16	[4.9e-11 7.4e-11]
G_4G_6	0.2893	2.881	0.002	2.068	0.019	[2.7e-06 5.1e-06]
G_4G_7	0.2721	3.109	9.37e-04	2.070	0.019	[1.3e-06 2.4e-06]
G_5G_6	0.2132	2.370	0.0089	5.538	1.5e-08	[2.7e-12 4.8e-12]
G_5G_7	0.2005	2.630	0.0043	5.533	1.6e-08	[1.3e-12 2.4e-12]
G_6G_7	0.9975	2.710	0.003	-2.446	0.993	[6.7e-05 6.7e-05]

The Second-order failure probability bounds system is calculated using the following formulas:

$$
\begin{aligned}
&P(F) = P(F1) \\
&+ P(F2) - P(F1 \cap F2) \\
&+ P(F3) - P(F1 \cap F3) - P(F2 \cap F3) + P(F1 \cap F2 \cap F3) \\
&+ P(F4) - P(F1 \cap F4) - P(F2 \cap F4) - P(F3 \cap F4) + P(F1 \cap F2 \cap F4) \\
&+ P(F1 \cap F3 \cap F4) + P(F2 \cap F3 \cap F4) - P(F1 \cap F2 \cap F3 \cap F4) \\
&+ P(F5) - \cdots
\end{aligned} \tag{5.1}
$$

The third order of this equation generally has a very small value so that we can neglect it. The equation (5.1) becomes:

$$P(F) = P(F1) + P(F2) - P(F1 \cap F2) + P(F3) - P(F1 \cap F3) - P(F2 \cap F3) + P(F4) - P(F1 \cap F4) - P(F2 \cap F4) - P(F3 \cap F4) + P(F5) - \cdots \quad (5.2)$$

5.4.3.1 Second order failure probability bounds for gear pair subsystem

The second-order failure probability bounds for the gear pair subsystem are defined as:

$$P(F)_{gear} = P(F_{b\_p}) + P(F_{b\_g}) + P(F_{c\_g}) - P(F_{b\_p} \cap F_{b\_g}) - P(F_{b\_p} \cap F_{c\_g}) - P(F_{b\_g} \cap F_{c\_g}) \quad (5.3)$$

The results are shown in Tab(5.11).

Table 5.11. Second-order failure probability bounds for the gear pair subsystem

Components of gear subsystem	*Failure Probability*	*Reliability index β*	*Absolute Error %*
Second-order Lower bound	**1.11836e-05**	**4.2398519**	2.0e-04
Second-order Upper bound	**1.309544e-05**	**4.2042893**	1.1 e-05
First-order Lower bound	5.70 e-06	4.38875	7.5e-03
First-order Upper bound	1.5363966e-05	4.168007	2.2e-04
MCS reduced model	1.2367e-05	4.21722	8.4e-05
MCS original model	1.3208e-05	4.202343	0

The results presented in Table 5.11 for the failure probability of the gear pair, obtained using the second-order failure probability upper bound method, are very close to those obtained through Monte Carlo Simulation (MCS) for both the reduced and original models. This similarity arises from the fact that correlations between failure modes are accounted for in the second-order bounds.

Furthermore, the results from the dimension reduction models align closely with those obtained via MCS, demonstrating that the reduced models is reliable for estimating the reliability of complex gear pair subsystems.

It is also noteworthy that bending and contact failures in the gears exhibit weak correlation, indicating that the subsystem's overall reliability is not significantly affected by interactions between these two failure modes. This distinction is advantageous, as it suggests that these failure mechanisms operate largely independently and do not strongly influence each other's probabilities.

5.4.3.2 Second-order failure probability bounds for of the ball bearing subsystem

Two identical bearings mounted on the pinion shaft and two identical gearings mounted on the gear shaft make up the ball bearings subsystem. Therefore, we define the second-order failure probability bounds for the roller bearings subsystem as follows:

$$P(F)_{bearings} = P(F_{br_{sh}p}) + P\left(F_{br_{shg}}\right) + P(F_{br_{sh}p}) + P(F_{br\_shg}) - P(F_{br_{sh}p} \cap F_{br\_shg}) - P(F_{br_{sh}p} \cap F_{br\_shg}) \quad (5.4)$$

The results of this section are illustrated in **Tab 5.12**.

Table 5.12. Second-order failure probability bounds for bearings subsystem

Components of ball bearing subsystem	*Failure Probability*	*Reliability index β*	*Absolute Error %*
Second-order Lower bound	**2.43897816 e-03**	**2.8149846**	1.6 e-02
Second-order Upper bound	**2.43897822 e-03**	**2.8149846**	1.6 e-02
First-order Lower bound	1.2194889e-03	3.0308110	1.4 e-1
First-order Upper bound	2.438978e-03	2.8149846	1.6 e-02
MCS reduced model	2.6641 e-03	2.78649155	6.6 e-03
MCS original model	2.59818304 e-03	2.794602	0

The failure probability of the bearings subsystem, assessed by the Second-Order System Bounds, is approximated at 0.001, signifying moderate overall reliability for this subsystem. The Monte Carlo Simulation (MCS) method gives a precise estimate of the failure probability, which supports the conclusion that the reliability is moderate. The correlation coefficient between the first and second bearing models is 0.3381, indicating a moderate connection. This indicates that the two components function with a certain level of interdependence; nonetheless, the failure of one does not substantially impact the other.

Furthermore, the failure probability of a bearing block consisting of four bearings is comparatively greater than that of a block containing only two identical bearings. This case

illustrates that in a series system, the probability of failure escalates with the addition of identical components.

In addition, as in the previous subsystem, the reduction dimension model demonstrates its effectiveness in resolving system reliability issues, yielding results that closely align with the MCS of the original model.

5.4.3.3 Second-order failure probability bounds for shafts subsystem

The second-order failure probability bounds for the shafts subsystem are defined as:

$$P(F)_{shafts} = P(F_{sh\_p}) + P(F_{sh\_g}) - P(F_{sh\_p} \cap F_{sh\_g}) \quad (5.5)$$

Table 5.13. Second-order failure probability bounds for the shaft subsystem

Components of Shafts subsystem	*Failure Probability*	*Reliability index β*	*Absolute Error %*
Second-order Lower bound	**1.3986059608e-04**	**3.6333910**	2.3 e-03
Second-order Upper bound	**1.39860597399e-04**	**3.6333910**	2.3 e-03
First-order Lower bound	1.39373405e-04	3.6342909	2.4 e-03
First-order Upper bound	2.069861e-04	3.5310128	4.4 e-03
MCS reduced model	1.617416667e-04	3.59572987	1.0 e-04
MCS original model	1.6312222e-04	3.59351693	0

This Table analyzes the shaft subsystem's reliability, focusing on both its components. The shaft subsystem failure probability is estimated using second-order upper bounds and Monte Carlo Simulation (MCS), which yield similar results. The second-order system bounds estimate the shaft subsystem failure probability to range from 10^{-4}, which indicates a high shaft subsystem reliability. A correlation coefficient of $\rho_{67} = 0.9975$ indicates an almost complete positive connection. This means that whether one shaft performs or fails, the other performs or fails, too.

Furthermore, the dimension reduction model proves successful in addressing system dependability challenges, producing results that nearly correspond with the MCS of the original model.

5.4.3.4 Second-order failure probability bounds for the speed reducer system

The second-order upper bound for the overall speed reducer system failure probability is defined by equation (5.2):

Table 5.14. Second-order failure probability bounds for the speed reducer system

Components of Speed reducer system	*Failure Probability*	*Reliability index β*	*Absolute Error %*
Second-order Lower bound	**2.5820857 e-03**	**2.7966107**	0.15
Second-order Upper bound	**2.5877415 e-03**	**2.7959036**	0.15
First-order Lower bound	1.21948885e-03	3.0308111	0.28
First-order Upper bound	2.6613284 e-03	2.7868289	0.14
MCS reduced model	4.1598 e-03	2.63881648	0.009
MCS original model	4.06837537 e-03	2.646342	0

The reliability analysis of the reducer system, encompassing the gear pair, roller bearings, and shaft subsystems, is computed using second-order upper bound. The overall speed reducer system has an increased probability of failure than its components $P_{f\_syst} = [2.582\text{e}-03 - 2.588\text{e}-03]$, indicating that the combined subsystem is less reliable than its separate components. The gear and shaft blocks exhibit high reliability, whereas the bearing block's moderate reliability indicates that enhancements can be implemented in one component without substantially impacting the other.

Furthermore, the dimension reduction model and the second-order upper bound approximation validate their efficacy in solving reliability issues, yielding results that closely align with the MCS of the original model.

5. 5 Conclusion

This chapter has presented a comprehensive approach to evaluating system failure probability bounds through dimensional reduction models applied to a speed reducer. By analyzing the role of independence between failure modes models, we have emphasized its significance in accurately estimating structural system reliability.

The bounding approximation methods, particularly second-order system bounds, provide practical upper and lower limits for failure probability estimation, improving predictive accuracy when correlations among failure modes are identified. The second-order bounds serve as a viable alternative, balancing computational efficiency with improved accuracy in reliability evaluation. These methods enable a more refined assessment of system reliability, particularly for multidimensional performance functions, thereby supporting reliability-based decision-making processes.

Furthermore, the dimension reduction model demonstrates its effectiveness in tackling system reliability challenges by efficiently handling highly nonlinear models, such as gear contact, bearings, and shaft models, while producing results that closely align with those obtained from Monte Carlo Simulation (MCS) of the original model, especially when the reduced variable have a very low importance factors, so their influence on the failure probability assessment is very low.

The next chapter will focus on enhancing the reliability and optimizing the design of a gear pair using Reliability-Based Robust Design Optimization (RBRDO) within the Sequential Optimization and Reliability Assessment (SORA) framework.

CHAPTER 6 RELIABILITY BASED ROBUST DESIGN OPTIMIZATION OF A GEAR PAIR

6.1 Introduction

Ensuring the reliability and robustness of a mechanical system at the design stage has become essential for effectively managing inherent uncertainties. In this chapter, the objective is to increase the reliability of a mechanical system based on sensitivity factors analysis using two methods: the first is to change the statistical parameters of the most influential variables on the performance model. The second approach applies a Reliability-Based Robust Design Optimization (RBRDO) technique to systematically account for uncertainties while optimizing the system's performance and robustness.

Initially, a reliability analysis is performed using the First- and Second-Order Reliability Methods (FORM and SORM), with Monte Carlo Simulation employed as a benchmark for validation. In addition, FORM is used to evaluate reliability sensitivity and elasticity factors, which facilitate the identification of the most influential parameters affecting system performance. These factors not only reveal variables that are most sensitive to statistical variations but also aid in reducing the design variable number within the RBRDO framework.

Subsequently, Reliability-Based Robust Design Optimization (RBRDO) is performed using the Sequential Optimization and Reliability Assessment (SORA) method, guided by the elasticity factor results. The SORA approach integrates reliability analysis with optimization procedures, enabling the development of designs that are not only optimal in performance but also robust against inherent uncertainties.

Both methodologies are applied to the gear pair subsystem presented in the previous chapters—one of the key components of the speed reducer discussed in chapters 4 and 5—which operates under severe loading conditions that significantly compromise its reliability. The study focuses on three critical failure modes commonly encountered in gear operation: bending stresses in the pinion and wheel teeth, as well as contact stress within the gear pair.

6.2 Reliability-based robust design optimization steps

According to Taguchi et al. (2005), Reliability-Based Robust Design (RBRD) is defined as a robustness concept that can be directly used as a design criterion. A robust design is characterized by its ability to minimize sensitivity to variations in the statistical properties of input random variables—such as mean, standard deviation, and distribution type—while ensuring feasibility and performance within an acceptable cost range. The Reliability-Based

Robust Design Optimization (RBRDO) approach adopted in this chapter follows a structured six-step methodology, as outlined below.

- **Step1. Limit stat functions**: Define the failure modes and their corresponding limit state functions. Additionally, specify all relevant random variables involved in the performance and failure models.

- **Step2. Reliability-based design analysis**: Conduct a Reliability-based design aimed at identifying the Most Probable Point (MPP) of failure using iterative optimization techniques such as FORM or SORM.

- **Step 3. Sensitivity and Elasticity Analysis**: Perform a detailed sensitivity and elasticity analysis for each random variable to quantify their influence on system reliability. This step is critical for identifying key parameters that significantly impact performance.

- **Step4. Parametric analysis:** Based on the results of the elasticity analysis, select the most influential parameters. This selection informs design improvement strategies and helps establish both the design variable vector and the random variable vector for the RBRDO process.

- **Step5. Reliability-Based Robust Design Optimization Formulation** The RBRDO problem is formulated to enhance system reliability and robustness under uncertainty. A bi-objective optimization approach is employed, which seeks to minimize both the mean and the variance of the performance function simultaneously. The mathematical formulation of the problem is expressed as:

$$\begin{cases} \text{minimize} \quad f1(\mathrm{x}) = [\mu_{\mathrm{G}}] \\ \text{minimize } f2(\mathrm{x}) = [\sigma_{\mathrm{G}}^2] \\ \text{Subject to} \quad \mathrm{Prob}[\mathrm{G}(\mathrm{d},\mathrm{X}) \geq 0] \geq \mathrm{R_T} \\ \mathrm{d_k^l} \leq \mathrm{d_k} \leq \mathrm{d_k^u} \end{cases} \tag{6.1}$$

The bi-objective optimization can be reformulated into a single objective function using a weighted sum approach, as represented in the following equation

$$\begin{cases} \text{minimize} \quad f(x) = [w \times \mu_G + (1-w) \times \sigma_G^2] \\ \text{subject to} \quad Prob[G(d,X) \geq 0] \geq R_T \\ d_k^l \leq d_k \leq d_k^u \end{cases} \tag{6.2}$$

$f(x)$ represents the objective function; with $\boldsymbol{w}$ denoting the weighting factor, it can be adjusted within the range of $0 \leq w \leq 1$.

$G(d,x)$ represents the probabilistic constraint, X represents random variables, and R_T

denotes the target reliability.

d_k k=1, 2.....n are the design variables.

The literature extensively documents a variety of algorithms capable of solving the aforementioned optimization problem. In this study, the **Sequential Optimization and Reliability Assessment (SORA)** method is adopted to determine the optimal values of the critical design parameters while satisfying a predefined reliability target. SORA decouples the optimization and the reliability assessment tasks in an iterative process. Each cycle distinctly separates the optimization and the reliability assessment phases, with the latter performed after deterministic optimization to verify constraint feasibility. The core principle of this approach involves systematically adjusting the boundaries of violated constraints in a feasible direction, leveraging reliable information obtained from the preceding iteration. As a result, both design accuracy and computational efficiency progressively improve with each successive cycle.

- **Step** 6. **Confirmation of Design Robustness:** The final step involves recalculating the sensitivity and elasticity factors based on the optimized design. These factors are then compared with those obtained prior to optimization to verify improvements in robustness and reliability. This comparison serves as a validation of the RBRDO process and ensures that the design is less sensitive to input uncertainties.

Figure (6.1) illustrates the key steps involved in the Reliability-Based Robust Design Optimization (RBRDO) process.

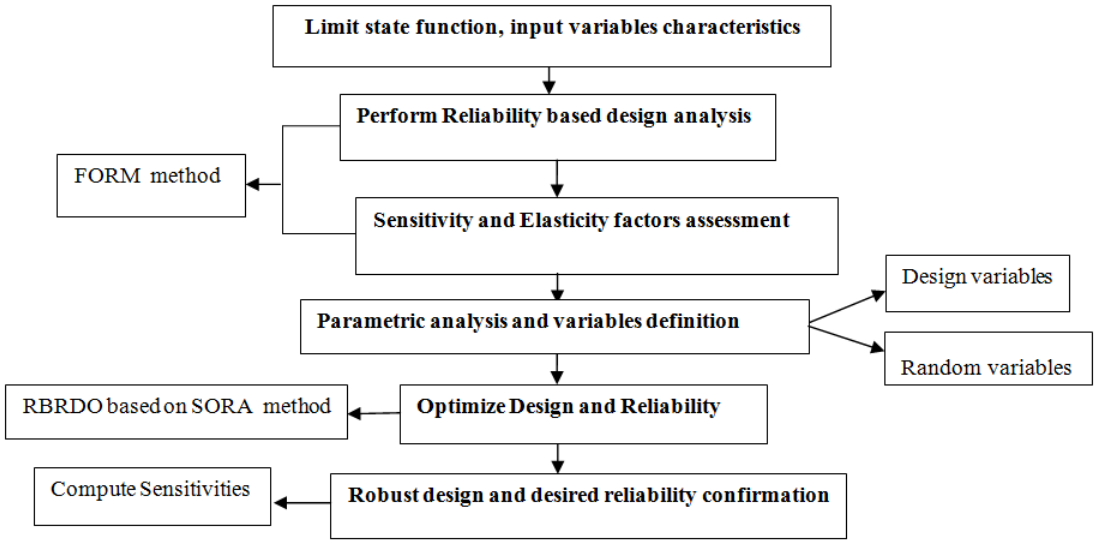

Figure 6.1. Key steps involved in the RBRDO process

6.3 Reliability-based robust design optimizations of the gear pair

This section presents the application of the RBRDO methodology to a gear pair, illustrating how the proposed approach can enhance reliability and robustness under severe operating conditions.

6.3.1 Reliability-based design of the gear pair

To conduct a reliability study, it is essential to define three distinct types of models: a physical model, a probabilistic model, and a performance model.

6.3.1.1Presentation of the physical model of the gear pair

Three failure scenarios that may arise during gear operation correspond to three distinct physical models: the bending stresses experienced by the pinion and gear, as well as the Hertzian tooth contact stress.

The assumed bending stress σ_F represents the maximum tensile stress at the surface of the tooth root, as defined in Standard ISO 6336-3:2006. This value can be calculated using equation:

$$\sigma_F = \frac{F_t}{b.m} Y_F Y_S Y_\beta Y_\varepsilon K_A K_V K_{F\alpha} K_{F\beta} \leq \sigma_{FP}$$

$$\sigma_{FP} = \sigma_{Flim} Y_{ST} Y_{NT} Y_{\delta relT} Y_{RrelT} Y_X$$

The assessment of contact stress is conducted using the standard equation Standard ISO 6336-2:2006:

$$\sigma_H = Z_H Z_E Z_\beta Z_\varepsilon \sqrt{\frac{F_t}{d_1 b} \frac{u \pm 1}{u} K_A K_V K_{H\beta} K_{H\alpha}} \leq \sigma_{HP}$$

$$\sigma_{HP} = \sigma_{Hlim} Z_{NT} Z_L Z_V Z_R Z_W Z_X$$

6.3.1.2 Presentation of the probabilistic model of the gear pair

All variables exhibit a standard normal distribution of the input data. The mean values and standard deviations of the random variables are derived from bibliographic sources [Zhang et al. (2003)], Yang et al. (2012)].

Almost random variables statistics are the same for the previous gear pair in chapter 5 and are given in given in Annex 1. The modified variables from the previous are given in **Table 6.1**

Table 6. 1: Random variables statistics

Gear pair variables	***symbol***	***Mean and standard deviation***
Pinion pitch diameter	d_1	*N(148.75,0.74375) mm*
Active face width	b	*N(200,1) mm*
Tangential force	F_t	*N(34644,519.66)N*

6.3.1.3 Presentation of the performance model of the gear pair

The first performance model is characterized by a bending model for the pinion, as represented by the following equation :

$$G_1(x) = \sigma_{FP1} - \sigma_{F1} \tag{6.3}$$

The second performance model is characterized by the bending model for the gear, as represented by equation:

$$G_2(x) = \sigma_{FP2} - \sigma_{F2} \tag{6.4}$$

The third performance model represents contact stress for a gear pair as represented by equation (6.9):

$$G_3(x) = \sigma_{HP} - \sigma_H \tag{6.5}$$

6.3.1.4 Reliability assessment results for the gear pair

The reliability results for each scenario $G_1(x)$, $G_2(x)$, and $G_3(x)$ are presented in Tables (6.2), (6.3), and (6.4), respectively. Additionally, results from published sources are presented, including those from the perturbation method (Zhang et al., 2003), as well as the Edgeworth Series methods (RE) and MCSa, as reported by Yang et al. (2012). The error of each method ($\boldsymbol{\varepsilon_R}$) in relation to the MCS results, along with the values of the convergence criterion and the number of limit state appeals, are also presented.

a. Bending stress reliability results for pinion and gear

Table 6.2 Bending reliability for pinion model

Pinion	***MCS***	***FORM***	***SORM***	***Perturbation method***	***MCS*** [a]	***RE Edgeworth***
Reliability R	0.99734	0.99742	0.99733	0.9963	0.9974	0.99644
Error ε_R (%)	-	0.008	0.001	0.104	0.006	0.090
Reliability index β	2.7867	2.7964	2.7860	2.754	2.6754	2.6754
Convergence criterion	Cov=0.0061	$\left\|\frac{G(x^*)}{G(x_0)}\right\|$=6.08×10^{-8}	-	-	-	
Appeals number	10^7	5	6	-	-	-

The reliability results for the bending reliability for gear model are mentioned in **Tab 6.3**

Table 6.3 Bending reliability for gear model

Gear	***MCS***	***FORM***	***SORM***	***Perturbation method***	***MCS*** [a]	***RE Edgeworth***
Reliability R	0.99760	0.99767	0.99759	0.9966	0.9974	0.99644
Error ε_R (%)	-	0.007	0.001	0.1	0.02	0.090
Reliability index β	2.8206	2.8294	2.8190	2.705	2.6754	2.6754
Convergence criterion	Cov=0.0065	$\left\|\frac{G(x^*)}{G(x_0)}\right\|$=6.4×10^{-8}	-	-	-	
Appeals number	10^7	5	6	-	-	-

The findings presented in Tables 6.2 and 6.3 indicate that FORM and SORM align with MCS. In this example, the SORM method demonstrates the highest accuracy, achieving an error rate of ($\varepsilon_R = 10^{-3}\%$) with a total of 6 appeals to the limit state.

Additionally, the SORM approximation predicts with greater accuracy than FORM. This observation may suggest the presence of nonlinearity in the response, and it demonstrates that SORM has effectively accounted for the curvatures of these limit states.

The results derived from the perturbation method and the Edgeworth series, as documented in published findings, exhibit a discrepancy when compared to the Monte Carlo Simulation (MCS) results, with error orders of $\varepsilon_R = 0.1\%$ and $\varepsilon_R = 0.09\%$, respectively.

b. Reliability based on contact stress for the gear pair

The reliability results for the contact reliability for gear pair model are mentioned in Tab 6.4.

Table 6.4 Contact gear pair reliability

Gear pair	***MCS***	***FORM***	***SORM***	***Perturbation method***	***MCS*** [a]	***RE Edgeworth***
Reliability R	0.999462	0.999496	0.999464	0.9985	0.9994	0.9989
Error ε_R (%)	-	0.003	0.0002	0.096	0.006	0.05
Reliability index β	3.2699	3.2880	3.2709	2.9685		2.9685
Convergence criterion	Cov=0.0136	$\left\|\frac{G(x^*)}{G(x_0)}\right\|$=4.56×10^{-7}	-	-	-	
Appeals number	10^7	5	5	-	-	-

Table 6.4presents the reliability results related to flank contact. It shows that the reliability values and corresponding reliability indices obtained using approximation methods—FORM and SORM—are in close agreement with those computed via Monte Carlo Simulation (MCS), with error rates of ε_R= 0.003% and ε_R= 0.0002%, respectively.

The convergence and consistency of the FORM and SORM methods used in this analysis are considered satisfactory; the ratio $\left|\frac{G(x^*)}{G(x_0)}\right|$ is found to be very close to zero, indicating that the estimated most probable point of failure lies near the limit state surface, thus confirming the accuracy of the approximation. Additionally, the Monte Carlo Simulation (MCS) results exhibit high precision, as reflected by a coefficient of variation $cov < 0.05$ underscoring the reliability of the probabilistic assessment.

Based on the presented results, the reliability index calculations indicate that the SORM method provides more accurate estimates of both reliability and the reliability index β at a lower computational cost compared to the Monte Carlo Simulation (MCS) technique. Furthermore, SORM demonstrates greater precision than the FORM method, particularly in the presence of nonlinear limit state functions. These findings validate the effectiveness of SORM for conducting reliability analyses in scenarios where nonlinearity significantly influences the system's behavior.

6.3.2 Reliability Sensitivity and elasticity analysis

6.3.2.1 Elasticity factors analysis

From a design perspective, elasticity with respect to the mean values provides valuable insights into which design dimensions should be tightly controlled or adjusted, whereas elasticity with respect to standard deviations offers guidance for implementing effective quality control measures. Calculating the elasticity of the failure probability with respect to the parameters of the random variables is thus essential for informed decision-making. To this end, the approximated FORM method can be employed to evaluate reliability elasticities for each random variable, both with respect to their mean values (as expressed in Eq. (3.31)) and their standard deviations (as given in Eq. (3.32)).

Figures 6.2 and 6.3 illustrate the elasticity factors with respect to the means and standard deviations of the input variables for the bending and contact stress models, respectively.

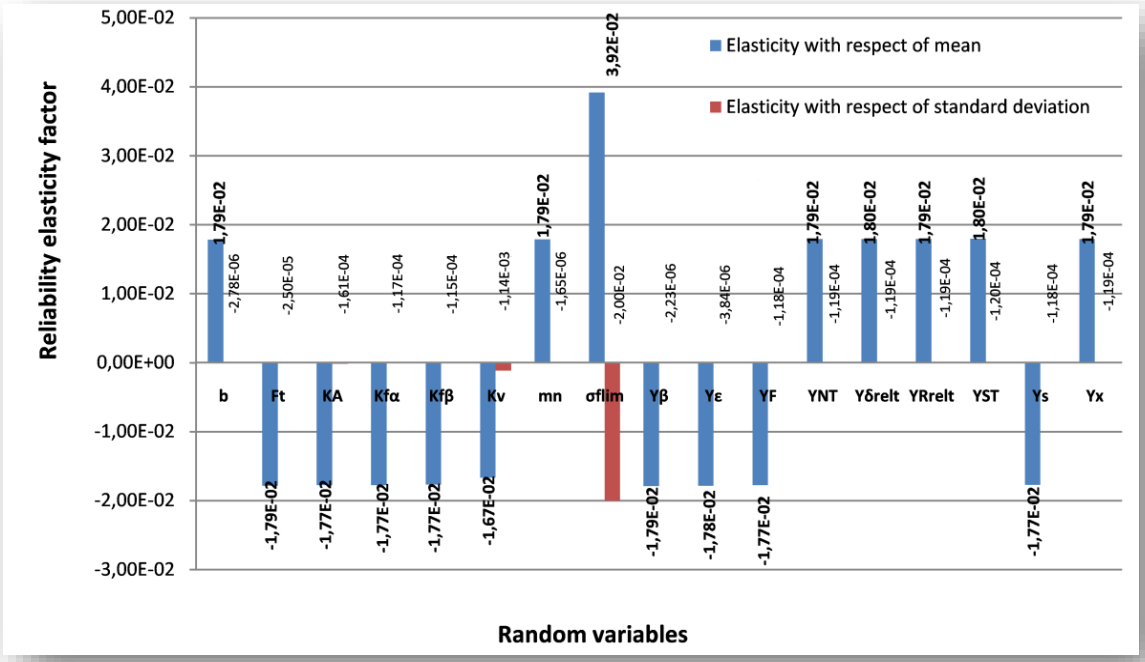

Figure 6.2 Reliability elasticity factors results of bending model

According to Fig (6.2), it is evident that the reliability elasticity with respect to the mean value of each variable significantly influences the failure probability. Most variables exhibit similar elasticity factor magnitudes—whether positive or negative—with the notable exception of the elasticity associated with the mean of σ_{Flim}. This variable emerges as the most influential factor, indicating that variations in σ_{Flim} have a pronounced impact on the probability of failure. Notably, the elasticity value is positive, suggesting a beneficial effect: the system's reliability increases by (3.92×10^{-2} %) or every 1% increase in σ_{Flim}. A similar positive effect is observed for other variables such as Y_{NT}, Y_{ST}, $Y_{\delta relT}$, Y_{RrelT}, Y_X, b and m_n; this finding aligns well with the results presented by Yang et al. (2012), who conducted a comparable sensitivity analysis on the same gear model. In contrast, the elasticity results concerning the standard deviations of the input variables reveal that $E_{\sigma_{\sigma Flim}}$ has the biggest influence on the bending model ($E_{\sigma_{\sigma Flim}}$ = -2.0×10-2), the remaining elasticity factors are comparatively negligible. This outcome suggests that the model is relatively insensitive to uncertainties in most standard deviations, indicating inherent robustness—except in the case of the standard deviation $E_{\sigma_{\sigma Flim}}$ of σ_{Flim} which demands strict control measures due to its substantial impact. The reliability elasticity analysis for the contact stress failure model is presented in Figure 6.3.

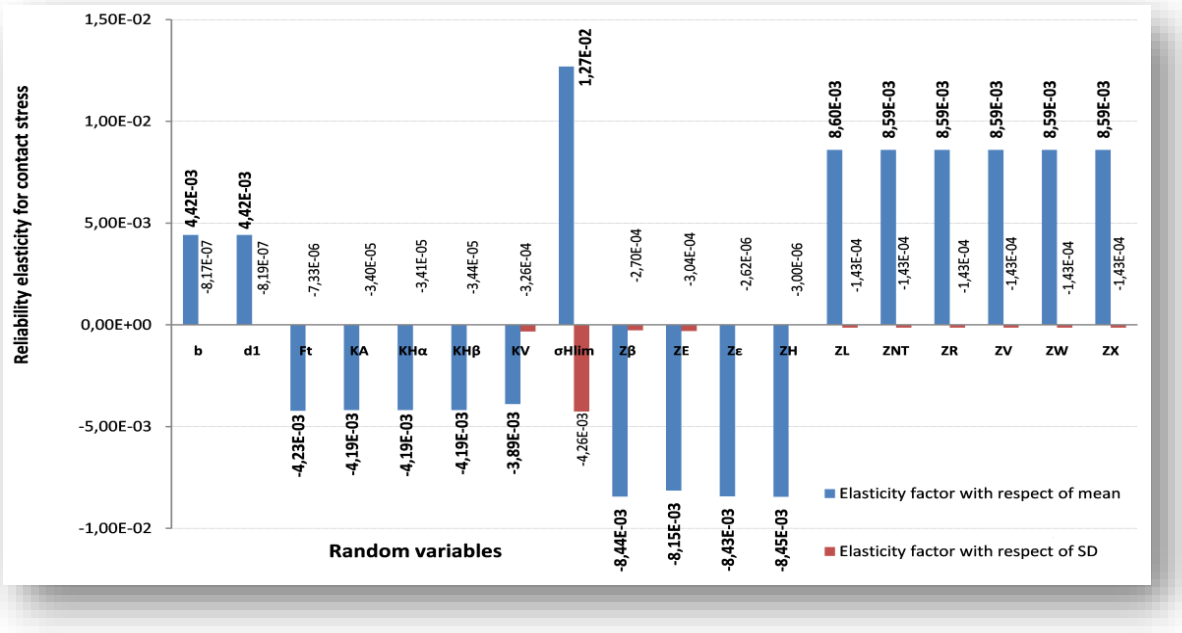

Figure 6.3 Reliability elasticity factors results of contact model

The results presented in Figure 6.3 indicate that the parameter σ_{Hlim} exerts the most significant influence on the reliability of the contact stress model. In comparison, the effects of the remaining variables are relatively minor. The analysis of the elasticity histogram for the contact stress model indicates that a 1% increase in the average variable σ_{Hlim} results in a increase of approximately (1.27×10^{-2} %) of *R*. The results indicate that implementing quality control measures for gear material is essential, as evidenced by the need to reduce the standard deviation of the variable σ_{Hlim}, which exhibits a significant elasticity factor of (4.26×10^{-3}). This elasticity analysis proves instrumental in identifying the most sensitive parameters, guiding design modifications and control strategies aimed at enhancing overall system reliability.

6.3.2.2 Sensitivity factors analysis

To quantitatively assess the individual impact of each design parameter on system reliability, sensitivity factors with respect to the means $\frac{\partial R}{\partial x_i}$ re computed using the FORM method. These results are subsequently compared with those obtained using the approach proposed by Yang et al. (2012), as presented in **Table 6.5**. This comparison serves to validate the accuracy and consistency of the current sensitivity analysis methodology.

Table 6.5 Sensitivity Factors results

contact stress	$\frac{\partial R}{\partial x_i}$ FORM	$\frac{\partial R}{\partial x_i}$ Edgeworth series		bending stress	$\frac{\partial R}{\partial x_i}$ FORM	$\frac{\partial R}{\partial x_i}$ Edgeworth series
b	$2{,}11\times10^{-5}$	$3{,}59\times10^{-5}$		b	$8{,}91\times10^{-5}$	$1{,}02\times10^{-4}$
d_1	$2{,}84\times10^{-5}$	$4{,}83\times10^{-5}$		F_t	$-5{,}14\times10^{-7}$	$-5{,}89\times10^{-7}$
Ft	$-1{,}22\times10^{-7}$	$-2{,}07\times10^{-7}$		K_A	$-1{,}77\times10^{-2}$	$-2{,}04\times10^{-2}$
K_A	$-4{,}19\times10^{-3}$	$-7{,}19\times10^{-3}$		$K_{F\alpha}$	$-1{,}53\times10^{-2}$	$-1{,}76\times10^{-2}$
$K_{H\alpha}$	$-3{,}61\times10^{-3}$	$-6{,}19\times10^{-3}$		$K_{F\beta}$	$-1{,}10\times10^{-2}$	$-1{,}27\times10^{-2}$
$K_{H\beta}$	$-2{,}49\times10^{-3}$	$-4{,}28\times10^{-3}$		K_v	$-1{,}12\times10^{-2}$	$-1{,}37\times10^{-2}$
K_V	$-2{,}62\times10^{-3}$	$-4{,}84\times10^{-3}$		$\boldsymbol{m}$	$4{,}46\times10^{-3}$	$5{,}10\times10^{-3}$
σ_{Hlim}	$9{,}76\times10^{-6}$	$2{,}01\times10^{-5}$		σ_{Flim}	$1{,}22\times10^{-4}$	$1{,}60\times10^{-4}$
Z_β	$-8{,}82\times10^{-3}$	$-1{,}50\times10^{-2}$		Y_β	$-2{,}23\times10^{-2}$	$-2{,}55\times10^{-2}$
Z_E	$-4{,}29\times10^{-5}$	$-7{,}57\times10^{-5}$		Y_ε	$-2{,}49\times10^{-2}$	$-2{,}85\times10^{-2}$
Z_ε	$-1{,}04\times10^{-2}$	$-1{,}77\times10^{-2}$		Y_f	$-7{,}50\times10^{-3}$	$-8{,}65\times10^{-3}$
Z_H	$-3{,}64\times10^{-3}$	$-6{,}19\times10^{-3}$		Y_n	$1{,}79\times10^{-2}$	$4{,}96\times10^{-2}$
Z_L	$9{,}34\times10^{-3}$	$2{,}84\times10^{-2}$		$Y_{\delta relt}$	$1{,}81\times10^{-2}$	$5{,}01\times10^{-2}$
Z_{NT}	$8{,}59\times10^{-3}$	$2{,}61\times10^{-2}$		Y_{Rrelt}	$1{,}68\times10^{-2}$	$4{,}66\times10^{-2}$
Z_R	$8{,}34\times10^{-3}$	$2{,}53\times10^{-2}$		Y_{st}	$8{,}54\times10^{-3}$	$2{,}36\times10^{-2}$
Z_v	$8{,}26\times10^{-3}$	$2{,}51\times10^{-2}$		Y_s	$-1{,}01\times10^{-2}$	$-1{,}17\times10^{-2}$
Z_w	$8{,}59\times10^{-3}$	$2{,}61\times10^{-2}$		Y_x	$1{,}79\times10^{-2}$	$4{,}96\times10^{-2}$
Z_x	$8{,}59\times10^{-3}$	$2{,}61\times10^{-2}$				

Table 6.5 reveals that the reliability sensitivity estimates with respect to the mean values of the random variables, as calculated using the FORM method, exhibit significantly larger errors when compared to those obtained via the Edgeworth method in the case of G3. In contrast, for case G1, the discrepancies between the two methods are relatively minor. Despite these differences, Yanfang et al. (2011) concluded that FORM remains one of the most widely adopted methods in reliability-based design, owing to its high computational efficiency and accuracy. Furthermore, FORM provides reliable approximations of sensitivity in the presence of strongly nonlinear limit state functions by leveraging the most probable point (MPP) approach.

6.3.3 Parametric analysis

The results of elasticity values with respect to means and standard deviations are utilized to identify which parameters warrant further exploration to achieve a more reliable gear pair. In the case, σ_{Flim} and σ_{Hlim} exhibit the highest elasticity factors, along with their respective standard deviations, which is why they have been selected as decision variables.

6.3.4 Possible improvements in design and reliability

1) ***Modification of Statistical Parameters**:* Enhancing the reliability of the gear pair may require adjustments to the statistical parameters of the input distributions. This can involve increasing the mean of beneficial random variables, reducing the standard deviations to minimize variability, or truncating the variables distribution law.
2) ***Implementation of RBRDO via the SORA Method:*** A structured Reliability-Based Robust Design Optimization (RBRDO) process should be executed using the Sequential Optimization and Reliability Assessment (SORA) method. This approach allows for the systematic optimization of the selected design variables, balancing performance and robustness in the presence of uncertainties, thereby improving overall system reliability.

6.3.4.1 Modification of statistical parameters

Based on the results of the parametric analysis, the most influential variables affecting the reliability of the gear pair are σ_{Hlim} (σ_{Flim}), Therefore, improving reliability can be approached by either increasing the mean values, reducing their standard deviations $\sigma_{\sigma Hlim}$ ($\sigma_{\sigma Flim}$), or truncate their distribution law. This means that gear pair reliability can be increased by increasing the material's allowable stress for contact and bending.

In the current study, the material characterized by $\sigma_{Flim} = 310\ N/mm^2$ and σ_{Hlim}=1300 N/mm^2 corresponds to a hardened wrought steel of grade ML (Minimum Limit), typically exhibiting a surface hardness ranging from 600 to 800 HV (Vickers hardness). However, as emphasized by Herring (2004) the fatigue strength of a material is not solely determined by nominal hardness values but is influenced by multiple interrelated factors, including:

Hardness Distribution: Case hardness, case depth, and core hardness.

***Microstructure**:* Percentage of retained austenite, grain size, carbide morphology, distribution of non-martensitic phases, and intergranular toughness.

***Design and Manufacturing Conditions**:* Residual compressive stresses, surface finish quality, and geometric features.

These considerations must be accounted for when selecting or treating materials to enhance the reliability and fatigue resistance of gear components under severe operating conditions.

A. Decreasing the standard deviation

The results regarding the elasticity values in relation to means and standard deviations are utilized to identify which parameters are significant for enhancing the reliability of the structure. In the gear pair case, special attention should be given to the experimental gear bending fatigue strength σ_{Flim}, so quality control on this variable is probably quite simple to implement. The variation coefficient of σ_{Flim} for pinion and wheel COV = 20%. This value is quite conservative due to a lack of information about it. In fact, according to Aziz and Chassapis (2011), the coefficient of variation of hardened alloy steel should be only chosen at about ± 10%. It is for this reason that changes in the standard deviation of this variable should be done to increase the gear pair reliability.

The following figures are obtained by reducing the standard deviation of σ_{Flim} and $\sigma_{Hlim.}$

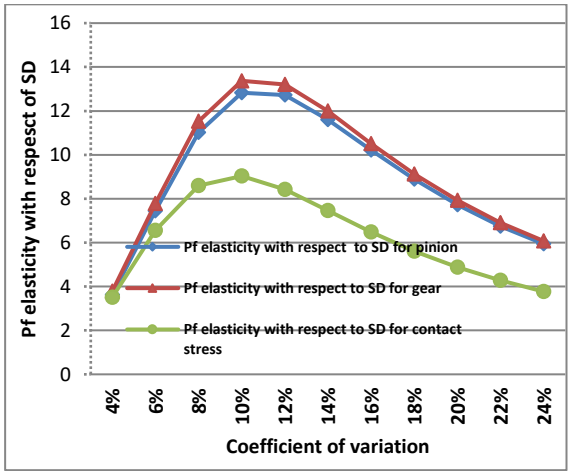

Figure 6.4 Failure probability elasticity factor

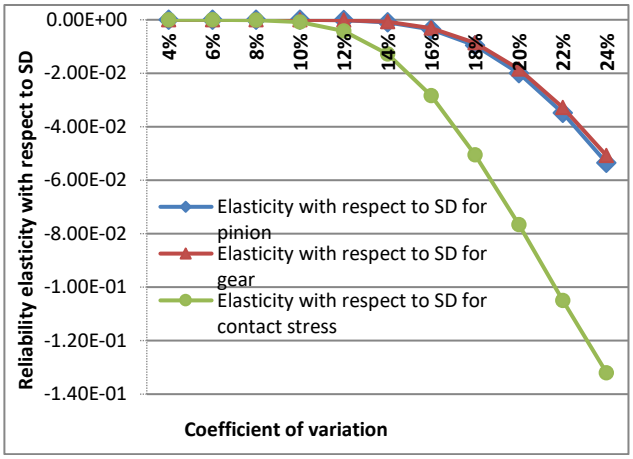

Figure 6.5 Reliability elasticity factor

Figure **6.4** shows that elasticity factors are maximized at the coefficient of variation value equal to 10% for the tree limits states equations. The increase of the elasticity factor in the interval COV= 20% to 10% is due to the increase in the speed of convergence of the failure probability compared to the variation in the standard deviation; this convergence becomes slower in the interval 10% to 4%. So, in terms of reliability cost, the value of COV=10% is considered an optimal solution for the design variables σ_{Flim} and σ_{Hlim}.

Figure **6.5** notes that the elasticity factor curve versus the variation of COV is always negative, confirming that an increase in the standard deviation is always unfavourable to reliability.

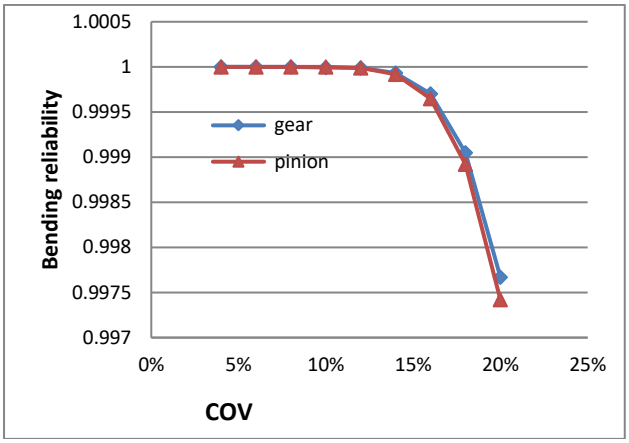

Figure 6. 6 Bending reliability vs COV

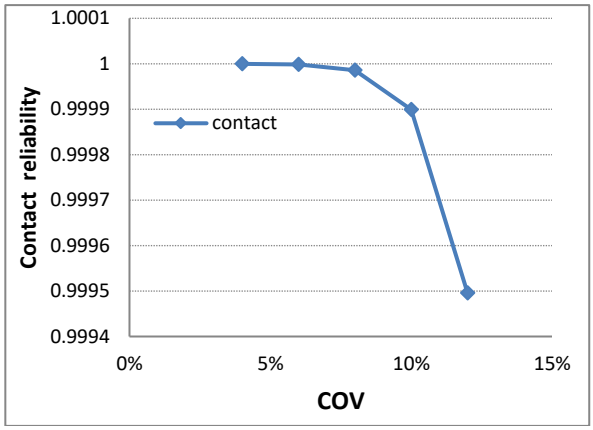

Figure 6.7 Contact gear pair reliability vs COV

From Figure 6, by varying the COV of σ_{Flim} from 20% to 10%, the increase in R in cases G_1 and G_2 as a function of the values of standard deviation could be quantified. It is noted that, for the same level of stress, reliability increases with a reduction of standard variation. Indeed, for a variation of COV value from 20% to 10%, the gear pair reliability increases from (R=0,99742) to (R=0,99999883) for the pinion and from (R=0,99767) to (R=0,99999186) for the wheel.

Figure 7 illustrates the standard deviation variation of σ_{Hlim} from 12% to 10%, corresponding to an increase in reliability varying from (R=0,999496) to (R=0,999899).

The results highlight the critical need for quality control on gear materials during the design or manufacturing phase. It is essential that the series produced maintains σ_{Flim} and σ_{Hlim} values as close as possible to their mean values. The causes of dispersion in the material primarily involve the preparation process, which may modify the material and its heterogeneity.

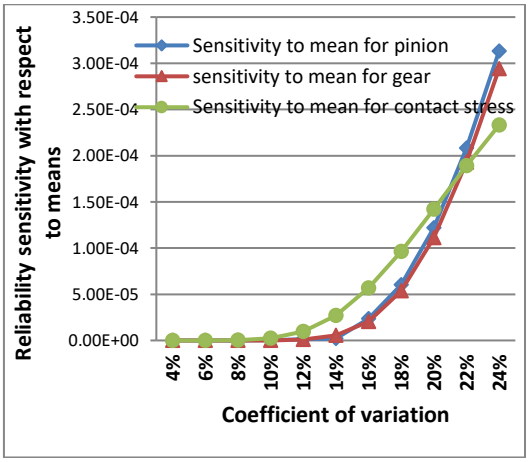

Figure 6. 8 Sensitivity factor vs COV

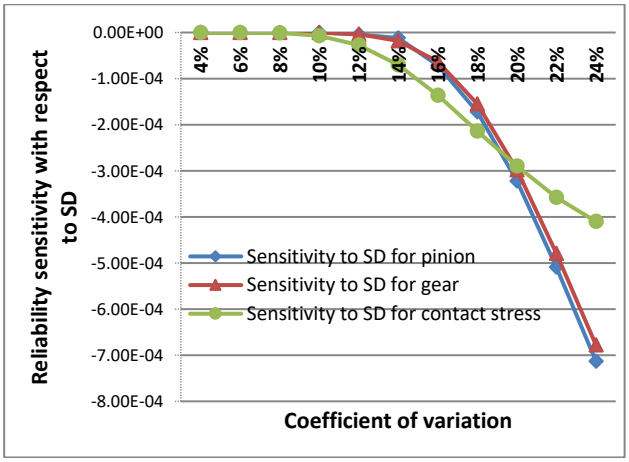

Figure 6.9 Sensitivity factor vs COV

Figures **6. 8** and **6.9** note that the sensitivities to mean and standard deviation of σ_{Flim} and σ_{Hlim} tend to zero when the coefficient of variation is reduced from 20% to 10%. As a result, the model is insensitive to these design variables and its reliability increases.

However, the results can serve as a decision-support tool. For example, they can improve quality control at the design and manufacturing stage by reducing deviations in allowable stresses σ_{Flim} and σ_{Hlim}.

According to Mayo (Mayo, 1998), these deviations can arise from various factors, including variations in material metallurgy and hardness, such as cleanliness, residual stresses, microstructure, quality, deformations induced by heat treatment, and poor machine tool condition. Consequently, minimizing these deviations requires strict control of these sources of uncertainty and the implementation of appropriate measures during design and manufacturing.

B.Changing law distributions

Two types of distributions are frequently utilized in the literature to characterize σ_{Flim} and σ_{Hlim}. Certain studies indicate that the allowable stresses conform to a normal distribution, while others propose that a logarithmic normal distribution is more appropriate. However, there is a deficiency in experimentation, as the lognormal distribution is referenced by Zhang et al. (2013). To clarify this effect, the analysis is carried out for a lognormal distribution for both σ_{Flim} and σ_{Hlim} to observe the evolution of R versus in function of variation in standard deviation from 6% to 20%.

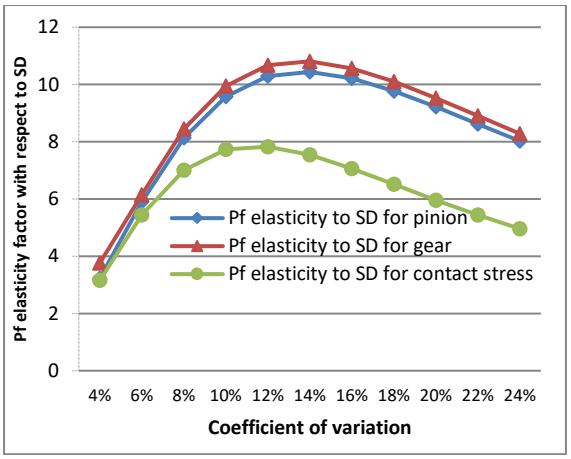

Figure 6.10 Elasticity factor vs COV

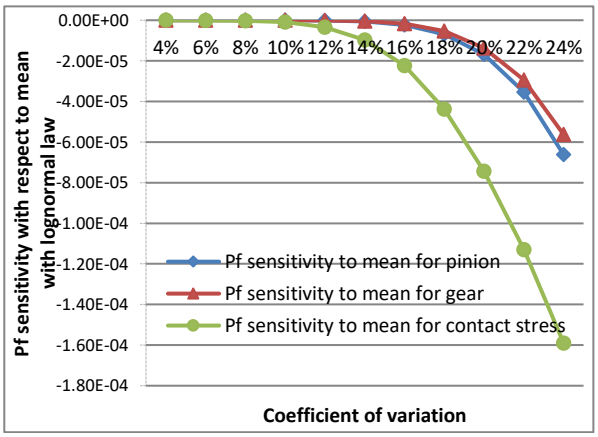

Figure 6.11 Elasticity factor vs COV

Fig.6.10 shows that elasticity factors are maximized at the coefficient of variation value equal to 12% for the tree limits states equations.

The increase of elasticity factors in the interval COV= 20% to 12% is due to the increase in the speed of convergence of the failure probability compared to the variation in the standard deviation. This convergence speed becomes slower in the interval 12% to 4%. So, in terms of reliability cost, the value of COV=12% is considered an optimal solution for the design variables σ_{Flim} and σ_{Hlim}.

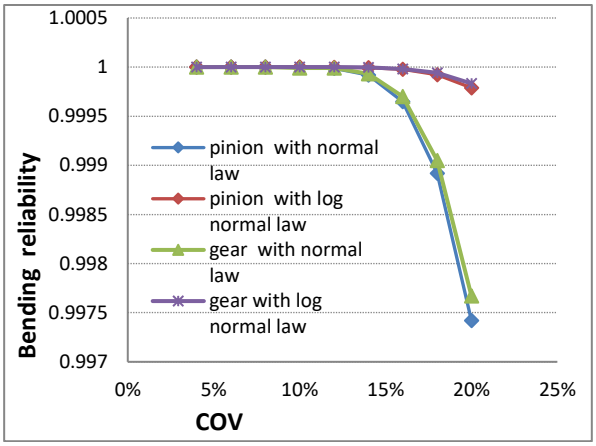

Figure 6.12 Bending *R* evolution vs COV for types

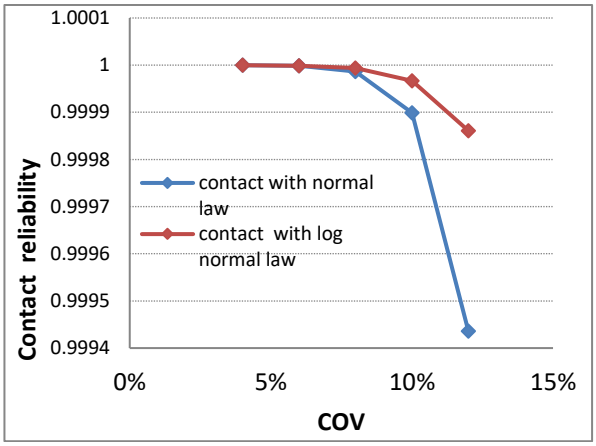

Figure 6.13 Contact *R* evolution vs COV for types of distribution law

As predicted, an important effect of the distribution law on the failure probability is confirmed in(Figures 12,13 and) since, for the same stress level, the failure probability values are always higher in the case of a lognormal distribution. For $\sigma_{\sigma_{\mathrm{Flim}}} = 62\ N/mm^2$, the pinion will have an R = 0,99742 in the case of a normal law (figure **6.**12). On the other hand, when the distribution is lognormal leads to an R =0,999789. The same effect is found in the case of contact stress, while $\sigma_{\sigma_{\mathrm{Hlim}}} = 156\ N/mm^2$, the contact

R= 0,999436 with a normal law, and R= 0,999861 with a lognormal law (figure **6.13**).

C. Changing mean values

From the results of elasticity shown in the histograms (**Figure 6.2, Figure 6.3**), it is clear that the average values of σ_{Flim} and σ_{Hlim} have a negative influence on the failure probability. Therefore the improvement of the reliability related to the bending and contact stress is done by the increase of the mean values of allowable stress values without changing the coefficients of variation. As an example, changing the variation of the σ_{Flim} mean from 200 N/mm^2 to 425 N/mm^2 and σ_{Hlim} mean from 1300 N/mm^2 to 1500 N/mm^2. This

corresponds to a new material belonging to grade MQ having a surface hardness in the range of 660 HV to 800 HV and a core hardness of 25 HR minimum. However, figures 14 and 15 illustrate these results.

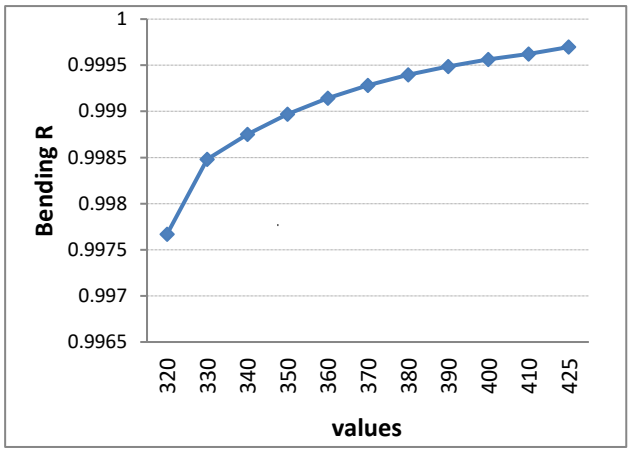

Figure 6.14 Reliability evolution vs σ_{Flim}

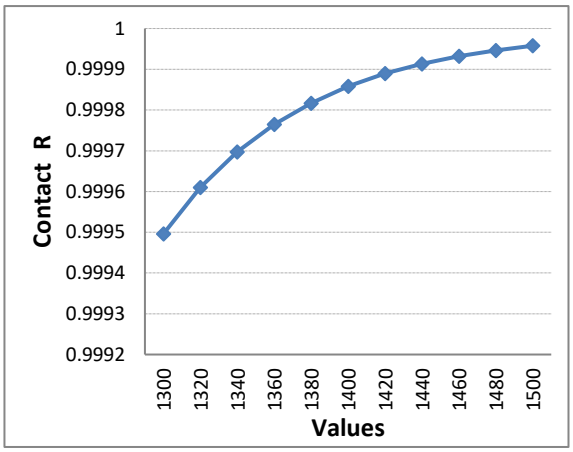

Figure 6.15 Reliability evolution vs σ_{Hlim}

Figures **6.**14 and **6.**15 show that increasing mean values of σ_{Flim} and σ_{Hlim} affect the gear reliability positively; for example, with a material of σ_{Flim} = 320 N/mm^2, the R= 0,99767 or a material of σ_{Flim} = 425 N/mm^2 leading to R= 0,999697. For the case of contact stress, when $\sigma_{Hlim} = 1300\ N/mm^2$, the R = 0,999496, or to have R= 0,9999578, a material of $\sigma_{Hlim} = 1500\ N/mm^2$ is needed.

As can be concluded, the shift from low-quality ML to medium-quality MQ has considerably increased reliability. Furthermore, in order to provide adequate performance for both bending strength and pitting resistance, the choice of material with characteristics that have direct consequences on the safety and reliability of the gear pair is necessary.

In practice, the choice of gear material depends on several factors: gear types and dimensions, speed and silent operation, required bending strength, and wear resistance. Standard ISO 6336-5:2003 provides numerical values for allowable stress numbers, specifically for bending and contact, of materials utilized in gears. It also includes specifications for material quality and heat treatment requirements.

6.3.4.2 Optimize Design and Reliability by proposed RBRDO formulation

A decoupled approach utilizing the Sequential Optimization and Reliability Assessment (SORA) method is implemented to achieve the desired reliability in the robust design of gear pair parameters. The RBDO methods are implemented using Matlab code to address this problem.

A RBRDO of a gear pair can be characterized as a bi-objective optimization problem. In this context, the objective functions $f_1(x)$ and $f_2(x)$ are defined as the minimum variances and mean values of each limit state function $G_1(x)$ and $G_3(x)$.

$$f_1(x) = \left[w \times \mu_{G_1} + (1-w) \times \sigma_{G_1}^2\right] \quad (6.6)$$

The parameters chosen as a design variable are: $100 \leq \sigma_{Flim} \leq 450,\ 25 \leq \sigma_{\sigma Flim} \leq 75$, utilizing starting parameters $[\sigma_{Flim0},\ \sigma_{\sigma Flim0}] = [310, 40]$.

$$f_1(x) = w \times (2.26 \times \sigma_{Flim} - 283.77) + (1-w) \times [5.1024712 \times \sigma_{\sigma Flim}{}^2 + (0.027783 \times \sigma_{Flim}{}^2)] \quad (6.7)$$

and: $$f_2(x) = \left[w \times \mu_{G_3} + (1-w) \times \sigma_{G_3}^2\right] \quad (6.8)$$

The parameters chosen as a design variable are:

$$600 \leq \sigma_{Hlim} \leq 1500\ ,\ 100 \leq \sigma_{\sigma Hlim} \leq 200$$

the initial values are: $[\sigma_{Hlim0}\ ,\ \sigma_{\sigma Hlim0}] = [1300, 156]$.

$$f_2(x) = [w \times (0.985 \times \sigma_{Hlim} - 700.926585) + (1-w) \times ((0.97 \times \sigma_{\sigma Hlim}{}^2) + (0.00631 \times \sigma_{Hlim}{}^2) + 3151.21)] \quad (6.9)$$

The materials align with the specified limit values to σ_{Flim} and σ_{Hlim} in the RBRDO process: $[\sigma_{Flim}, \sigma_{Hlim}]_{min} = [100\ N/mm^2, 600N/mm^2]$ correspond to " flame or induction hardened wrought and cast steel" quality ML, hardness HV=[485-615].

$[\sigma_{Flim},\ \sigma_{Hlim}]_{max} = [450\ N/mm^2, 1500N/mm^2]$ correspond to " case hardened wrought steel" quality MQ, hardness HV=[660-800].

The materials align with the specified limit values $\sigma_{Flim} = 310\ N/mm^2$ and σ_{Hlim}=1300 N/mm^2. They are hardened wrought steel grade ML (stands for the minimum requirement), with a surface hardness from 600 to 800 HV (Vickers hardness).

ISO 6336:5 (2003) specifies numerical values for allowable stress numbers, including bending and contact, for materials utilized in gears. This standard outlines the requirements for material quality and heat treatment.

From equation $G(d^k, \mu_x^k - s_i^{k+1},\ P_{MPP}^{k+1})$, The probabilistic constraints are designated as G_1 and G_3; there are no random parameters (P_{MPP}^{k+1})) present.

The weight coefficients w are determined for two distinct sets of values: w=0; w=1. The evolution of design variables, objective function values, and statistics for G_1 and G_3 following the RBRDO design based on the SORA method for target reliability of $R_T = 99.99\%$ (corresponding to $\beta = 3.73$) has been calculated and presented in tables (4.6), (4.7), (4.8), and (4.9).

Utilizing these sets for each objective function will yield four optimal designs.

Table 6.6 Design 1 for the objective function $\mathbf{f_1(x)}$ in the case where $w = 0$

cycles	σ_{Flim}	$\sigma_{\sigma Flim}$	$f_1(x)$	*G1*	σ_{G1}
Original design	310	62	/	-114.8	213.5
1	125.63	25	3.627×10^{3}	-257.789	101.85
2	249,48	25	4.918×10^{3}	1.256	105.27
3	248.36	25	4.903×10^{3}	-0.0458	105.22
4	248.38	25	4.903×10^{3}	0.0016	105.22
5	248.38	25	4.903×10^{3}	-4.54×10^{-5}	105.22

Table 6.7 Design 2 for the objective function $\mathbf{f_1(x)}$ in the case where $w = 1$

cycles	σ_{Flim}	$\sigma_{\sigma Flim}$	$f_1(x)$	*G1*	σ_{G1}
Original design	310	62	/	-114.8	213.50
1	125.63	40.27	0.0044	-360.89	149.50
2	294.25	40.03	380.90	5.525	146.70
3	291.23	40.05	374.08	-0.722	146.63
4	291.36	40.05	374.38	-0.722	146.63
5	291.36	40.05	374.38	-0.722	146.63

Table 6.8 Design 3 for the objective function $\mathbf{f_2(x)}$ in the case where $w = 0$

cycles	σ_{Hlim}	$\sigma_{\sigma Hlim}$	$f_2(x)$	*G3*	σ_{G1}
Original design	1300	156	/	-61.37	145.92
1	711,24	100	1.6050×10^{4}	-434.32	108.84
2	1215,98	100	2.2178×10^{4}	1.299	120.41
3	1214,37	100	2.2154×10^{4}	-0.346	120.34
4	1214,43	100	2.2155×10^{4}	-0.346	120.34
5	1214,43	100	2.2155×10^{4}	-0.346	120.34

Table 6.9 Design 4 for the objective function $\mathbf{f_2(x)}$ in the case where $w = 1$

cycles	σ_{Hlim}	$\sigma_{\sigma Hlim}$	$f_2(x)$	*G3*	σ_{G1}
Original design	1300	156	/	-61.37	145.92
1	1300	156	/	-61.37	145.92
2	711,23667	155,71	2.0×10^{-8}	-593.674	150.10
3	1376,66	155.999	655.78	4.596	156.46
4	1370,47	155,999	649.68	-0.589	156.33
5	1370,71	155,999	649.91	-0.589	156.33

The optimization results presented in tables (4.16), (4.17), (4.18), and (4.19) indicate that variations in weight coefficient values result in differing design variable values. The four designs exhibit significant differences for the scenario where w=1, the optimization of tables (4.17) and (4.19) is limited to σ_{Flim} and σ_{Hlim}. The values obtained after the convergence of the objective functions are 291.36 N/mm^2 and 1370.71 N/mm^2, respectively.

Tables (4.16) and (4.18) (case w=0) indicate that when standard deviations are treated as design parameters, their values attain the lower bound, with optimal values of $\sigma_{Flim}$and σ_{Hlim}equal to 248.38 $N/mm^2$and 1214.43 N/mm^2, respectively.

6.3.4.3 Confirmation of the robustness of the design

Reliability sensitivity analysis respecting the means should be conducted for each random variable in $\boldsymbol{G1}$ and $\boldsymbol{G3}$. The results are presented in Tables (4.20) and (4.21).

Table 6.10 Reliability sensitivity for bending model with respect to mean

Random variables for bending stress	*Reliability Sensitivity factors for cov=20%*	*Reliability Sensitivity factors for w=0*	*Reliability Sensitivity factors for w =1*
$\boldsymbol{b}$	8.01×10^{-5}	5.55×10^{-6}	3.9×10^{-6}
$\boldsymbol{F_t}$	-4.62×10^{-7}	-3.18×10^{-8}	-2.24×10^{-8}
$\boldsymbol{K_A}$	-1.6×10^{-2}	-1.09×10^{-3}	-7.71×10^{-4}
$\boldsymbol{K_{F\alpha}}$	-1.37×10^{-2}	-9.43×10^{-4}	-6.65×10^{-4}
$\boldsymbol{K_{F\beta}}$	-9.93×10^{-3}	-6.82×10^{-4}	-4.81×10^{-4}
$\boldsymbol{K_v}$	-1.01×10^{-2}	-7.48×10^{-4}	-5.25×10^{-4}
$\boldsymbol{m}$	4.0×10^{-3}	2.78×10^{-4}	1.95×10^{-4}
$\boldsymbol{\sigma_{Flim}}$	1.11×10^{-4}	1.25×10^{-5}	8.77×10^{-6}
$\boldsymbol{Y_\beta}$	-2.0×10^{-2}	-1.38×10^{-3}	-9.74×10^{-4}
$\boldsymbol{Y_\varepsilon}$	-2.24×10^{-2}	-1.55×10^{-3}	-1.01×10^{-3}
$\boldsymbol{Y_F}$	-7.44×10^{-3}	-5.11×10^{-4}	-3.60×10^{-4}
$\boldsymbol{Y_N}$	1.61×10^{-2}	1.32×10^{-3}	8.88×10^{-4}
$\boldsymbol{Y_{\delta relt}}$	1.6×10^{-2}	2.3×10^{-3}	1.5×10^{-3}
$\boldsymbol{Y_{Rrelt}}$	1.51×10^{-2}	2.2×10^{-3}	1.4×10^{-3}
$\boldsymbol{Y_{st}}$	7.68×10^{-3}	1.11×10^{-3}	7.17×10^{-4}
$\boldsymbol{Y_s}$	2.8×10^{-3}	5.62×10^{-4}	3.97×10^{-4}
$\boldsymbol{Y_x}$	1.61×10^{-2}	2.34×10^{-3}	1.56×10^{-3}

Tables (4.10) and (4.11) indicate that the reliability sensitivities to the means of each random variable (DR/Dx) decrease when design parameters are optimized through RBRDO.

Consequently, models exhibit reduced sensitivity to variations in design variables, resulting in enhanced robustness of the two designs and an increase in their reliability.

The results highlight the critical need for quality control on gear materials during the design or manufacturing phase. It is essential that the series produced maintains σ_{Flim} and σ_{Hlim} values that deviate minimally from their means.

Table 6.11 Reliability sensitivity for contact model with respect to means

Random variables for contact stress	***Reliability Sensitivity factors for cov=12%***	***Reliability Sensitivity factors for w=1***	***Reliability Sensitivity factors for w=0***
b	$2{,}11\times10^{-5}$	4.61×10^{-6}	6.14×10^{-6}
d_1	$2{,}83\times10^{-5}$	6.21×10^{-6}	8.27×10^{-6}
F_t	$-1{,}22\times10^{-7}$	-2.66×10^{-8}	-3.54×10^{-8}
K_A	$-4{,}19\times10^{-3}$	-9.22×10^{-4}	-1.23×10^{-3}
$K_{H\alpha}$	$-3{,}61\times10^{-3}$	-7.89×10^{-4}	-1.05×10^{-3}
$K_{H\beta}$	$-2{,}49\times10^{-3}$	-5.45×10^{-4}	-7.24×10^{-4}
K_V	$-2{,}62\times10^{-3}$	-5.76×10^{-4}	-7.50×10^{-4}
σ_{Hlim}	$9{,}73\times10^{-6}$	2.033×10^{-6}	2.58×10^{-6}
Z_β	$-8{,}82\times10^{-3}$	-1.93×10^{-3}	-2.56×10^{-3}
Z_E	$-4{,}27\times10^{-5}$	-9.41×10^{-6}	-1.24×10^{-5}
Z_ε	$-1{,}04\times10^{-2}$	-2.28×10^{-3}	-3.03×10^{-3}
Z_H	$-3{,}64\times10^{-3}$	-7.95×10^{-4}	-1.06×10^{-3}
Z_L	$9{,}34\times10^{-3}$	2.08×10^{-3}	2.81×10^{-3}
Z_{NT}	$8{,}59\times10^{-3}$	1.91×10^{-3}	2.58×10^{-3}
Z_R	$8{,}34\times10^{-3}$	1.85×10^{-3}	2.47×10^{-3}
Z_v	$8{,}26\times10^{-3}$	1.84×10^{-3}	2.48×10^{-3}
Z_w	$8{,}59\times10^{-3}$	1.91×10^{-3}	2.58×10^{-3}
Z_x	$8{,}59\times10^{-3}$	1.91×10^{-3}	2.58×10^{-3}

The causes of dispersion in materials primarily include alterations resulting from the preparation process, which can affect the material's heterogeneity. The objective is to minimize deviations through stringent control of sources of uncertainty and the implementation of appropriate actions during the design and manufacturing processes.

6.4 Conclusion

The Reliability-Based Robust Design Optimization (RBRDO) of a gear pair has been conducted, yielding highly promising results. Initially, system reliability concerning the critical failure event was assessed using multiple approaches, including Monte Carlo Simulations (MCS) and the First- and Second-Order Reliability Methods (FORM/SORM). As is customary, the MCS method was employed to validate the accuracy of the applied approximation techniques. Notably, in the given case study, SORM demonstrated greater efficiency in balancing computational cost and response precision due to the nonlinear nature of the limit state functions.

Furthermore, the findings indicate that failure is primarily governed by bending stress in both the pinion and the wheel, which proves to be slightly more critical than contact stress for the studied gear pair.

Additionally, FORM was utilized to evaluate sensitivity and elasticity with respect to the mean and standard deviations of each random variable parameter. These insights facilitate the selection of key parameters for design optimization, effectively reducing the dimensionality of the optimization problem. The SORA method, on the other hand, reformulates the RBRDO problem into a deterministic design optimization before performing a reliability assessment through an efficient inverse Most Probable Point (MPP) search algorithm (PMA). This approach enables the reliability analysis to commence from the optimal design point and rapidly converge toward the final optimum solution.

Ultimately, using the SORA method, the optimal values of means and standard deviations with high elasticity factors were determined. The confirmation phase demonstrated that reliability sensitivity coefficients were significantly reduced, highlighting the diminished impact of uncertainties during the robust optimization process. This study underscores the effectiveness of achieving a robust design with a desired level of reliability in a computationally efficient manner. Moreover, it emphasizes the critical role of elasticity analysis in optimizing the design and manufacturing process, reinforcing its importance in engineering applications.

CONCLUSION AND FUTURE RESEARCH

Conclusion

Reliability analysis of multi-component systems, such as speed reducers, is essential for ensuring performance and durability. Since the reliability of a system depends on the reliability of its parts, probabilistic methods are needed to measure the dependability of these parts accurately and then of the system as a whole. However, interactions between components and the presence of numerous random variables increase computational complexity, making traditional methods inefficient. Therefore, developing a scalable approach that balances accuracy and computational efficiency is crucial for improving reliability evaluations.

This thesis has developed an efficient methodology for estimating the reliability of a multi-component system, with a focus on a speed reducer, using a Dimensionality Reduction Method (DRM). The proposed approach effectively addresses the complexity of high-dimensional reliability problems with correlated variables, while maintaining both the variability of the reduced variables and the interpretability of the results. This work contributes a robust and scalable framework for reliability analysis in complex engineering systems. Furthermore, it opens pathways for improving the reliability and optimizing the design of gear reducers by systematically accounting for uncertainties in all model input variables. In this context, three main contributions have been presented in this thesis.

The first contribution has concentrated on creating reduced-dimensional models using the results of cosine direction factors and the correlations of failure modes in speed reducer subsystems. A new approach is introduced for the Structural System Reliability-Based Dimension Reduction Method (SSR-DRM), grounded in the First-Order Reliability Method (FORM). We analyze each component's reliability using original, reduced-dimensional, and deterministic models to determine which of the latter two accurately reflects the original one. The failure probabilities are estimated through FORM and Monte Carlo Simulation (MCS) as a benchmark.

The second contribution has extended the application of the reduced models to

estimate the reliability of the speed reducer subsystems, then of the system as a whole, modeled as a series configuration of its components. First-order failure probability bounds were established, followed by the application of Ditlevsen's second-order upper bound method to refine the reliability estimation.

The third contribution has analyzed the previous gear pair subsystem under harsh conditions, which reduce its reliability and reflect real-world challenges. The objective is to increase its reliability using two methods: the first is by changing the statistical parameters of the most important parameters, and the second is by applying the suggested Reliability-Based Robust Design Optimization (RBRDO) method, in which the Sequential Optimization and Reliability Assessment (SORA) technique finds the best parameter values.

The implementation of programs under MATLAB software package for all calculations has improved the reproducibility and applicability of the proposed techniques.

The results

The comparison between the original, reduced, and deterministic models demonstrated that the reduced dimension model provided the most accurate reliability representation for all speed reducer subsystems. The failure probability estimates obtained through FORM and Monte Carlo Simulation (MCS) further confirmed the effectiveness of this approach.

The results obtained through the application of the First-order failure probability bounds and Ditlevsen's second-order upper bound method for the Reduced Dimension Model are closely aligned with those obtained by the original model, confirming the accuracy of the proposed (SSR-DRM) methodology. In addition, These results have shown effectively the dominant failure mode affecting the gear reducer system, providing essential insights for improving design and maintenance strategies.

The important factor results obtained using FORM, like direction cosines and elasticity factors, show how the response changes depending on all random variables and their statistical parameters. This makes it easy to figure out which parameters are concerned by the reduced dimension process and also to suggest ways to improve the products.

The best values for the means and standard deviations of the most important parameters are found using the proposed Reliability-Based Robust Design Optimization (RBRDO) process. The confirmation phase of this process revealed that the reliability

sensitivity coefficients had decreased. This suggests that the robust optimization procedure successfully reduced the impact of uncertainties, resulting in a robust design.

This study has shown that a robust design with the desired reliability can be achieved quickly and simply by using elasticity factors results, demonstrating the importance of sensitivity factors analysis in the designing and manufacturing process.

Overall, this study provides a systematic and computationally efficient framework for reliability assessment and optimization of speed reducers under uncertainty by integrating Dimension Reduction Techniques with Structural Reliability estimation and Optimization Methods. This research enhances the precision and practicality of mechanical reliability engineering.

Future works

Future work may explore the extension of this framework in the following recommendations:

- Investigate alternative reliability analysis techniques, such as higher-order reliability methods or machine learning-based approaches, to further enhance computational efficiency and accuracy.
- Extend the methodology to account for time-dependent failure mechanisms and degradation processes in mechanical components.
- Validate the proposed models using experimental data to improve their practical applicability and reliability predictions and develop more robust design optimization strategies that incorporate real-world constraints, such as manufacturing tolerances and maintenance schedules.

Annex 1

Table Random variables statistics for the gear pair [Zhang et al.(2003)], Yang et al. (2012), Ziat (2022)]

Random variables of Bending stresses	***Symbol***	***Mean values and standard deviations***		***Random variables of Contact stress***	***Symbol***	***Mean values and standard deviations***
		Pinion	***Gear***			
Normal module	m	*N*(4 ,0.02)	*N*(4, 0.02)	***Pinion pitch diameter***	d_1	*N(148.75,0.74375) mm*
Active face width	b	*N(200,1) mm*	*N(200, 1)mm*	***Work harden factor***	Z_W	*N(1,0.033)*
Rated tangential tooth force at transverse pitch	F_t	*N(34644,519.66)N*	*N(34644, 519.66)N*	***Rated tangential tooth force at transverse pitch***	F_t	*N(34644 ,519.66)N*
Experimental gear bending fatigue strength	σ_{Flim}	*N(310 ,62)N/mm²*	*N(310, 62) N/mm²*	***Experimental flank contact fatigue strength***	σ_{Hlim}	*N(1300,156) N/mm²*
Tooth form factor	Y_F	*N(2.36, 0.07788)*	*N(2.14, 0.07062)*	***Contact ratio factor***	Z_ε	*N(0.81, 0.00405)*
Dedendum stress concentration factor	Y_S	*N(1.75, 0.05775)*	*N(1.94, 0.06402)*	***Nodal field factor***	Z_H	*N(2.32, 0.0116)*
Contact ratio factor	Y_ε	*N(0.715, 0.003575)*	*N(0.715, 0.003575)*	***Elastic factor***	Z_E	*N(189.8, 9.49)*$\sqrt{N/mm^2}$
Helix angle factor	Y_β	*N(0.8,0.004)*	*N(0.8, 0.004)*	***Helix angle factor***	Z_β	*N(0.957, 0.004785)*
Experimental gear dedendum stress concentration factor	Y_{ST}	*N(2.1 , 0.0693)*	*N(2.1, 0.0693)*	***Lubricant factor***	Z_L	*N(0.92, 0.03036)*
Life factor	Y_{NT}	*N(1 , 0.033)*	*N(1, 0.033)*	***Life factor***	Z_{NT}	*N(1, 0.033)*
Relative sensitive factor	$Y_{\delta relT}$	*N(0.99 ,0.03267)*	*N(1.01,0.03333)*	***Tooth fineness factor***	Z_R	*N(1.03, 0.03399)*
Relative surface condition factor	Y_{RrelT}	*N(1.065, 0.035145)*	*N(1.065, 0.035145)*	***Velocity factor***	Z_V	*N(1.04, 0.03432)*
Size factor	Y_X	*N(1, 0.033)*	*N(1, 0.033)*	***Size factor***	Z_X	*N(1, 0.033)*
Work condition factor	K_A	*N(1, 0.033)*	*N(1, 0.033)*	***Work condition factor***	K_A	*N(1, 0.033)*
Dynamic load factor	K_V	*N(1.484 ,0.1613)*	*N(1.484,0.1613)*	***Dynamic load factor***	K_V	*N(1.484, 0.1613)*
Longitudinal load distribution factor	$K_{F\alpha}$	*N(1.16 ,0.03828)*	*N(1.16, 0.03828)*	***Transverse load distribution factor***	$K_{H\beta}$	*N(1.68, 0.05544)*
Transverse load distribution factor	$K_{F\beta}$	*N(1.603 ,0.052899)*	*N(1.603, 0.052899)*	***Longitudinal load distribution factor***	$K_{H\alpha}$	*N(1.16, 0.03828)*

BIBLIOGRAPHY

Abdi, S., Sharifzadeh, S., & Amiri, S. (2021, March). Reliability Model Development for Wind Turbine Drivetrain with Brushless Doubly-Fed Induction Machine as Generator. In 2021 22nd IEEE International Conference on Industrial Technology (ICIT) (Vol. 1, pp. 228-233). IEEE.

Abdo, T., & Rackwitz, R. (1991). A new beta-point algorithm for large time-invariant and time-variant reliability problems. In Reliability and Optimization of Structural Systems' 90 (pp. 1-12). Springer, Berlin, Heidelberg.

AGMA 2001-D04. Fundamental Rating Factors and Calculation Methods for Involute Spur and Helical Gear Teeth.

Akinci, I., Yilmaz, D., & Çanakci, M. (2005). Failure of a rotary tiller spur gear. Engineering failure analysis, 12(3), 400-404

Alvarado-Hernandez, A. I., Zamudio-Ramirez, I., Jaen-Cuellar, A. Y., Osornio-Rios, R. A., Donderis-Quiles, V., & Antonino-Daviu, J. A. (2022). Infrared Thermography Smart Sensor for the Condition Monitoring of Gearbox and Bearings Faults in Induction Motors. Sensors, 22(16), 6075.

Amanda Egerton. (August 31, 2016). Markov Analysis – A Brief Introduction.

Andrzej, S. Nowak., & Niels, C. Lind. (1995). Probabilistic Structural Mechanics Handbook Probability-Based Design Codes, DOI: 10.1007/978-1-4615-1771-9_15.

Armaan, A., Keshav, S., & Srinivas, G. (2020). A step towards safety: material failure analysis of landing gear. Materials Today: Proceedings, 27, 402-409.

Standard Test Method for Evaluating the Scuffing Load Capacity of Oils.

Aziz, E.S.S and Chassapis, C. (2011), "Probabilistic Simulation Approach to Evaluate the Tooth-Root Strength of Spur Gears with FEM-Based Verification", Engineering, Vol. **3** No. 12, p.1137

Baravalle, M. (2017). Risk and Reliability Based Calibration of Structural Design Codes Principles and Applications.

Beermann, S. (2018). Reliability, Lifetime and Safety Factors. Gear Technology, 8.

Bertsche, B. (2008). Reliability in automotive and mechanical engineering: determination of component and system reliability. Springer Science & Business Media.

Bhandari, V. B. (2020). Design of machine elements third edition.

Bhaumik, S. K., Rangaraju, R., Parameswara, M. A., Venkataswamy, M. A., Bhaskaran, T. A., & Krishnan, R. V. (2002). Fatigue failure of a hollow power transmission shaft. Engineering failure analysis, 9(4), 457-467.

Bhaumik, S. K., Sujata, M., Kumar, M. S., Venkataswamy, M. A., & Parameswara, M. A. (2007). Failure of an intermediate gearbox of a helicopter. Engineering Failure Analysis, 14(1), 85-100.

Bibal, A., & Frénay, B. (2019). Measuring quality and interpretability of dimensionality reduction visualizations. In SafeML ICLR Workshop.

Billinton, R., & Allan, R. N. (1992). Reliability evaluation of engineering systems (Vol. 792). New York: Plenum press.

Bloch, H. P. (1998). Improving machinery reliability (Vol. 1). Gulf professional publishing.

Breitung, K. (1984). Asymptotic approximations for multinormal integrals. Journal of Engineering Mechanics, 110(3), 357-366.

Bryan Christiansen. (2023). Benefits And Shortfalls Of 5 Reliability Techniques For Analyzing Fault Tolerance. https://www.modernanalyst.com/

Byun, J. E., & Song, J. (2020). Bounds on reliability of larger systems by linear programming with delayed column generation. Journal of Engineering Mechanics, 146(4), 04020008. https://doi.org/10.1061/(ASCE)EM.1943-7889.0001717

Calderon-Salmeron, G., Schwack, F., Joshi, P., & Glavatskih, S. (2023). A Reliability Case Study of the Impact of Tribology on Wind Turbine Gearboxes.

Carlos Gonzalez 2015 what's the difference between bearings? .machinedesign.com

Chen, Z., Qiu, H., Gao, L and Li, P. (2013). An optimal shifting vector approach for efficient probabilistic design , Structural and Multidisciplinary Optimization, Vol. 47 No. 6, p. 905-920.

Chen, Z., Li, X., Chen, G., Gao, L., Qiu, H., & Wang, S. (2018). A probabilistic feasible region approach for reliability-based design optimization. Structural and Multidisciplinary Optimization, 57(1), 359-372.

Chen, Z., Wu, Z., Li, X., Chen, G., Gao, L., Gan, X., ... & Wang, S. (2019). A multiple-design-point approach for reliability-based design optimization. Engineering Optimization, 51(5), 875-895.

Chengbing, H., & Xinxin, F. (2012). Institutions function and failure statistic and analysis of wind turbine. Physics procedia, 24, 25-30.

Choi, S. K., Grandhi, R., & Canfield, R. A. (2006). Reliability-based structural design. Springer Science & Business Media.

Center, N. S. W. (1998). Handbook of reliability prediction procedures for mechanical equipment. Carderock Division, Naval Surface Warfare Center.

Clark, C. E., Barter, G., Shaler, K., & DuPont, B. (2022). Reliability-based layout optimization in offshore wind energy systems. Wind Energy, 25(1), 125-148.

DNV (2012) CLASSIFICATION NOTES no. 41.2, Calculation of Gear Rating for Marine Transmissions, DET NORSKE VERITAS AS, Norway, may 2012 (DNV Internet site: www.dnv.com).

Cremona, C., Poulin, B., Colas, A. S., Michel, J., Marcotte, C., Vion, B., ... & Sadone, R. (2013, May). Calibration of partial safety factors for the assessment of existing bridges. In Assessment, Upgrading and Refurbishment of Infrastructures", IABSE Conference Rotterdam (pp. 290-291).

Dawei, Z. H. U., Jinyu, Z. H. O. U., Chunqiu, L. I. U., & Zhiling, W. A. N. G. (2021). A short review of reliability-based design optimization. In IOP Conference Series: Materials Science and Engineering (Vol. 1043, No. 3, p. 032041). IOP Publishing.

Der Kiureghian, A., & Liu, P. L. (1986). Structural reliability under incomplete probability information. Journal of Engineering Mechanics, 112(1), 85-104.

Ditlevsen, O., (1979) Narrow reliability bounds for structural systems. Journal of Structural Mechanics, 7, 453-472.

Ditlevsen, O., & Madsen, H. O. (1996). Structural reliability methods (Vol. 178). New York: Wiley.

Du, X., & Chen, W. (2004). Sequential optimization and reliability assessment method for efficient probabilistic design. J. Mech. Des., 126(2), 225-233.

Du, X., & Chen, W. (2002, January). Sequential optimization and reliability assessment method for efficient probabilistic design. In International Design Engineering Technical Conferences and Computers and Information in Engineering

Conference (Vol. 36223, pp. 871-880).

Dwyer-Joyce, R. S. (1999). Predicting the abrasive wear of ball bearings by lubricant debris. Wear, 233, 692-701.

Dwyer-Joyce, R. S., Hamer, J. C., Sayles, R. S., & Ioannides, E. (1990). Surface damage effects caused by debris in rolling bearing lubricants, with an emphasis on friable materials. Rolling Element Bearings: Towards the 21st Century.

Ebrahimi, B., & Bataleblu, A. A. (2024). Intelligent reliability-based design optimization: Past and future research trends. In Developments in Reliability Engineering (pp. 787-826). Elsevier.

Efficient plant: https://www.efficientplantmag.com/2012/07/failure-analysis-of-machine-shafts/; visited 15/05/2023

Eftekharnejad, B., Addali, A., & Mba, D. (2012). Shaft crack diagnostics in a gearbox. Applied Acoustics, 73(8), 723-733.

Elusakin, T., & Shafiee, M. (2022). Fault diagnosis of offshore wind turbine gearboxes using a dynamic Bayesian network. International Journal of Sustainable Energy, 41(11), 1849-1867.

Eurocode (2002) Basis of structural design. CEN, Brussels

Errichello, R. (2013). Gear Bending Fatigue Failure and Bending Life Analysis. Encyclopedia of Tribology, 1467-1468.

Errichello, R., & Muller, J. (2002). How to analyze gear failures. Journal of Failure Analysis and Prevention, 2(6), 8-16.

Fan, W., Liu, C., Wang, Z., & Li, Z. (2024). Improved FORM and SORM based on improved modified symmetric rank 1 algorithm and adaptive Kriging model. Journal of Mechanical Design, 146(10).

Fernandes, P. J. L., & McDuling, C. (1997). Surface contact fatigue failures in gears. Engineering Failure Analysis, 4(2), 99-107.

Fischer, K., Besnard, F., & Bertling, L. (2011). Reliability-centered maintenance for wind turbines based on statistical analysis and practical experience. IEEE Transactions on Energy Conversion, 27(1), 184-195.

Forsthoffer, W. E. (2011). Forsthoffer's best practice handbook for rotating machinery.

Elsevier.

Gao, P., Xie, L., & Hu, W. (2018). Reliability and random lifetime models of planetary gear systems. Shock and Vibration, 2018.

Gautham, B. P., Gupta, P., Kulkarni, N. H., Panchal, J. H., Allen, J. K., & Mistree, F. (2013, August). Robust Design of Gears with Material and Load Uncertainties. In International Design Engineering Technical Conferences and Computers and Information in Engineering Conference (Vol. 55898, p. V03BT03A046). American Society of Mechanical Engineers.

Gayton, A. Mohamed, J. Sorensen, M. Pendola, M. Lemaire, Calibration methods for reliability-based design codes, *Structural Safety 26*(1) (*2004*) *91-*

Gear Manual Writing Committee, Gear Handbook, 2nd edn. (Machinery Industry Press, New York, 2013).

Giovanni, A. G. P. B. G. (2016). Failure analysis of a half-shaft of a Formula SAE Racing. CEP, 21941, 972.

Glenn E. Gabryel 2002 Optimize shaft surface finish for maximum seal performance 2002 Plant Services Articles

Godfrey, D. (2003). Fretting corrosion or false brinelling?. Tribology and Lubrication Technology, 59(12), 28-31.

Golabi, S. I., Fesharaki, J. J., & Yazdipoor, M. (2014). Gear train optimization based on minimum volume/weight design. Mechanism and machine theory, 73, 197-217.

Goswami, S., Chakraborty, S., Chowdhury, R., & Rabczuk, T. (2019). Threshold shift method for reliability-based design optimization. Structural and Multidisciplinary Optimization, 60, 2053-2072.

Goswami, P., & Rai, R. N. (2023). A Systematic Review on Failure Modes and Proposed Methodology to Artificially Seed Faults for Promoting PHM Studies in Laboratory Environment for an Industrial Gearbox. Engineering Failure Analysis, 107076.

Grączewski, A., & Ligaj, B. (2015). Calculations of cylindrical tooth wheels in view of iso 6336 standard and recommendations of classification society CN 41.2-DNV-GL. Journal of Polish CIMEEAC, 10(1), 75-83.

Gu, Y. K., Xu, B., Huang, H., & Qiu, G. (2020). A fuzzy performance evaluation model for a gearbox system using hidden Markov model. IEEE Access, 8, 30400-30409.

Gunjegaonkar, D. S., Bhattacharya, S., & Sequeira, S. R. (2009). Design Analysis and Development of a New 5F/1R Synchromesh Rear Mounted Gearbox for Mini Truck

for an Emerging Markets (No. 2009-26-0021). SAE Technical Paper.

Haldar, A. and Mahadevan, S. (2000), Probability, reliability, and statistical methods in engineering design, John Wiley, Sons Inc, New York

Hariom, P., Kumar, V., & Chandrababu, D. (2016). A Review of Fundamental Shaft Failure Analysis. International Research Journal of Engineering and Technology, 3(10), 389-395..

Hasofer, A. M., & Lind, N. C. (1974). Exact and invariant second-moment code format. Journal of the Engineering Mechanics division, 100(1), 111-121.

He, Y., Song, B., & Zhang, D. (2017, March). Uncertainty-based improved multidisciplinary design optimization methods. In 2017 IEEE 2nd Advanced Information Technology, Electronic and Automation Control Conference (IAEAC) (pp. 1113-1117). IEEE.

Helton, J. C. (1994). Treatment of uncertainty in performance assessments for complex systems. Risk analysis, 14(4), 483-511.

Helton, J. C., & Davis, F. J. (2003). Latin hypercube sampling and the propagation of uncertainty in analyses of complex systems. Reliability Engineering & System Safety, 81(1), 23-69.

Herring, D. H. (2004). Gear heat treatment: the influence of materials and geometry. Gear Technology, 21(2), 35-40.

Hohenbichler, M., & Rackwitz, R. (1982). First-order concepts in system reliability. Structural safety, 1(3), 177-188.

Hoogeveen, M., & Mao, K. (2022). The Conceptualisation, Development, Design and Optimisation of an Integrated In-Hub Planetary Gearbox System for a Formula Student Race Car.

Hristovska, E. (2024). Concept for evaluating the safety of a dynamically loaded gearbox reducer. Acta Polytechnica, 64(6), 230-538.

Hu, Y., Liu, S. J., Chang, J. H., & Zhang, J. G. (2015). An intelligent method for contact fatigue reliability analysis of spur gear under EHL. Journal of Central South University, 22(9), 3389-3396.

Huang, H. Z., Zhang, X., Meng, D. B., Wang, Z., & Liu, Y. (2013). An efficient approach to reliability-based design optimization within the enhanced sequential optimization and reliability assessment framework. Journal of Mechanical Science and Technology, 27(6), 1781-1789.

Huangfu, Y., Zhao, Z., Ma, H., Han, H., & Chen, K. (2020). Effects of tooth modifications on

the dynamic characteristics of thin-rimmed gears under surface wear. Mechanism and Machine Theory, 150, 103870.

Hunter, D. (1976). An upper bound for the probability of a union. Journal of Applied Probability, 13(3), 597-603. https://doi.org/10.2307/3212481.

Inturi, V., Balaji, S. V., Gyanam, P., Pragada, B. P. V., Geetha Rajasekharan, S., & Pakrashi, V. (2023). An integrated condition monitoring scheme for health state identification of a multi-stage gearbox through Hurst exponent estimates. Structural Health Monitoring, 22(1), 730-745.

ISO 15243 2004 Rolling bearings – Damage and failures – Terms, characteristics and causes.

ISO 15243 2017 Bearings—Damage, R. (2017). Failures—Terms, Characteristics and Causes. International Organization for Standardization: Geneva, Switzerland.

ISO 8402 (1986) Quality vocabulary. International Standards Organization, Geneva.

ISO 2394 (1998) General principles on reliability for structures. ISO, Geneva

ISO 281:2007. Rolling Bearings—Dynamic Load Ratings and Rating Life

ISO/TR 13989. International standard: ISO TR 13989, Calculation of scuffing load capacity of cylindrical, bevel and hypoid gears, 2010.

Jia, W., Sun, M., Lian, J., & Hou, S. (2022). Feature dimensionality reduction: a review. *Complex & Intelligent Systems*, *8*(3), 2663-2693.

Jia, Y., Li, Y., Xu, M., Cheng, Y., & Wang, R. (2024). A fault diagnosis scheme for harmonic reducer under practical operating conditions. Measurement, 227, 114234.

Jiang, R., Zhang, K., Ma, Z., & Wang, D. (2015). Fault mode, effects and criticality analysis for overheating fault of wind turbines gearbox and generator.

Jiang, Z., Hu, W., Dong, W., Gao, Z., & Ren, Z. (2017). Structural reliability analysis of wind turbines: A review. Energies, 10(12), 2099.

Jiang, G., Jia, C., Nie, S., Wu, X., He, Q., & Xie, P. (2022). Multiview enhanced fault diagnosis for wind turbine gearbox bearings with fusion of vibration and current signals. Measurement, 196, 111159.

Jolliffe, I. T. (2002). Principal component analysis for special types of data (pp. 338-372). Springer New York.

Kabir, S., & Papadopoulos, Y. (2019). Applications of Bayesian networks and Petri nets in safety, reliability, and risk assessments: A review. Safety science, 115, 154-175.

Karpat, F., Kalay, O. C., Dirik, A. E., & Karpat, E. (2022). Fault Classification of Wind

Turbine Gearbox Bearings Based on Convolutional Neural Networks. Transdisciplinary Journal of Engineering and Science, 13, 71-83.

Keller, J. (2017). Gearbox reliability collaborative gearbox 3 planet bearing calibration (No. NREL/TP-5000-67370). National Renewable Energy Lab.(NREL), Golden, CO (United States).

Kim, H., Howland, P., Park, H., & Christianini, N. (2005). Dimension reduction in text classification with support vector machines. Journal of machine learning research, 6(1).

Kimura, Y., Sekizawa, M., & Nitanai, A. (2002). Wear and fatigue in rolling contact. Wear, 253(1-2), 9-16.

Kissling, U., & Stangl, M. (2017). The documentation of gearbox reliability–an upcoming demand. In Int. Conf. Gears, Garching, Germany (pp. 1051-1062).

KISSsoft/KISSsys. "Calculation Programs for Machine Design," www.KISSsoft.AG.

Kiureghian Song, J., & Der Kiureghian, A. (2003). Bounds on system reliability by linear programming. Journal of Engineering Mechanics, 129(6), 627-636.

Kounias, E. G. 1968. "Bounds for the probability of a union, with applications." Ann. Math. Stat. 39 (6): 2154–2158. https://doi.org/10.1214/aoms/1177698049.

Kwak, B. M., & Lee, T. W. (1987). Sensitivity analysis for reliability-based optimization using an AFOSM method. Computers & structures, 27(3), 399-406.

Lanzutti, A., Gagliardi, A., Raffaelli, A., Simonato, M., Furlanetto, R., Magnan, M., ... & Fedrizzi, L. (2017). Failure analysis of gears, shafts and keys of centrifugal washers failed during life test. Engineering Failure Analysis, 79, 634-641.

Lee, H., Kwak, W., & Han, I. (1995). Developing a business performance evaluation system: An analytic hierarchical model. The Engineering Economist, 40(4), 343-357.

Lee, I., Choi, K.K. & Gorsich, D. (2010). System reliability-based design optimization using the MPP-based dimension reduction method. Struct Multidisc Optim 41, 823–839 https://doi.org/10.1007/s00158-009-0459-0.

Lee, J. O., Yang, Y. S., & Ruy, W. S. (2002). A comparative study on reliability-index and target- performance-based probabilistic structural design optimization. Computers & structures, 80(3-4), 257-269.

Lemaire, M. (2013). Structural reliability. John Wiley & Sons.

Lemaire, M., & Pendola, M. (2006). Phimeca-soft. Structural safety, 28(1-2), 130-149.

Lemaire, M., Chateauneuf, A., & Mitteau, J. C. (2009). Structural reliability. London: ISTE.

Lechner, G., & Naunheimer, H. (1999). Automotive transmissions: fundamentals, selection, design and application. Springer Science & Business Media.

Lim, J., Lee, B., & Lee, I. (2014). Second-order reliability method-based inverse reliability analysis using Hessian update for accurate and efficient reliability-based design optimization. International Journal for Numerical Methods in Engineering, 100(10), 773-792.

Lobato, F. S., Lara-Molina, F. A., & Libotte, G. B. (2025). A comparative study of direct and inverse reliability methods applied to robotic manipulators design. In Reliability Assessment and Optimization of Complex Systems (pp. 1-21). Elsevier.

Li, J., Mourelatos, Z., & Singh, A. (2012). Optimal preventive maintenance schedule based on lifecycle cost and time-dependent reliability. SAE International Journal of Materials and Manufacturing, 5(1), 87-95.

Li, M. X., Kang, J. C., Sun, L. P., & Wang, M. (2017, April). Reliability analysis of offshore wind turbine gearbox. In 6th International Conference on Marine Structures.

Li, D. Q., Jiang, Z. Y., & Zhao, X. (2016, June). Ship Multidisciplinary robust design optimization under multidimensional stochastic uncertainties. In The 26th International Ocean and Polar Engineering Conference. OnePetro.

Li, S., & Kahraman, A. (2014). A micro-pitting model for spur gear contacts. International Journal of Fatigue, 59, 224-233.

Liang, J., Mourelatos, Z. P., & Tu, J. (2004, January). A single-loop method for reliability-based design optimization. In International Design Engineering Technical Conferences and Computers and Information in Engineering Conference (Vol. 46946, pp. 419-430).

Liang, Q., Yang, Y., Zhang, H., Peng, C., & Lu, J. (2022). Analysis of simplification in Markov state-based models for reliability assessment of complex safety systems. Reliability Engineering & System Safety, 221, 108373.

Lin, X., Janak, S. L., & Floudas, C. A. (2004). A new robust optimization approach for scheduling under uncertainty:: I. Bounded uncertainty. Computers & chemical engineering, 28(6-7), 1069-1085.

Liu, W. (2014). The failure analysis of the repeat geartooth breakage in a 40 MW steam

turbine load gearbox and the butterfly in the carburized case. Engineering Failure Analysis, 46, 9-17.

Liu, P. L., & Der Kiureghian, A. (1991). Optimization algorithms for structural reliability. Structural safety, 9(3), 161-177.

Liu, Q. Y., & Zhou, Z. R. (2001). Effect of tangential force on wear behaviour of steels in reciprocating rolling and rolling–sliding contact. Wear, 250(1-12), 357-361.

Liu, Q. Y., & Zhou, Z. R. (2001). Effect of tangential force on wear behaviour of steels in reciprocating rolling and rolling–sliding contact. Wear, 250(1-12), 357-361.

Liu, H., Liu, H., Zhu, C., & Parker, R. G. (2020). Effects of lubrication on gear performance: A review. Mechanism and Machine Theory, 145, 103701.

Liu, G., Liu, H., Zhu, C., Mao, T., & Hu, G. (2021). Design optimization of a wind turbine gear transmission based on fatigue reliability sensitivity. Frontiers of Mechanical Engineering, 16, 61-79.

Littmann, W. E. (1970). The mechanism of contact fatigue. NASA Special Publication, 237, 309.

Loewenthal, S. H., Moyer, D. W., & Needelman, W. M. (1982). Effects of ultra-clean and centrifugal filtration on rolling-element bearing life.

Loc, N. H. (2021, March). Reliability based design of shaft for gearbox. In IOP Conference Series: Materials Science and Engineering (Vol. 1109, No. 1, p. 012017). IOP Publishing.

Loganathan, T. M., Purbolaksono, J., Inayat-Hussain, J. I., Muthaiyah, G., & Wahab, N. (2010). Pitting corrosion of triggering initial fractures of palm oil screw press machine shafts. Engineering Failure Analysis, 17(5), 1086-1093.

Madsen, H. O., Krenk, S., & Lind, N. C. (2006). Methods of structural safety. Courier Corporation.

Maláková, S., Puškár, M., Frankovský, P., Sivák, S., & Harachová, D. (2021). Influence of the Shape of Gear Wheel Bodies in Marine Engines on the Gearing Deformation and Meshing Stiffness. Journal of Marine Science and Engineering, 9(10), 1060.

Malakzadeh, K., & Daei, M. (2020). Hybrid FORM-Sampling simulation method for finding design point and importance vector in structural reliability. Applied Soft Computing, 92, 106313.

Mankhi, T. A., AL-Bedhany, J. H., & Legutko, S. (2022). Investigation of subsurface microcracks causing premature failure in wind turbine gearbox bearings. Results in Engineering, 16, 100667.

Mayo, P. (1998). Designing reliability into industrial gear drives. Gear Technology(USA), 15(5), 22-23.

MIL-STD-1629A, Military Standard: Procedures for Performing a Failure Mode, Effects and Criticality Analysis -http://everyspec.com/MIL-STD/MIL-STD-1600-1699/ .

Mogal, S. P., & Lalwani, D. I. (2017). Fault diagnosis of bent shaft in rotor bearing system. Journal of Mechanical Science and Technology, 31(1), 1-4.

Musial, W., Butterfield, S., & McNiff, B. (2007). Improving wind turbine gearbox reliability (No. NREL/CP-500-41548). National Renewable Energy Lab.(NREL), Golden, CO (United States).

Musto, J. C. (2010). The safety factor: case studies in engineering judgment. International Journal of Mechanical Engineering Education, 38(4), 286-296.

Murotsu, Y. (1983) Reliability analysis of frame structure through automatic generation of failure modes. In Reliability theory and its application in structural and soil mechanics (pp. 525-540). Dordrecht: Springer Netherlands.

Mylonas, N., Mollas, I., Bassiliades, N., & Tsoumakas, G. (2024). Exploring local interpretability in dimensionality reduction: Analysis and use cases. *Expert Systems with Applications*, *252*, 124074.

Nie, M., & Wang, L. (2013). Review of condition monitoring and fault diagnosis technologies for wind turbine gearbox. Procedia Cirp, 11, 287-290.

Noor, S. M. (2007). Failure Analysis of Driveshaft of Toyota SEG (Doctoral dissertation, UMP).

Naunheimer, H., Bertsche, B., Ryborz, J., Novak, W., Naunheimer, H., Bertsche, B., ... & Novak, W. (2011). Specification and Design of Shafts. Automotive Transmissions: Fundamentals, Selection, Design and Application, 278-299.

Nwosu, H. U., & Iwuoha, A. U. (2010). Gearbox Failure Analysis (pp. 62-74). Journal of Innovative Research in Engineering and Science, 1, 1.

Oila A, PhD thesis, (2003). University of Newcastle-upon-Tyne.

Oila, A., & Bull, J. (2005). Assessment of the factors influencing micropitting in rolling/sliding contacts. Wear, 258, 1510–1524.

Ouyang, T., Mo, X., Lu, Y., & Wang, J. (2022). CFD-vibration coupled model for predicting cavitation in gear transmissions. International Journal of Mechanical Sciences, 225, 107377.

Öztürk, H. (2006). Gearbox health monitoring and fault detection using vibration analysis.

Pan, A. X., & Yang, Z. G. (2022). Cause analysis and countermeasure on premature failure of a driven gear for the high-speed train. Engineering Failure Analysis, 139, 106487.

Pandey, D. K., & Lim, H. C. (2020). Pinion failure analysis of a helical reduction gearbox in a kraft process. Applied Sciences, 10(8), 2935.

Pantazopoulos, G., Zormalia, S., & Vazdirvanidis, A. (2010). Investigation of fatigue failure of roll shafts in a tube manufacturing line. Journal of failure analysis and prevention, 10(5), 358-362.

Park, J. W. (2023). Sequential sampling and reliability analysis method with improved accuracy and efficiency for reliability-based design optimization.

Peeters, J. F. W., Basten, R. J., & Tinga, T. (2018). Improving failure analysis efficiency by combining FTA and FMEA in a recursive manner. Reliability engineering & system safety, 172, 36-44.

Pei, J., Han, X., Tao, Y., & Feng, S. (2021). Lubrication reliability analysis of spur gear systems based on random dynamics. Tribology International, 153, 106606.

Pinterest, https://www.pinterest.com/pin/782641241519670304/; 21/02/2026

Software for reliability analysis developed by Phimeca Engineering S.A. http ://www.phimeca.com/.

Rackwitz, R. (2001). Reliability analysis—a review and some perspectives. Structural safety, 23(4), 365-395.

Rackwitz, R., & Flessler, B. (1978). Structural reliability under combined random load sequences. Computers & Structures, 9(5), 489-494.

Radoń, U., & Zabojszcza, P. (2025). The Application of Structural Reliability and Sensitivity Analysis in Engineering Practice. Applied Sciences, 15(1), 342.

Rahman, S., & Xu, H. (2004). A univariate dimension-reduction method for multi-dimensional integration in stochastic mechanics. Probabilistic Engineering Mechanics, 19(4), 393-408.

Randall FA. The safety factor of structures in history. Professional Safety, 1976; January:12–28. probably the latter half of the 19th century.

Rausand, M., & Høyland, A. (2003). System reliability theory: models, statistical methods, and applications (Vol. 396). John Wiley & Sons.

Raut, S. P., & Raut, L. P. (2014). A review of various techniques used for shaft failure analysis. International Journal of Engineering Research and General Science, 2(2), 2091-2730.

Rezaei, E., Poursina, M., & Rezaei, M. (2020). Experimental Investigation of Spur Gear Tooth Crack Location and Depth Detection using Short-time Averaging Method and Statistical Indicators. International Journal of Engineering, 33(10), 2079-2086.

Ribrant, J. (2006). Reliability performance and maintenance-a survey of failures in wind power systems. Unpublished doctoral dissertation, XR-EE-EEK, 4, 6.

Rupesh, Bhortake., Vaibhav, Kharabe, Kiran Shende., & Rohan Kadam. (2017). Bending and Wear Analysis of Spur Gear. International Research Journal of Engineering and Technology (Vol. 04 Issue: 05, pp. 2051-2053).

SAE ARP4761 Standard - Guidelines and Methods for Conducting the Safety Assessment Process on Civil Airborne Systems and Equipment - http://standards.sae.org/wip/arp4761a/

Saleem, M. A., Diwakar, G., & Satyanarayana, M. R. S. (2012). Detection of unbalance in rotating machines using shaft deflection measurement during its operation. IOSR J. Mech. Civ. Eng, 3(3), 08-20.

Sann, S., Tomeh, E., & Petr, T. (2024). Methods of detection and localization of the sources of noise and vibration on car gearboxes: a review. Journal of Vibroengineering, 26(4), 808-842.

Santana, H., Parco, D., Galdos, C., Calcina, A., De la Cruz, R., & Moggiano, N. (2023, May). Design of 10: 1 speed reducer for an elevator. In Journal of Physics: Conference Series (Vol. 2512, No. 1, p. 012011). IOP Publishing.

Sara, T. (2020). The Fractographic Investigation of an Aeroengine Accessory Gearbox Quill Shaft. Fatigue of Aircraft Structures, 2020(12), 36-46.

Scutti, J. J., & McBrine, W. J. (2002). Introduction to failure analysis and prevention. Materials Park, OH: ASM International, 2002., 3-23.

Shafiee, M., Enjema, E., & Kolios, A. (2019). An integrated FTA-FMEA model for risk

analysis of engineering systems: a case study of subsea blowout preventers. Applied Sciences, 9(6), 1192.

Sheng, S. (2016). Wind Turbine Gearbox Reliability Database. Condition Monitoring, and O&M Research Update.

Sheng, L., Li, W., Ye, G., & Feng, K. (2022). Nonlinear dynamic analysis of gear system in shearer cutting section under wear failure. Proceedings of the Institution of Mechanical Engineers, Part K: Journal of Multi-body Dynamics, 236(1), 99-112.

Singh, A., Mourelatos, Z. P., & Li, J. (2009, January). Design for lifecycle cost using time-dependent reliability. In International Design Engineering Technical Conferences and Computers and Information in Engineering Conference (Vol. 49026, pp. 1105-1119)

Singh, K., Kaushik, M., & Kumar, M. (2022). Integrating α-cut interval based fuzzy fault tree analysis with Bayesian network for criticality analysis of submarine pipeline leakage: A novel approach. Process Safety and Environmental Protection, 166, 189-201.

Soleimani-Babakamali, M. H., Lourentzou, I., & Sarlo, R. (2021). Does the curse of dimensionality apply to unsupervised shm? investigating the trade-off between loss of information and generalizability to unseen structural conditions. In 13th International Workshop on Structural Health Monitoring: Enabling Next-Generation SHM for Cyber-Physical Systems, IWSHM 2021 (pp. 644-650). DEStech Publications Inc.

Song, J., Kang, W. H., Lee, Y. J., & Chun, J. (2021). Structural system reliability: Overview of theories and applications to optimization. ASCE-ASME Journal of Risk and Uncertainty in Engineering Systems, Part A: Civil Engineering, 7(2), 03121001

Standard, I. S. O. (2006). 6336-2: 2003, Calculation of Load Capacity of Spur and Helical Gears—Part 2: Calculation of Surface Durability (Pitting). International Organization for Standardization, Geneva, Switzerland.

Standard, B., & ISO, B. (2006). Calculation of load capacity of spur and helical gears. ISO, 6336(1), 1996.

JCSS (2001) Probabilistic model code. Joint Committee on Structure Safety.

Su, C., Yang, Y., Wang, X., & Hu, Z. (2016, October). Failures analysis of wind turbines: Case study of a Chinese wind farm. In 2016 Prognostics and System Health Management Conference (PHM-Chengdu) (pp. 1-6). IEEE.

Taguchi, G., Chowdhury, S., & Wu, Y. (2004). Taguchi's quality engineering handbook. (No Title).

Tang, X., Xu, Y., Sun, X., Liu, Y., Jia, Y., Gu, F., & Ball, A. D. (2023). Intelligent fault diagnosis of helical gearboxes with compressive sensing based non-contact measurements. ISA transactions, 133, 559-574.

Tavner, P. J., Xiang, J., & Spinato, F. (2007). Reliability analysis for wind turbines. Wind Energy: An International Journal for Progress and Applications in Wind Power Conversion Technology, 10(1), 1-18.

Tavner, P. J., Greenwood, D. M., Whittle, M. W. G., Gindele, R., Faulstich, S., & Hahn, B. (2013). Study of weather and location effects on wind turbine failure rates. Wind energy, 16(2), 175-187.

Tazi, N., Châtelet, E., & Bouzidi, Y. (2017). Using a hybrid cost-FMEA analysis for wind turbine reliability analysis. Energies, 10(3), 276.

Tchangani, A., & Pérès, F. (2020). Modeling interactions for inoperability management: from fault tree analysis (FTA) to dynamic bayesian network (DBN). *IFAC-PapersOnLine*, *53*(3), 342-347

testbook. (2026) https://testbook.com/mechanical-engineering/spur-gear-definition-and-working. 22/02/2026

Tharwat, A. (2021) Independent component analysis: An introduction. Applied Computing and Informatics, 17(2), 222-249.

Tu, J., Choi, K. K., & Park, Y. H. (1999). A new study on reliability-based design optimization. 557-564.

Park, Y. H. (2001). Design potential method for robust system parameter design. AIAA journal, 39(4), 667-677.

Tvedt, L. (1983). Two second-order approximations to the failure probability. Technical Report RDIV/20-004-83, Det Norske Veritas.

Van Der Maaten, L., Postma, E. O., & Van Den Herik, H. J. (2009). Dimensionality reduction: A comparative review. Journal of machine learning research, *10*(66-71), 13.

Vanmarcke E.H. (1973) Matrix formulation of reliability analysis and reliability-based design. Computers and Structures, 3, 757-770.

Vencl, A., Gašić, V., & Stojanović, B. (2017, February). Fault tree analysis of most common rolling bearing tribological failures. In IOP Conference Series: Materials Science and Engineering (Vol. 174, No. 1, p. 012048). IOP Publishing.

Wall, M. E., Rechtsteiner, A., & Rocha, L. M. (2003). Singular value decomposition and principal component analysis. In A practical approach to microarray data analysis (pp. 91-109). Boston, MA: Springer US.

Wang, Q., Zhu, Y., Zhang, Z., Fu, C., Dong, C., & Su, H. (2016). Partial load: a key factor resulting in the failure of gear in the wind turbine gearbox. Journal of Failure Analysis and Prevention, 16(1), 109-122.

Wang, J., Liu, Y., Zhao, G., Ye, N., & Yang, L. (2022). An improved reliability index based on regional equivalent conversion. Quality and Reliability Engineering International, 38(4), 2031-2048.

Wang, M. H., Chen, F. H., & Lu, S. D. (2023). Research on Fault Diagnosis of Wind Turbine Gearbox with Snowflake Graph and Deep Learning Algorithm. Applied Sciences, 13(3), 1416.

Wink, C. H. (2012). Predicted scuffing Risk to spur and Helical Gears in Commercial Vehicle Transmissions. Gear Technology-The journal of Gear Manufacturing, 6, 82-86.

World Pumps. Selecting the right grease for rolling bearings, World Pumps 2015 31–33.

Wu, J., Yan, S., & Xie, L. (2011). Reliability analysis method of a solar array by using fault tree analysis and fuzzy reasoning Petri net. Acta Astronautica, 69(11-12), 960-968.

Xu, H., & Rahman, S. (2004). A generalized dimension-reduction method for multidimensional integration in stochastic mechanics. International Journal for Numerical Methods in Engineering, 61(12), 1992-2019.

Yanfang, Z., Yanlin, Z., & Yimin, Z. (2011). Reliability sensitivity based on first-order reliability method. Proceedings of the Institution of Mechanical Engineers, Part C: Journal of Mechanical Engineering Science, 225(9), 2189-2197.

Yang, S. Q., Huang, B., & Mao, L. P. (2013). Design Planetary Gear Reducer of ROV Thruster Using Evidence Theory. In Advanced Materials Research (Vol. 616, pp. 1988-1992). Trans Tech Publications Ltd.

Yang, X., Du, M., Zhao, D., & Zhang, J. (2018, August). Simultaneous Reliability-based

Optimal Design with Calibration for a Transmission Shaft in DCV. In 2018 6th International Conference on Mechanical, Automotive and Materials Engineering (CMAME) (pp. 66-70). IEEE.

Yang, Z., Zhang, Y. M., Zhang, X. F., & Huang, X. Z. (2012). Reliability-based sensitivity design of gear pairs with non-Gaussian random parameters. Applied Mechanics and Materials, 121, 3411-3418.

Yucesan, M., Gul, M., & Celik, E. (2021). A holistic FMEA approach by fuzzy-based Bayesian network and best–worst method. Complex & Intelligent Systems, 7, 1547-1564.

Zaman, M. A. U. (2019). On the Reliability-Based Design Optimization (RBDO) of A Speed Reducer. International Journal of Engineering Innovation & Research Volume 8, Issue 1, ISSN: 2277 – 5668

Zhang, R., & Mahadevan, S. (2000). Model uncertainty and Bayesian updating in reliability-based inspection. Structural Safety, 22(2), 145-160.

Zhang, G., Wang, G., Li, X., & Ren, Y. (2013). Global optimization of reliability design for large ball mill gear transmission based on the Kriging model and genetic algorithm. Mechanism and Machine Theory, 69, 321-336.

Zhang, H., Song, L., Li, X., Choy, Y., Liu, H., & Tao, F. (2025, January). Adaptive surrogate-assisted sampling pool reduction strategy for low failure probability estimation. In Proceedings of the Institution of Civil Engineers-Transport (pp. 1-45). Emerald Publishing Limited.

Zhang, X., Gao, H., Huang, H. Z., Li, Y. F., & Mi, J. (2018). Dynamic reliability modeling for system analysis under complex load. Reliability Engineering & System Safety, 180, 345-351.

Zhang, X., Han, P., Xu, L., Zhang, F., Wang, Y., & Gao, L. (2020). Research on bearing fault diagnosis of wind turbine gearbox based on 1DCNN-PSO-SVM. IEEE Access, 8, 192248-192258.

Zhang, Y., Liu, Q., & Wen, B. (2003). Practical reliability-based design of gear pairs. Mechanism and Machine Theory, 38(12), 1363-1370.

Zhang, Z., Liu, H., Wu, T., Xu, J., & Jiang, C. (2024). A novel reliability-based design optimization method through instance-based transfer learning. Computer Methods in Applied Mechanics and Engineering, 432, 117388.

Zhao, G., Zhao, X., Qian, L., Yuan, Y., Ma, S., & Guo, M. (2022). A Review of Aviation Spline Research. Lubricants, 11(1), 6.

Zheng, M. (2023). Research on time-varying reliability of wind power gearbox with failure correlation. Journal of Theoretical and Applied Mechanics, 119-127.

Ziat, A., Zaghar, H., Taleb, A. A., & Mohammed, S. (2022, May). Robust and Reliable Optimization of a Pair of Gear Wheels. In *International Conference on Integrated Design and Production*

LIST OF PUBLICATIONS

Karar, N., Felkaoui, A., & Djeddou, F. (2020). Reliability based robust design optimization based on sensitivity and elasticity factors analysis. *Journal of Materials and Engineering Structures «JMES»*, *7*(1), 97-111.